ABSTRACT

Title of dissertation: DEVELOPMENT OF A MODEL FOR FLAMING COMBUSTION OF DOUBLE-WALL CORRUGATED CARDBOARD

Mark B. McKinnon, Master of Science, 2012

Dissertation directed by: Professor Stanislav I. Stoliarov
Department of Fire Protection Engineering

Corrugated cardboard is used extensively in a storage capacity in warehouses and frequently acts as the primary fuel for accidental fires that begin in storage facilities. A one-dimensional numerical pyrolysis model for double-wall corrugated cardboard was developed using the Thermakin modeling environment to describe the burning rate of corrugated cardboard. The model parameters corresponding to the thermal properties of the corrugated cardboard layers were determined through analysis of data collected in cone calorimeter tests conducted with incident heat fluxes in the range 20-80 kW/m^2. An apparent pyrolysis reaction mechanism and thermodynamic properties for the material were obtained using thermogravimetric analysis (TGA) and differential scanning calorimetry (DSC). The fully-parameterized bench-scale model predicted burning rate profiles that were in agreement with the experimental data for the entire range of incident heat fluxes, with more consistent predictions at higher heat fluxes.

DEVELOPMENT OF A MODEL FOR FLAMING COMBUSTION OF DOUBLE-WALL CORRUGATED CARDBOARD

By

Mark B. McKinnon

Thesis submitted to the Faculty of the Graduate School of the
University of Maryland, College Park in partial fulfillment
of the requirements for the degree of
Master of Science
2012

Advisory Committee:

Assistant Professor Stanislav I. Stoliarov, Chair
Associate Professor Peter B. Sunderland
Associate Professor Arnaud Trouvé

Acknowledgements

I would like to thank everyone that I have met during my tenure at the University of Maryland because the intelligence and passion of these students and faculty served to inspire much of the work completed for this project. These people include all the students in my research group, all the faculty of the Fire Protection engineering department, Dr. Marc Nyden, and the scientists in the Engineering Lab at NIST. I would also like to thank everyone with whom I collaborated at the Cooper Union because those collaborations shaped me as a scientific-minded individual but also taught me the importance and power of cross-discipline collaboration.

I would like to thank my parents for supporting me and motivating me in every possible way for as long as I have been alive. My parents truly inspire me and are, in no small part, the motivation for me to become who I am today. I would also like to thank my siblings. Without the constant sibling rivalry I would have never been motivated to pursue a technical background or graduate studies.

Dr. Artur Witkowski deserves as much recognition for this project as I do. Artur spent countless hours fitting data curves in the initial stages of this model and provided the groundwork for the final model presented in this paper. Without his collaboration on this project, the results would not be as impressive as those presented here.

The person that deserves the most significant acknowledgement is my advisor, Dr. Stanislav Stoliarov. Without his guidance and patience over this project, nothing would have been accomplished. I remember one episode in particular when I was talking to Artur about the model and it appeared that we had reached a dead end. I felt disheartened at the prospect that the work we had completed over several weeks appeared

to be fruitless. Artur mentioned that he had felt this way several times before but after meeting with Dr. Stoliarov and modifying the interpretation of a given experiment or parameter, he always came away from the meeting with a newfound optimism that model was on the right track. Dr. Stoliarov brought unparalleled knowledge and experience to this project and he acted as the driving force behind the successful interpretation of the experimental data.

I would like to thank FM Global for provided the funding for this project. Jing Li and Natallia Safronava conducted milligram-scale tests that provided much of the foundation of the milligram-scale model development.

Table of Contents

List of Figures

List of Tables

1. Introduction

1.1 Background

Warehouse storage presents a potential fire hazard mainly due to the orientation and configuration of the stored commodities. In most storage facilities, commodities are stored closely together in combustible packaging on racks that can range up to 30 m high. A small fire can spread rapidly due to the proximity of combustible goods. The configuration of storage racks can lead to large flame spread velocities causing considerable damage regardless of the presence of sprinklers [1]. The economic impact from warehouse fires is, on average, considerably higher than the economic impact of fires in residential and office buildings because it includes property damage and business interruption costs. It is worthwhile to develop a comprehensive understanding of the initiation and spread of fire in warehouse storage applications to propose new fire safety measures that effectively reduce the societal, economic, and environmental impacts of warehouse fires.

The fire protection community has come to focus on computational modeling more than full-scale testing because of the lower cost of computer modeling. Full scale tests for commodities packaged and stored in warehouse geometries require a facility equipped to handle a large-scale test, the payload and storage structure, and technical experts capable of conducting the test which can all lead to high costs. The cost of large scale tests can be justified by the potential lifesaving data that is collected in the tests, but experimental data generally does not provide accurate extrapolations for large scale tests conducted with different parameters and in different geometries.

Large-scale fire dynamics are complex and changes in the stored commodity, storage density, or orientation and configuration of storage racks could significantly change the data collected in a full-scale test. It is economically advantageous to develop a computational model that can accurately predict the data of interest by solving governing equations as opposed to conducting full-scale tests for every possible combination of test parameters and geometry.

Comprehensive computational fluid dynamics (CFD) models designed to predict the flame spread and heat release rate of a full-scale warehouse fire require different submodels for the gaseous phase and the condensed phase. Multiple submodels are usually required because the spatial and temporal scales required for accurate resolution of the condensed phase processes are different from those required for the processes that occur in the gas phase. Using different solution methods for the gas and condensed phase improves the efficiency and reduces the computational cost of the model.

Understanding the processes involved in the pyrolysis of condensed phase fuels is important to characterizing the ignition and growth stages of fires. A condensed phase pyrolysis submodel that accurately predicts the temperature and mass flux of volatiles evolved from a fuel are essential to produce accurate predictions with CFD codes. A condensed phase pyrolysis submodel produces data concerning the mass flux of volatile species out of the solid as the solid degrades. The mass flux output from the pyrolysis model can be used by the gas-phase submodel to calculate characteristics of the resulting flame. Radiative and convective heat fluxes from the flame can be calculated and the effect of the flame on the materials in the surrounding environment can be determined.

One of the major obstacles to accurate comprehensive models describing the pyrolysis and subsequent oxidation of condensed phase fuels is a lack of measured material-specific properties to be used as model parameters. Though several studies have been completed to determine the flammability and combustibility characteristics of lignocellulosic fuels, there have been few studies directed at corrugated cardboard, which presents a unique host of challenges because of its structure.

The structure of corrugated cardboard presents an interesting physical modeling challenge because of the presence of a complex, non-homogeneous section consisting of the non-planar fluted medium and air. Since the Thermakin program [2] utilized in this investigation produced a one-dimensional model, the curvature of the fluted material cannot be exactly represented and the situation must be simplified. This problem was addressed by defining effective properties that, in some cases, differ from the real physical material properties of the material [3].

1.2 Lignocellulosic Materials

Corrugated cardboard is often used in industry for packaging and storage, where it is used to store myriad materials and products. Corrugated cardboard boxes used to house commodities can be the primary fuel for fires that start in storage areas, so it is important to understand the ignition and heat release characteristics of cardboard. The heat release rate of a combusting fuel can directly contribute to flame spread and fire growth in an enclosure fire. An understanding of the pyrolysis of corrugated cardboard is important in analyzing the development and growth of warehouse fires [3]. It has also been claimed that the subsequent oxidation of corrugated cardboard char could also be an

important contributor to the growth and spread of fire in an area used primarily for storage [4].

Corrugated cardboard is a member of a class of materials mainly composed of cellulose, hemicelluloses, and lignin, generally called lignocellulosic materials. Cellulose, hemicelluloses, and lignin are organic polymers that act as the structural components of the cell wall of plant cells. Cellulose is characterized by long, unbranched chains and a crystalline structure. Hemicellulose refers to any of a group of polymers existing in plant cell walls that are characterized by relatively shorter, branched chains and an amorphous structure.

Combustion of lignocellulosic materials tends to occur in two distinct phases. Flaming combustion is characterized by the presence of a diffusion flame above the surface of the material. It has been noted in the literature that the fuel-rich side of a diffusion flame has a low concentration of oxygen [5]. The model produced in this investigation was constructed under the assumption that reactions between oxygen and the cardboard material did not contribute to the production of volatile species from the condensed phase fuel. The heat generated by the flame increases the temperature of the fuel, which causes pyrolysis of the condensed phase fuel, resulting in the production of combustible gases and a stable, porous, carbon-rich material called char. The combustible gases generated during pyrolysis volatilize and mix with the air to produce a flammable mixture at the surface of the sample. When the flammable mixture is ignited, through autoignition or piloted ignition, a steady flame sheet is generated at the surface of the sample.

Flameless combustion, or smoldering, occurs when the flammable gas concentration above the sample can no longer sustain a flame. After the initial flaming combustion, the remaining char generally continues to pyrolyze while reacting with ambient air. The oxidation of the char produces inorganic residue, commonly referred to as ash, and product gases, typically CO_2 and CO. It had been observed that smoldering combustion has a higher heat of combustion than flaming combustion, but flaming combustion involves larger masses and releases heat at rate about an order of magnitude larger than smoldering combustion.

1.3 Existing Pyrolysis Models for Lignocellulosic Materials

Several pyrolysis models suitable for lignocellulosic materials exist with a wide variety of complex phenomena represented in each. Pyrolysis models can be divided into two groups according to the method used to describe the transformation of unreacted fuel to volatile species and char. Thermal models rely on energy conservation equations to determine the burning rate. Comprehensive models generally calculate the rate of the pyrolysis process with energy and mass conservation equations in combination with a chemical kinetic reaction mechanism.

Thermal models calculate the production rate of volatile species through an energy balance. These models are constructed under the assumption that pyrolysis occurs at a single temperature, effectively decoupling the chemical kinetics from other processes occurring during pyrolysis. This assumption is mathematically equivalent to the assumption that the chemical reactions occur much faster than the heat transfer through the material [6]. Comprehensive models were developed because the assumption that chemical reactions occur much faster than diffusion processes is not always valid. The

Thermakin modeling environment can be classified as a comprehensive model that incorporates chemical kinetics with energy and mass conservation equations. The review article written by Moghtaderi provides a more detailed discussion of thermal and comprehensive pyrolysis models [6].

Comprehensive models can be further divided based on the reaction scheme invoked to describe the transformation of solid virgin fuel to the products of pyrolysis. Chemical kinetics is used to describe the rates of reactions that occur during a process as a function of temperature and species concentration. Reaction schemes describe the various chemical pathways for the reactions that cause the reactants to form reaction products.

There are three general classes of reaction schemes in the literature. One-step global reaction schemes depend on a single reaction to describe the total mass evolution for the pyrolysis process. One-step, multi-reaction schemes use several parallel, competitive reactions that consist of a single step from the virgin material to each respective pyrolysis product. Multi-step semi-global schemes represent the most realistic reaction mechanisms and are characterized by primary reactions as well as secondary reactions that describe the further degradation of initial pyrolysis products. The determination of the reaction scheme that best characterizes the chemical processes can potentially have a considerable effect on the results of the pyrolysis model and the large-scale CFD fire model which uses the pyrolysis model [6].

The pyrolysis kinetics of cellulose and lignocellulosic materials have been studied extensively. Most of the studies focused on cellulose were conducted to improve the

understanding and efficiency of using biomass as an alternative fuel source. Studies focused on developing kinetic models for biomass pyrolysis produce reaction mechanisms that are inherently different than those focused on developing a pyrolysis model for a fire scenario because reaction kinetics depend heavily on test conditions and specifically on the heating rate [7]. Biomass fuel studies usually involve conducting experiments with isothermal heating with large sample masses whereas fire studies generally employ linear heating of relatively small samples. Few studies have been conducted on determining the pyrolysis kinetics of cardboard [8] [9]. Several of the most widely used multi-reaction semi-global schemes were considered in this investigation with more extensive discussions available in several review papers [10] [11] [12].

Broido and his colleagues [13][14] are credited with developing the first kinetic model with predictive capabilities that attempted to account for the complexities of cellulose pyrolysis in a series of papers published from 1971-1976. The kinetic scheme that they developed featured an initial reaction producing active cellulose from cellulose, followed by two competitive reaction pathways. One reaction pathway produced solid intermediates and gaseous volatiles in consecutive reactions and the other reaction pathway produced volatile tars. The kinetic scheme was developed based on isothermal mass loss measurements for relatively large samples of filter paper (on the order of 100 mg) conducted in a furnace with an inert atmosphere. A schematic representation of the general reaction scheme suggested by Broido is provided in Figure 1-1.

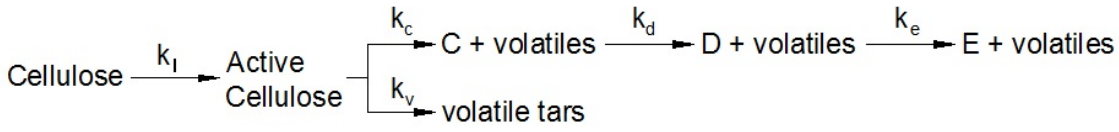

Figure 1-1: Broido Reaction Scheme

Bradbury, Sakai, and Shafizadeh simplified the Broido reaction scheme by reducing the number of intermediate species-producing reactions. The investigators developed the reaction scheme based on isothermal tests with shredded filter paper samples with masses on the order of 250 mg. The simplified model is generally referenced as the Broido-Shafizadeh model and is widely accepted today along with the kinetic parameters determined by the investigators [15]. The Broido-Shafizadeh reaction scheme is provided in Figure 1-2.

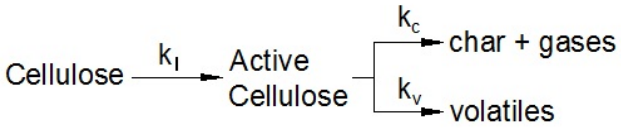

Figure 1-2: Broido-Shafizadeh Reaction Scheme for Cellulose

Though the Broido-Shafizadeh reaction model is well accepted, it has met criticism because several researchers have been unable to replicate the experimental data used to develop the kinetics model. Varhegyi, et al. conducted linear heating thermogravimetric studies on pure cellulose with samples ranging from 0.5-3 mg as well as isothermal tests in the same temperature ranges as the previous investigators. Varhegyi, et al. proposed the initiation reaction to form active cellulose from the initial cellulose was unnecessary because the reaction occurred either infinitely fast or did not occur at all above a certain temperature and did not affect the agreement between the model prediction and experimental data. It was found that a three reaction model based, in part, on the Broido-Shafizadeh scheme could accurately predict the results of the

thermogravimetric study [16]. The reaction scheme proposed by Varhegyi, et al. is provided in Figure 1-3.

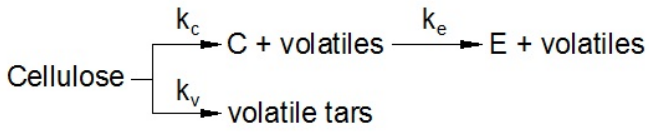

Figure 1-3: Reaction Scheme Proposed by Varhegyi, et al.

A reaction scheme for the pyrolysis and subsequent oxidation of wood was developed in a study by Shafizadeh and Chin [17]. The scheme featured three parallel primary reactions to produce gaseous volatiles, condensed phase volatiles (tars), and char. The scheme also featured two secondary reactions to characterize the further degradation of tars to solid char and gaseous volatiles. These secondary reactions are generally called "cracking" of the tar in the literature. The scheme was proposed based on data collected in a thermal evolution analysis conducted on cottonwood and Douglas fir needles. A schematic representation for the pyrolysis portion of the Shafizadeh reaction scheme is provided in Figure 1-4. Thurner, et al. used the reaction scheme proposed by Shafizadeh to model the pyrolysis of wood in an isothermal environment with good agreement between the model prediction and the mass fraction data for each component collected during experiments [18].

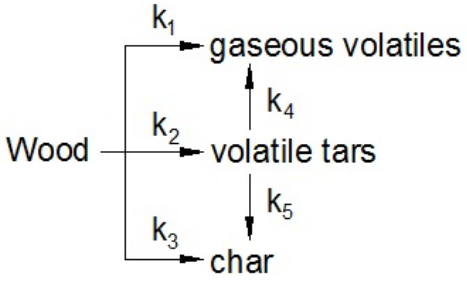

Figure 1-4: Reaction Scheme Proposed by Shafizadeh for the Pyrolysis of Wood

The four multi-step reaction schemes discussed here were developed in attempts by the investigators to describe the mass loss rate kinetics of cellulose and lignocellulosic materials with some insight to the chemical pseudo-species involved in the pyrolysis process. All of these schemes involve parallel reactions and the inclusion of high molecular weight volatiles termed tars as a pseudo-species in the reaction scheme. These reaction schemes have been developed for specific solid fuels subjected to specific heating environments. The literature can inform the production of a reaction mechanism in the current study but it is likely that none of these reaction schemes can accurately describe the pyrolysis of corrugated cardboard. The literature also provides a comparison for the kinetic parameters determined for the pyrolysis process studied in the current investigation.

Several investigators have employed optimization software or graphical methods to determine the kinetic parameters that provide the best fit for experimental data [8] [9][19]. In the studies that used optimization techniques, the reaction scheme was generally formulated based on schemes available in the literature or on qualitative analysis of the data. A variety of optimization algorithms have been used with varying degrees of success, though in one study several of the optimized parameters were outside the range of physical possibility [8]. Optimization codes can be useful for determining the kinetic parameters of a chemical reaction but a physical understanding of the affect of varying the kinetic parameters remains the most important requirement for fitting data. Some investigators have found success in describing the reaction kinetics for lignocellulosic materials with a single reaction [20] and two successive reactions [8] [9] [21]. Some investigators have used thermogravimetric data to attempt to determine the

composition of lignocellulosic materials to inform better representative models [22] [7]. The reaction scheme adopted for each study was able to adequately fit the data collected in that specific study. There is no standard method for conducting thermogravimetric analysis (TGA) tests or analyzing the results, so the variety of reaction schemes and kinetic parameters available in the literature can only offer a rough starting point for the reaction scheme specific to this study.

The treatment of the kinetic parameters has been shown to be important in the construction of a pyrolysis model to which much research has been dedicated [23]. Equally important is the treatment of the physical processes occurring in the condensed phase during pyrolysis. Investigators tend to disagree on the assumptions required to accurately describe the pyrolysis process for lignocellulosic fuels, but all investigators agree that the pyrolysis of charring materials is a complex process that incorporates a variety of physical and chemical phenomena. These physical and chemical processes are governed by the conservation equations, which require material properties for all the components included in the model. Salvador, et al. developed a one-dimensional model to describe the combustion of a porous homogeneous medium composed of cardboard and polyethylene [24]. To facilitate the construction of the model, the investigators made several assumptions. The main assumptions built in to the model were that local thermal and chemical equilibrium was achieved and oxidation did not occur in the condensed phase material. The investigators also chose to neglect the heat flux contribution from the flame. The target data identified in this study was the mass loss rate profile collected in cone calorimeter tests. The model was validated by comparing the temperature profiles collected during cone calorimeter tests.

Studies have been conducted on the burning rate and flame spread characteristics of corrugated cardboard in a vertical orientation common in warehouse and industrial storage settings [1] [25]. These studies provide confirmation for some of the properties and parameters that define the corrugated cardboard in the bench-scale model. Upward flame spread is inherently different from one-dimensional pyrolysis because it is a two-dimensional process that introduces buoyancy-driven flow, flame turbulence, and possibly significant oxidation reactions to the pyrolysis model. Though the pyrolysis of solid fuel is inherently different between a horizontal, one-dimensional orientation and upward flame spread, the model generated in this investigation describes a subset of physical phenomena required to predict upward flame spread.

The two apparatuses utilized in this investigation to collect experimental data were a cone calorimeter (Govmark CC-1) and a thermal analyzer capable of simultaneous thermogravimetry and scanning differential calorimetry (Netzsch STA 449 F3). The experiments with the cone calorimeter were intended to simulate flaming pyrolysis of the cardboard sample surface in a typical fire scenario. The simultaneous thermal analyzer allowed data to be collected regarding the reaction kinetics of the cardboard on a milligram scale in a well-defined atmosphere at a dynamic, well-defined temperature.

Thermogravimetric data have been used in past investigations to determine an effective reaction mechanism that describes the thermal degradation process of lignocellulosic materials specific to the individual study. Cone calorimeter tests have also been conducted in past investigations to verify the results of combustion models. [26] Both of these techniques have been employed during this investigation.

1.4 Thermakin Background

The Thermakin modeling environment [2] was used in this investigation to determine model parameters from experimental data and was ultimately used to construct a one-dimensional model to predict the results of cone calorimeter tests at heat fluxes ranging from 20-80 kW/m^2. Thermakin solves the non-steady energy and mass conservation equations accounting for chemical reactions described by a reaction mechanism. The sample material is defined in Thermakin geometrically as a series of layers with specified thicknesses and chemically as material components defined by specific physical and chemical properties. This investigation was conducted using the one-dimensional Thermakin program. The Thermakin modeling environment has been validated with investigations on charring and non-charring polymers [27][28][29].

Chemical and physical properties are defined for each component material in the Thermakin framework. These properties include the density, heat capacity, thermal conductivity, mass transport coefficient, emissivity, and absorption coefficient. The emissivity and absorption coefficient are assumed constant for each component throughout the simulation. The other properties are defined as functions of temperature with the following equation where the property is generically denoted p:

$$p(T) = p_0 + p_1 T + p_n T^n$$

Reactions are defined in Thermakin as occurring between one or two components to produce between zero and two components. The energy evolved from each reaction can be defined as a temperature-dependent quantity in the same manner as the chemical and physical properties. The reactions defined in the reaction mechanism are governed by Arrhenius reaction rates defined in the following equation:

$$r = A \exp\left(\frac{-E_a}{RT}\right)\left[\frac{m_1}{V}\right]\left[\frac{m_2}{V}\right]$$

The pre-exponential factor, A, and activation energy, E_a, are the kinetic parameters specified in the Thermakin program to define the reaction rate as a function of temperature and the concentration of the components denoted in the equation by $[m_1/V]$ and $[m_2/V]$.

Mass and energy conservation equations are solved by Thermakin assuming the heat exchange between the gases and the solid material of the sample is instantaneous. It is also assumed that the momentum from the gases transported in the solid material is negligible. The conservation of mass equations for each component include contributions from reactions as well as mass transport. Mass transport is assumed to be driven by concentration gradients. The conservation of energy equation is solved accounting for heat generation from reactions, conduction from adjacent elements, and convection from adjacent elements.

Boundary conditions are defined at the top and bottom surfaces of the computational domain in Thermakin. The boundaries can be defined with the capability of mass transport from the material to the surroundings. The mass transport can be specified with a linear function generally used to remove pyrolyzate gases from the solid sample at the top surface. An exponential function can be applied as the boundary condition to simulate surface reactions.

The heat transfer boundary condition must be specified for convective and radiative heat flow. The atmospheric temperature can be defined as a linear function of

time to modify the convective heat flow boundary condition during simulation. The radiative heat flow boundary condition can be specified with up to two linear heat flux phases and can be specified as periodic to repeat the heat flux program. A critical mass flux for ignition can be defined to simulate flaming combustion of the solid sample. The critical mass flux causes the convective and radiative boundary condition to change to account for the excess heat flux caused by the presence of a flame on the material surface [8].

The one-dimensional Thermakin program divides the computational domain into rectangular finite elements and calculates the temperature and concentration of each component in all the elements at every time step. The conservation equations are solved with a Crank-Nicolson scheme characterized by the following equation:

$$y_i^{t+\Delta t} = y_i^t + \frac{\left[F_i\left(y_i^t, y_j^t, y_k^t, \ldots\right) + F_i\left(y_i^{t+\Delta t}, y_j^{t+\Delta t}, y_k^{t+\Delta t}, \ldots\right)\right]}{2}\Delta t$$

Where the variable y_i^t is the mass of a component in the element being considered or the temperature of the element being considered at time t and $y_i^{t+\Delta t}$ is the same property at time t + Δt. F_i in the above equation is the rate of change of the property denoted by i. The rates of change of the properties are functions of the component masses and element temperatures defined by the conservation equations provided by Stoliarov and Lyon [2]. The resulting equations for each element and each component are linearized and solved at each time step.

The models constructed with the Thermakin program can be divided in two categories based on the operating assumptions for each model. The models used to

simulate the milligram-scale tests conducted in the STA apparatus were constructed assuming the sample was thermally thin. Under this assumption, the material heated instantaneously and evenly via convection from the atmosphere. The convection coefficient was sufficiently high to induce instantaneous heating. The model was defined such that heat was transferred to the sample through pure convection without a contribution from radiation. The models constructed in the thermally thin mode followed the same temperature program as the temperature program for tests conducted with the STA apparatus.

The models constructed to simulate bench-scale tests required few assumptions a priori about the heat and mass transfer characteristics of the sample and test procedure. Heat was transferred to the material with a radiation boundary condition set to the external heat flux measured in the physical tests. As the sample material was heated, convective cooling to the atmosphere occurred with the convection coefficient set to 10 W/m^2K and a constant ambient temperature of 300 K was assumed [30].

1.5 Objectives

This paper presents a method for the development of a 1-D thermal-kinetic model for corrugated cardboard pyrolysis. The first objective of this investigation was to determine the parameters required to describe the structure and thermal transport characteristics of the material. Most of the thermal transport properties for the material were measured directly or indirectly, through analysis of experimental data.

The second objective of this investigation was to develop a model using the parameters determined through experimental testing. A bench-scale model was constructed to predict the results of a cone calorimeter test with external heat flux ranging

from 20-80 kW/m^2. Similar investigations involving charring and non-charring polymers have been conducted recently with promising results [28][31][27].

The final objective of this investigation was to compare the mass loss rate curves predicted by the fully parameterized model to the mass loss rate data collected in cone calorimeter tests. In comparison of the mass loss rate curves, possible sources of error were identified and designated as objectives in the continuation of this research.

The thermal-kinetic model of burning produced in this investigation could be coupled with a computational fluid dynamics code as a boundary condition to describe the rate of production of volatile gases from corrugated cardboard as a function of the local incident heat flux.

2. Experimental

2.1 Sample Material

The corrugated samples specific to this investigation complicate modeling because the unequal thickness of the two fluted sections. The samples specific to this study were double wall cardboard designated as 69-23B-69-23C-69. The numbers in the cardboard designation refer to the areal density of the layer in [lb/1000ft^2]. The letters signify the flute designation. B-flute is characterized by 47 ± 3 flutes per foot (154 ± 10 flutes per m) and a layer height of approximately 3/32 inches (2.38 mm). C-flute is characterized by 39 ± 3 flutes per foot (128 ± 10 flutes per m) and a layer height of 9/64 inches (3.57 mm) [32].

The thickness of the linerboards was measured as 0.64 ± 0.03 mm. The density of the linerboards was calculated as approximately 520 kg/m^3. The thickness of the C-fluted medium section was measured as 3.4 mm and the thickness of the B-fluted medium section was measured as 2.1 mm though there were variations in these dimensions. The variations in these data were attributed to deformation of the samples during shipping and handling. The density of the thick fluted section was measured as 49 kg/m^3 and the density of the thin fluted section was measured as 74 kg/m^3. Due to the scatter in the dimension measurements of the fluted section thickness, the uncertainty of these densities was hard to determine.

A schematic representation of the corrugated cardboard material is provided in Figure 2-1 and a picture of the material is provided in Figure 2-2. The thickness of the entire composite material was measured as 7.4 mm with a density of approximately 174 kg/m^3.

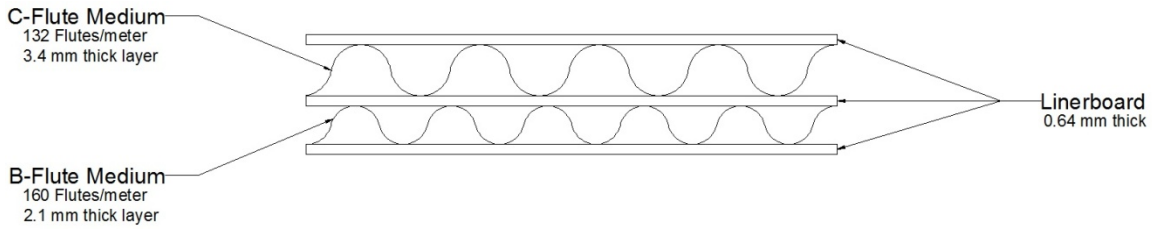

Figure 2-1: Structure of a Corrugated Cardboard Sample

Figure 2-2: Picture of a Corrugated Cardboard Sample

2.2 Bench-scale experiments

The bench-scale testing was conducted with a type of oxygen consumption calorimeter known as a cone calorimeter [33]. The cone calorimeter is designed with a cone-shaped coil of wire that heats via resistance when a current is passed through the wire. The heat flux from the heater to the sample depends on the temperature of the heater coil. The temperature of the heater depends on the voltage supplied to the resistive coil. The temperature of the heater, and effectively the heat flux from the heater, are set with a control system that depends on feedback from a Schmidt-Boelter heat flux gauge mounted 25 mm from the heater surface.

The heater is oriented such that an approximately uniform heat flux falls incident on the surface of the sample. The sample is usually placed on a holder that rests atop a balance to track the mass of the sample over the course of the test. A ventilation system is included in the apparatus with a well-defined flow rate of 0.024 m^3/s. A pump is connected to the ventilation system to sample the gases in the exhaust and feed the sampled gas to a gas analyzer.

The oxygen consumption calorimeter is called such because ventilation gas sampling is conducted primarily to detect the concentration (volume fraction) of oxygen in the exhaust gas. By comparing the concentration of oxygen in the exhaust gases during combustion of the sample to the concentration of oxygen in the exhaust gases during a baseline measurement when there is no sample present, the mass of oxygen consumed in the combustion process can be determined. It has been observed in investigations that the mass of oxygen consumed in the combustion process is directly proportional to the heat release rate during that process [34] [35].

The cone calorimeter tests were conducted following the procedure outlined in the standard. The tests were used in this investigation to collect data for the corrugated cardboard samples on the bench scale in an orientation that approximated one-dimensional behavior. The gas analyzer and balance were automatically calibrated according to [33]. The relationship between the oxygen consumed and the heat release rate is defined as the C-factor. The C-factor was determined during the cone calorimeter calibration procedure by measuring the oxygen consumed by a 5 kW methane flame. The equation that defines the C-factor [33] is provided below.

$$C = \frac{5.0}{1.10(12.54 \times 10^3)} \sqrt{\frac{T_c}{\Delta P}} \frac{1.105 - 1.5X_{O_2}}{{X_{O_2}}^0 - X_{O_2}}$$

Heat release rates and mass loss rates from flaming and subsequent smoldering of the samples were collected with the standard cone calorimeter test procedure. The times to important benchmarks during the tests were measured with a timer during observation of the cone calorimeter tests. The standard test procedure was modified for cone

calorimeter tests conducted to collect temperature distribution data and flame heat flux data

Though there can be some variation in the procedure of cone calorimeter tests, the tests completed in this study employed a spark igniter approximately 12 mm from the surface of the sample unless otherwise noted. The energy absorbed by the sample from the heater led to thermal degradation and the evolution of volatile gaseous species from the sample. The concentration of volatile species above the sample reached the lower flammability limit for piloted ignition and ignition occurred, resulting in a sustained flame above the surface of the sample that persisted until the mass flux of volatile species from the sample decreased past the lower flammability limit.

It was hypothesized that the heat flux profile from a circular heater to a square-shaped sample could cause uncertainties in the data collected from cone tests and a deviation from the assumptions of the model because of a non-uniform heat flux distribution over the entire surface of the sample. Initial tests were conducted with a heat flux gauge to determine the spatial variability of the heat flux across the surface of the sample. The heat flux was measured at every point in a square grid of 25 equally-spaced points at distance of 25 mm from the heater. The heat flux distribution data collected in these initial tests is provided in Figure 2-3.

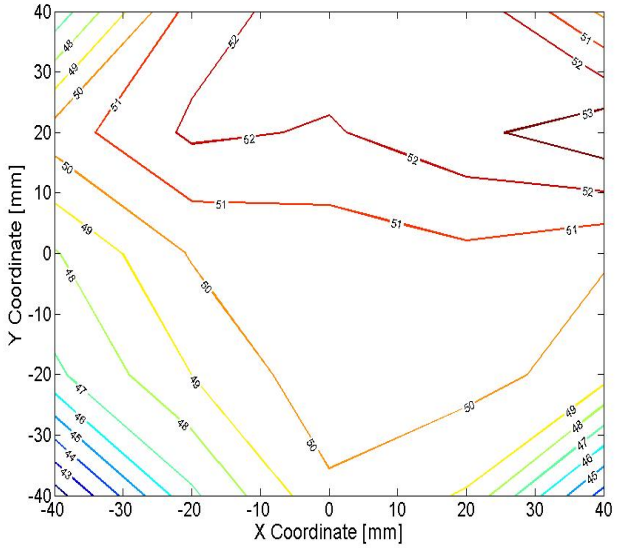

Figure 2-3: Spatial Heat Flux Distribution with the Sample Surface 25 mm from the Heater at a Heat Flux Set Point of 50 kW/m^2

The uniformity metric for the heat flux profile was defined as the mean of the heat flux at each point, normalized by the heat flux set point. The uniformity of the heat flux distribution for the square profile at a heat flux set point of 50 kW/m^2 is 0.992. It is evident from the figure that cone uniformity of the cone calorimeter diminishes considerably at the corners of the sample. The uniformity of a square sample with the corners removed 20 mm from each edge was calculated as 0.9998. Based on the spatial distribution of heat flux and limitations of manufacturing capabilities, it was determined that an octagonal shaped sample derived from a square with the corners removed 20 mm from each edge represented the best compromise.

Several cone calorimeter tests were completed with corrugated cardboard exposed to external heat fluxes of 20, 40, 60 and 80 kW/m^2. The cardboard samples were allowed to dry in a desiccator in the presence of Drierite for a minimum of 48 hours before testing to obtain measurements with little contribution from moisture. The samples were wrapped in heavy gauge aluminum foil such that one face of the sample could accept a

radiant heat flux. The sample was placed on top of 30 mm of Kaowool PM insulation and positioned 25 mm from the cone heater surface.

It was observed during preliminary tests that layers of the corrugated cardboard tended to peel away from the sample as the glue binding the layers degraded at high temperatures. Exfoliation of layers resulted in unreliable and unacceptable mass loss rate and heat release rate data. Several solutions were considered to eliminate exfoliation or minimize its effect during testing, but it was determined that many of the solutions introduced an unacceptable level of uncertainty to the tests. It was decided that the method of preventing exfoliation that introduced the smallest thermal mass to the system and obscured the sample surface least would also introduce the smallest amount of uncertainty and error.

The solution that was accepted consisted of the sample held in place with four 1.7 mm diameter steel wires. A plan view of the sample is provided in Figure 2-4 and a section view of the cone heater and sample setup is shown in Figure 2-5.

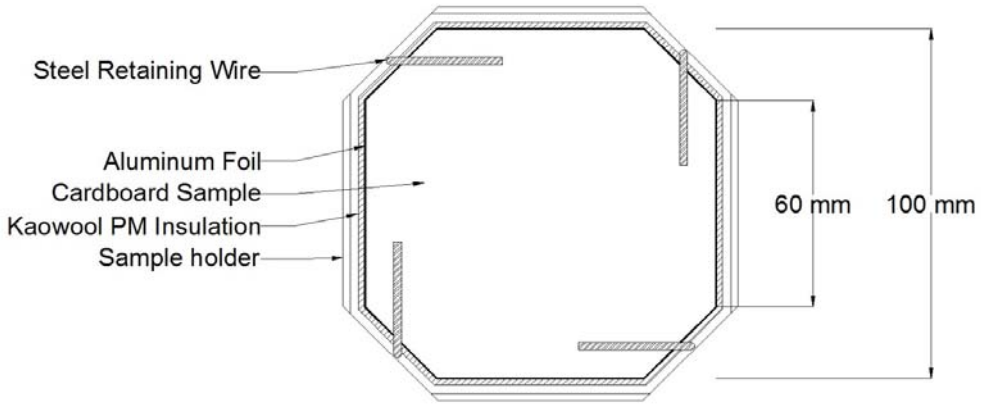

Figure 2-4: Sample Holder Schematic

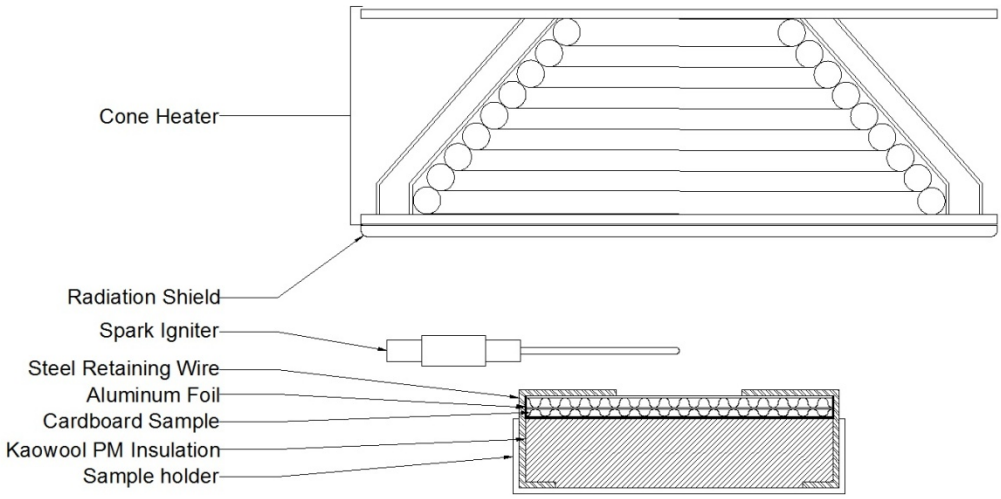

Figure 2-5: Schematic of Cone Calorimeter Experimental Setup

The cardboard samples, as depicted in Figure 2-1, had two different thicknesses of the fluted medium layers. It was determined that the samples must be tested in the two orientations with each fluted section facing the heater to compare the data collected between the two orientations and the repeatability of the data collected for each orientation. Tests were also completed with the edges of the cardboard sample sealed with aluminum tape to test whether more consistent results could be obtained by preventing possible lateral venting of volatiles. Tests conducted in the fire propagation apparatus at FM Global used the same designation of corrugated cardboard with the edges sealed with aluminum tape [31].

The results of the tests with the C-flute layer facing the heater were considered repeatable with an average variation of less than 5% of the instantaneous mean in the flaming portion. Tests were also completed to verify the repeatability of testing either side of the sample based on the test orientation defined by FM Global [3]. The heat release rate data collected with the C-flute layer facing the heater and the B-flute layer

facing the heater are shown in Figure 2-6. The data from the tests is included with the instantaneous average curve. A comparison of these tests indicates a considerable impact of the sample orientation on the heat release rate profile.

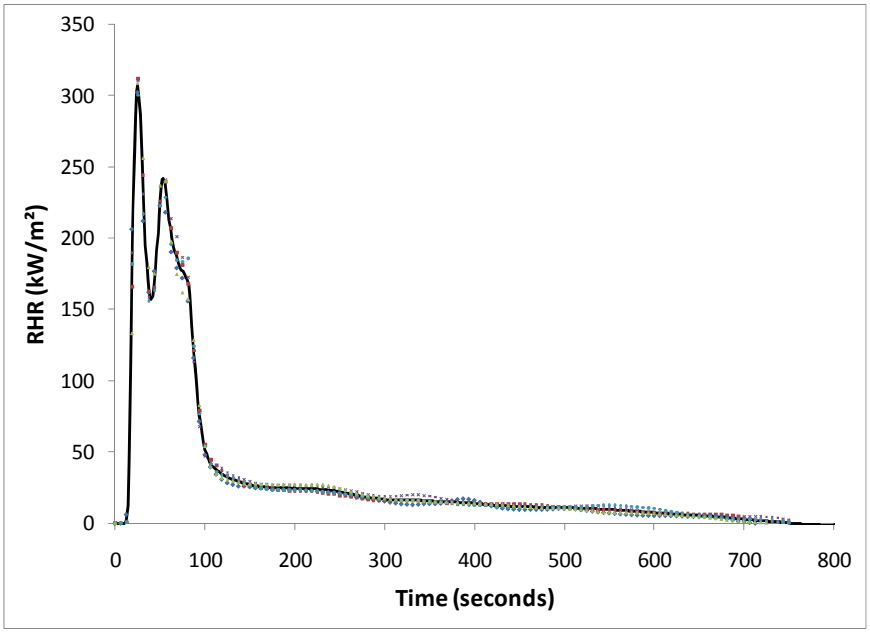

(a)

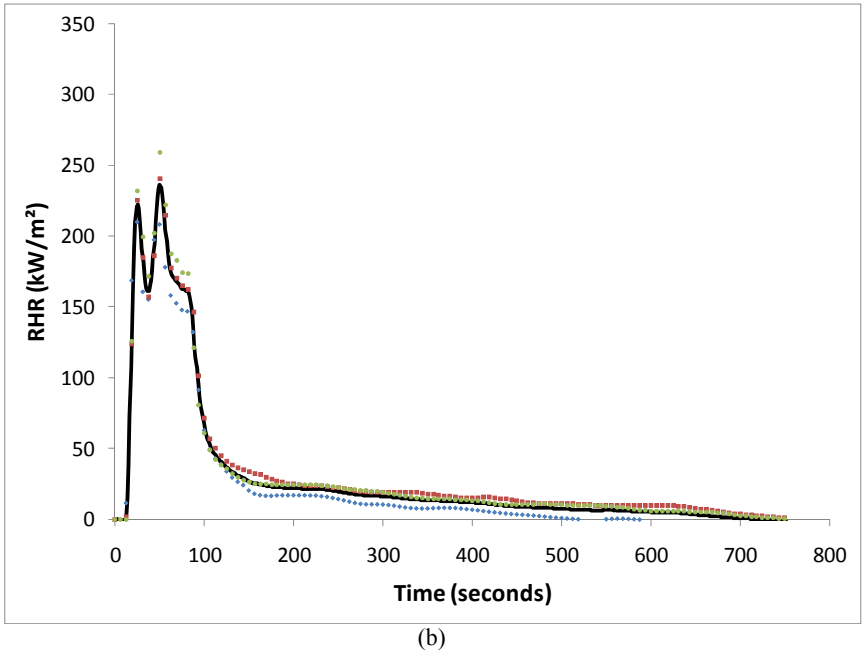

(b)

Figure 2-6: Rate of Heat Release Data for 40 kW/m^2 Oriented with: (a) C-Flute Layer Facing the Heater (b) B-Flute Layer Facing the Heater

The rates of heat release for the tests completed with the edges sealed are provided in Figure 2-7.

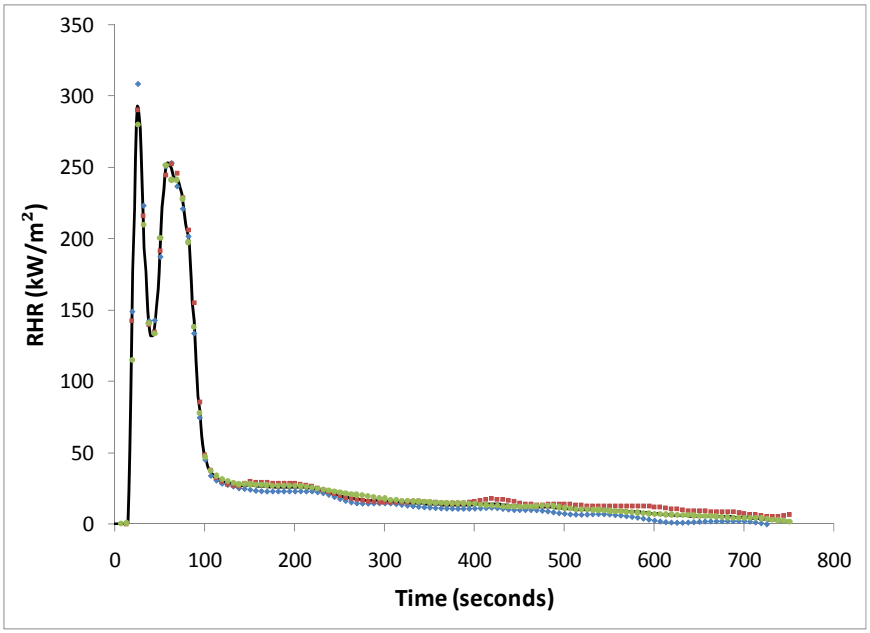

(a)

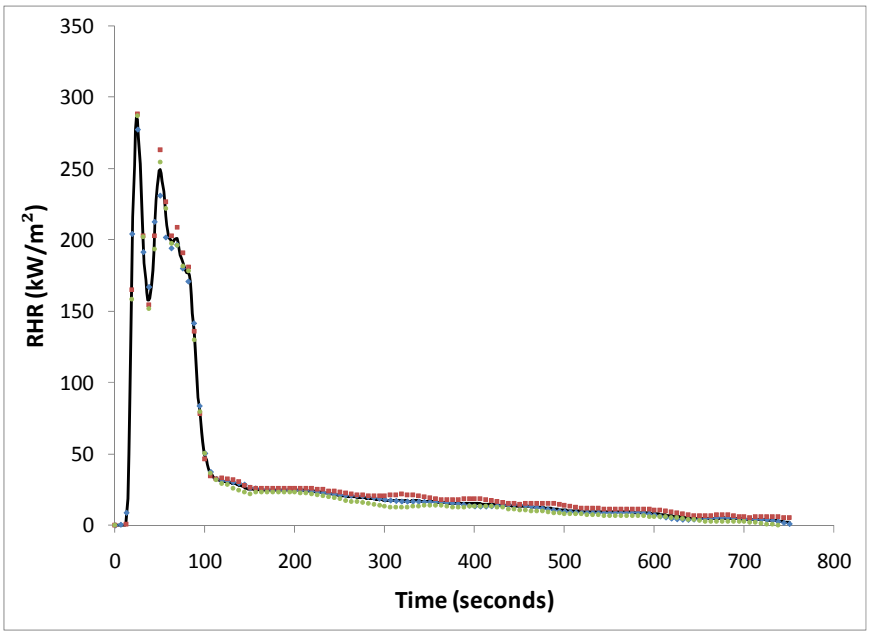

(b)

Figure 2-7: Rate of Heat Release Data for 40 kW/m^2 with: (a) C-Flute Layer Facing the Heater with Edges Sealed (b) B-Flute Layer Facing the Heater with Edges Sealed

The resulting data appeared to be approximately as repeatable as the results obtained when the edges of the samples were not sealed. The results obtained by testing the cardboard in the calorimeter with the B-flute layer facing the heater and the edges sealed, the sample orientation used by the FM Global researchers, showed good agreement with the results of the tests completed with the edges unsealed and the C- flute layer facing the heater.

The mean curves calculated from the data collected in each of the four configurations described previously were plotted together to provide a comparison between all orientations. The plot of all these data is provided in Figure 2-8. Initially all tests were conducted in the orientation with the C-flute medium facing the heater without the edges sealed with tape. A homogeneous model was proposed when the cone calorimeter tests were conducted. The homogeneous model did not depend on the orientation of the sample, though a non-homogeneous model did depend on the orientation of the sample. The orientations were tested a posteriori to determine the consistency of orientation used in this investigation compared to the data collected in related investigations.

The tests completed with the sample oriented such that the C-flute medium section was facing the heater without the edges sealed appeared to agree closely with the data collected when the sample was oriented such that the thinner fluted section faced the heater with the edges sealed. Therefore, the data collected in the former configuration was considered consistent with the related investigations and appropriate for the current investigation and model.

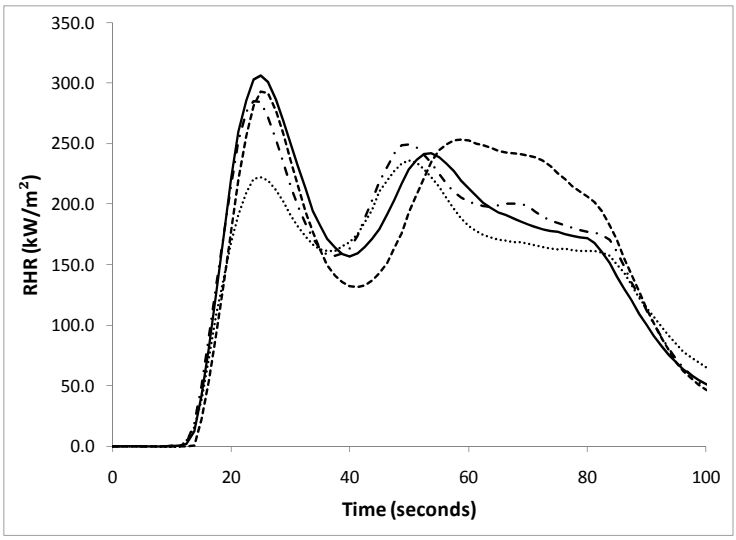

Figure 2-8: Average Rate of Heat Release Curves for the Four Orientations Examined - (-) C-Flute Layer Facing the Heater (--) C-Flute Layer Facing Heater with Edges Sealed (…) B-Flute Layer Facing the Heater (._.) B-Flute Layer Facing the Heater with Edges Sealed

Five cone calorimeter tests were completed at each heat flux of 20, 40, 60, and 80 kW/m^2. The heat flux was set automatically with a control system based on feedback from a water-cooled Schmidt-Boelter heat flux gauge under the heater. The data for 20, 40, and 60 kW/m^2 were collected by the calorimeter at a rate of 0.8 Hz. The data collected for 80 kW/m^2 were collected by the calorimeter at a rate of 1 Hz. The discrepancy between the sampling rates in these tests was due to an update of the cone calorimeter software between tests.

Cone calorimeter tests were conducted with incident heat fluxes of 20 kW/m^2 and 60 kW/m^2 with thermocouples inserted in each of the three linerboard sections. The thermocouples that were inserted in the linerboards were 0.25 mm diameter, grounded, type K thermocouples with Inconel 600 sheaths. These thermocouples were chosen because they were the smallest diameter sheathed thermocouple available. The diameter of the thermocouples was 39% of the thickness of the linerboards in which they were inserted. The small diameter ensured a fast response and a small contribution of thermal

mass to the system. The approximate positions of the thermocouples are depicted in Figure 2-9 with the distances measured from the sample surface to the middle of the thermocouple. The temperature data was collected with the thermocouples at a rate of 1 Hz. Mass loss rate data was not collected during the tests with thermocouples inserted in the samples because preliminary tests concluded the presence of the thermocouples and the data acquisition components yielded unreliable mass loss data.

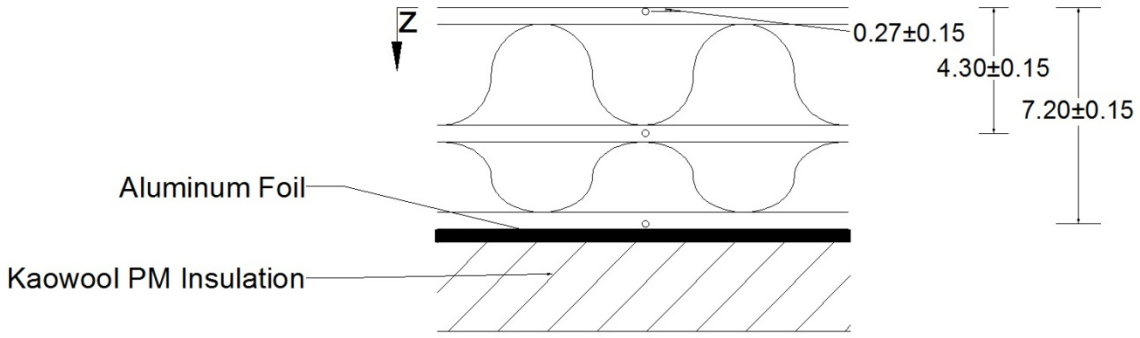

Figure 2-9: Approximate Locations of Thermocouples Inserted in Linerboards with all Dimensions Provided in Millimeters

Several tests were conducted with the surface of the cardboard sample covered with black paint that had an emissivity of 0.95 and thermocouples inserted into the linerboards. These tests were conducted with an incident heat flux of 20 kW/m^2 and the spark igniter was not used to ignite the sample. The igniter was not inserted over the sample in an effort to increase the amount of time the thermocouples collected meaningful data before the possibility that structural changes from the presence of the flame caused the thermocouples to become displaced. Introducing the flame to this test caused a change that was hard to account for in the definition of the heat flux boundary condition at the upper surface.

These tests were intended to determine the thermal conductivity of the virgin cardboard material while the surface emissivity was well-defined. These tests were also

intended to determine the emissivity of the unaltered virgin cardboard material by providing a comparison to the temperature data collected from tests on unaltered cardboard samples.

A 6.35-mm diameter water-cooled Schmidt-Boelter heat flux gauge was embedded in the corrugated cardboard for several cone calorimeter tests. The heat flux gauge was oriented such that the surface of the gauge was flush with the sample surface. Tests were conducted with incident heat fluxes of 20 and 60 kW/m^2 and the heat flux gauge in two locations. The heat flux gauge was positioned in the center of the sample and in a location close to the edge of the sample. The two separate locations were used to provide insight about the spatial distribution of the heat flux fed back to the sample surface.

The intended purpose of the tests conducted with the heat flux gauges was to measure the heat flux generated by the flame that was incident on the cardboard surface. The magnitude of the flame heat flux is a parameter required for bench-scale modeling of flaming combustion. The heat flux data was collected at a rate of 2 Hz. Mass loss rate and heat release rate data was not collected during the tests with the heat flux gauge embedded in the samples because preliminary tests concluded the presence of the heat flux gauge yielded unreliable mass loss rate data.

A single linerboard layer was inserted between the heater and the heat flux gauge to measure the radioactive heat flux that was transmitted through the linerboard to the heat flux gauge. The procedure was repeated with a 6.35 mm-thick piece of Kaowool-PM insulation to provide a comparison to the cardboard material. These tests were

conducted to determine the absorption coefficient of the linerboard material relative to the Kaowool insulation.

2.3 Milligram-Scale Experiments

Milligram-scale experiments were conducted to analyze the reaction mechanics and thermodynamics of the corrugated cardboard material. Thermogravimetric analyses were completed with various heating programs in an inert atmosphere to determine the chemical kinetics of the pyrolysis reactions that occur at the elevated temperatures experienced during flaming combustion. The heat of the pyrolysis reaction and the heat capacities of the virgin cardboard material and char were determined from data collected in differential scanning calorimetry tests.

2.3.1 Thermogravimetric Analysis

Thermogravimetric analysis (TGA) is a test method that measures the instantaneous mass and mass loss rate of the sample as a function of the temperature of the sample. The mass and mass loss rate data are of interest to this investigation because global reaction kinetics can be determined from these data. The global reaction kinetics describe the total mass loss rate of the sample as a function of temperature.

A file was used to grind the edge of a cardboard sample to generate powder, and the powder was allowed to dry in a desiccator in the presence of Drierite for a minimum of 48 hours. The corrugated cardboard powder was compacted in an alumina (Al_2O_3) crucible such that approximately half the crucible was filled. The sample masses prepared in this manner were in the range of 6-10 mg. The density of the sample depended on the extent to which the sample was compacted, and the effect of the density was investigated by varying the extent to which the sample was compacted for several

tests. Initial tests used samples that ranged in mass up to 25 mg. Analysis of the data concluded the sample density did not significantly affect the results but large sample masses produced inconsistent data.

The temperature program for the TGA tests consisted of a conditioning period when the temperature of the sample was held constant at 40°C for 20 minutes, followed by heating to 840°C at a rate of 10°C/min. This 20 minute conditioning period at 40°C was included to ensure the sample was purged of oxygen before data was collected. Three additional TGA tests were conducted with the same temperature program with a heating rate of 5 K/min to investigate the effect of the lower heating rate on the mass loss rate profile and reaction mechanism. The nitrogen flow rate for all TGA tests conducted in inert atmosphere was 50 mL/min which was toward the lower limit of the range recommended by the manufacturer.

The heating rate of 10 K/min was chosen because it is the most prevalent heating rate used in the literature [8][9][12][16][28][27]. This heating rate is low enough that the sample does not experience significant temperature or mass gradients, making the effects of mass and heat transfer negligible. A heating rate of 10 K/min is also high enough that the some material in the sample could possibly experience this heating rate in the bench-scale cone calorimeter tests. The peak heating rate measured in cone calorimeter tests was approximately 800 K/min, though a more representative average heating rate for the cone calorimeter tests was on the order of 30 K/min with considerable spatial temperature gradients.

Each layer of the composite corrugated cardboard material was prepared as a powder in the same manner as the entire composite material. TGA tests were conducted on the powder generated from each of these layers to determine if the composition and, in effect, the chemical kinetics and thermodynamics of each layer was different. The procedure for the TGA tests was the same as the procedure used to test the powder generated from the entire composite material with a heating rate of 10°C/min.

2.3.2 Differential Scanning Calorimetry

Differential scanning calorimetry (DSC) is a testing method that measures the heat flow to the sample as a function of the sample temperature. The method of DSC used in this investigation was heat flux DSC. Heat flux DSC measures the temperature difference between the sample and a reference crucible that is generally left empty. The temperature of each crucible is measured by a thermocouple in contact with the bottom of the crucible. The temperature difference between the sample and the reference is related to the heat flow to the sample through a calibration curve determined based on the melting points of inorganic salts.

The apparatus constantly measures the temperature of the sample and reference crucibles, and the heat flow to the sample can be calculated from this temperature difference. DSC derives its name from calculating the differential energy flowing to the sample as the atmosphere and sample temperature is scanned along a well-defined program.

DSC was used in this investigation to determine the heat capacity and the effective heat of reaction for the pyrolysis of the virgin cardboard material. The corrugated cardboard was ground to a powder and allowed to dry in the desiccator for a

minimum of 48 hours. The sample masses ranged from 6 to 10 mg for the DSC tests. The corrugated cardboard powder was compacted as densely as possible in a platinum crucible such that the sample material made contact with the entire bottom of the crucible.

The tests were conducted in the Netzsch 449 F3 Jupiter STA. The DSC tests were set up with the crucible lids covering the sample and reference crucibles to ensure uniform heating and temperature of the sample and both crucibles. The temperature program for the DSC tests consisted of a conditioning period when the temperature of the sample was held constant at 40°C for 20 minutes, followed by heating to 840°C at a rate of 10°C/min. The temperature was held constant at 840°C for ten minutes at the end of the tests to ensure the apparatus reached the final temperature of 840°C. The nitrogen flow rate for all DSC tests was 50 mL/min.

2.3.3 Pyrolysis-Combustion Flow Calorimetry

Pyrolysis-Combustion Flow Calorimetry is a testing method based on pyrolyzing a sample in an inert atmosphere similar to the principle of TGA tests [36]. The gaseous volatiles evolved during the pyrolysis process flow to a combustion chamber where a reaction occurs with excess oxygen and the heat release rate of the combustion of the volatiles is measured using oxygen-consumption calorimetry. The heating rate for the pyrolysis process is generally on the order of 1 K/s. PCFC data can be used to assign complete heats of combustion to the pyrolyzate evolved from each reaction in the reaction mechanism. Five PCFC tests were conducted on corrugated cardboard samples prepared in the same manner as the samples used in the TGA and DSC tests.

3. Experimental Results and Discussion

3.1 Bench-Scale Testing

3.1.1 Rate of Heat Release and Mass Loss Rate

The heat release rate and mass loss rate data collected while the sample was flaming in five tests at each of the aforementioned incident heat fluxes are provided in the following figures. The data for 20 kW/m^2 is provided in Figure 3-1, 40 kW/m^2 is provided in Figure 3-2, 60 kW/m^2 is provided in Figure 3-3, and 80 kW/m^2 is provided in Figure 3-4. The plots present the raw heat release rate data collected in the tests at a rate of 0.8 Hz along with the curve of the instantaneous mean. The discrete data are plotted to demonstrate the uncertainty in the mean curve and the repeatability of the curve trends between tests. The cone calorimeter data collected when the sample was smoldering are provided along with some discussion about the different physical phenomena contributing to the considerable difference in mass loss rate and heat release rate profiles during smoldering combustion in Appendix II – Char Smoldering.

A linear correction was applied to the total mass evolution data to eliminate zero point drift of the balance. The mass loss rate was calculated from a numerical differentiation of the corrected total mass data. The recorded instantaneous mass data was relatively noisy, and numerical differentiation tended to amplify the noise in the data. The average uncertainty in the instantaneous mean of mass loss rate due to variations in the data collected at all heat fluxes was approximately 16%., General trends about the mass loss rate and heat release rate data can be extracted from the following figures . The plots display the period of the tests between ignition and flame extinction.

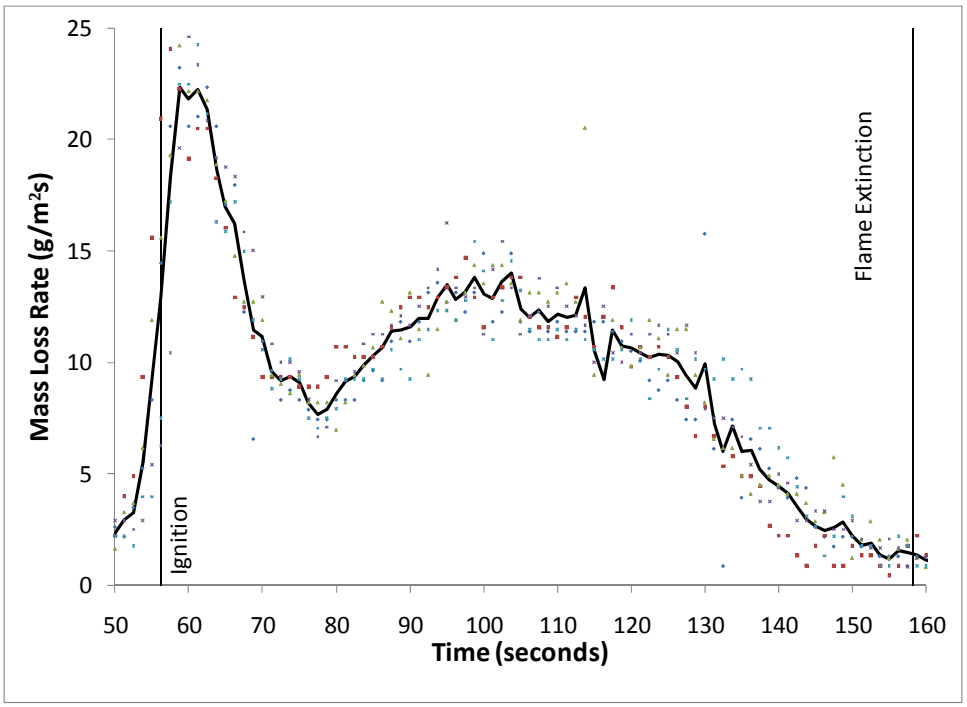

(a)

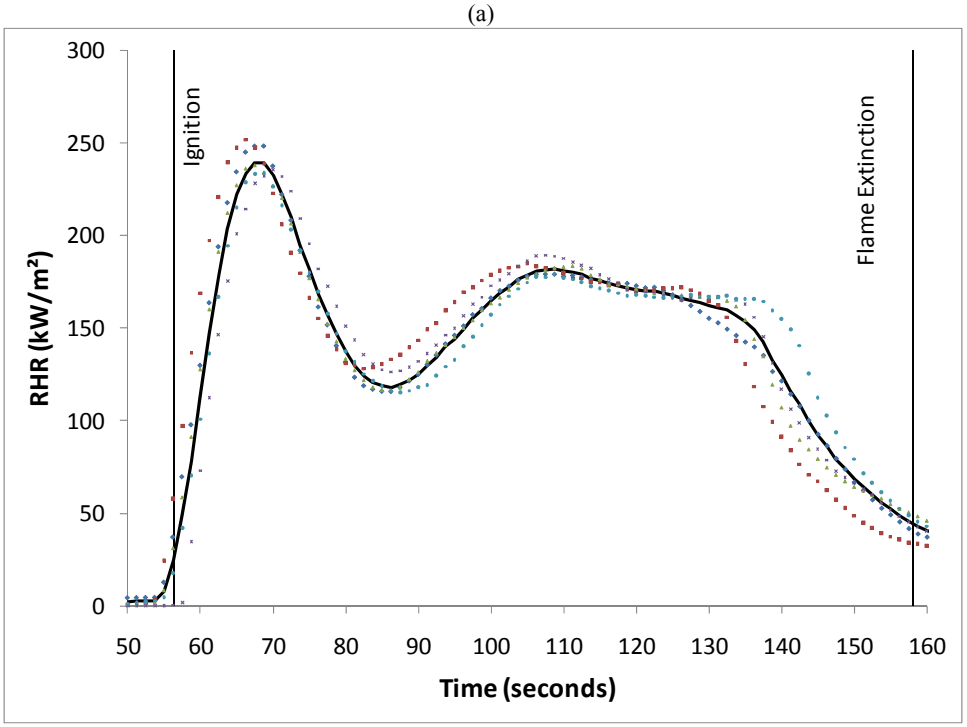

(b)

Figure 3-1: Data Collected from the Cone Calorimeter at an Incident Heat Flux of 20 kW/m^2 : (a) Mass Loss Rate Curve (b) Rate of Heat Release Curve

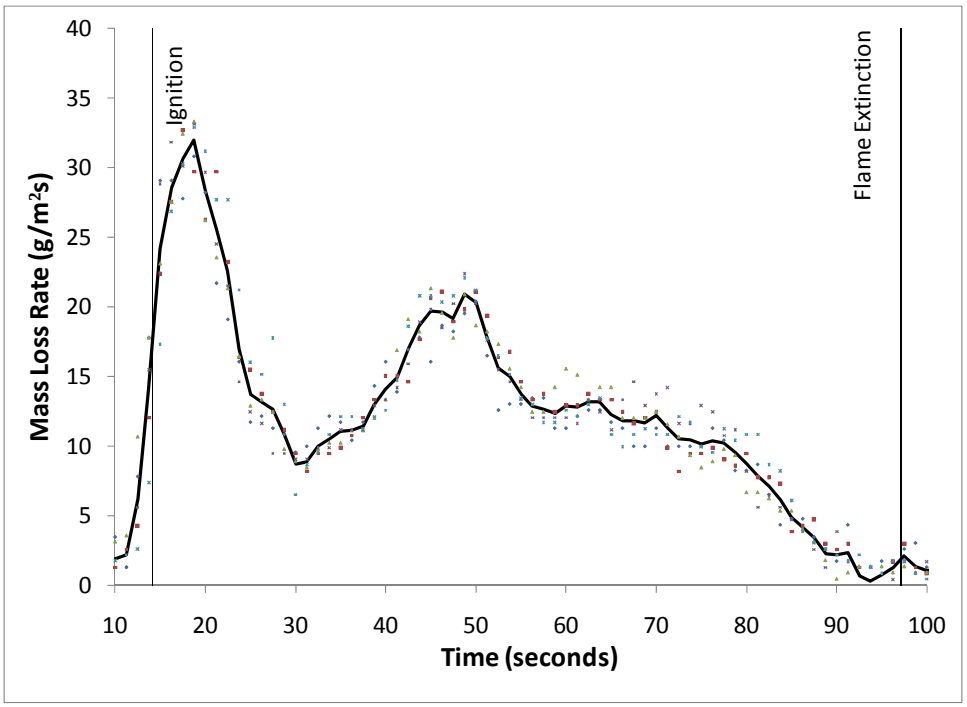

(a)

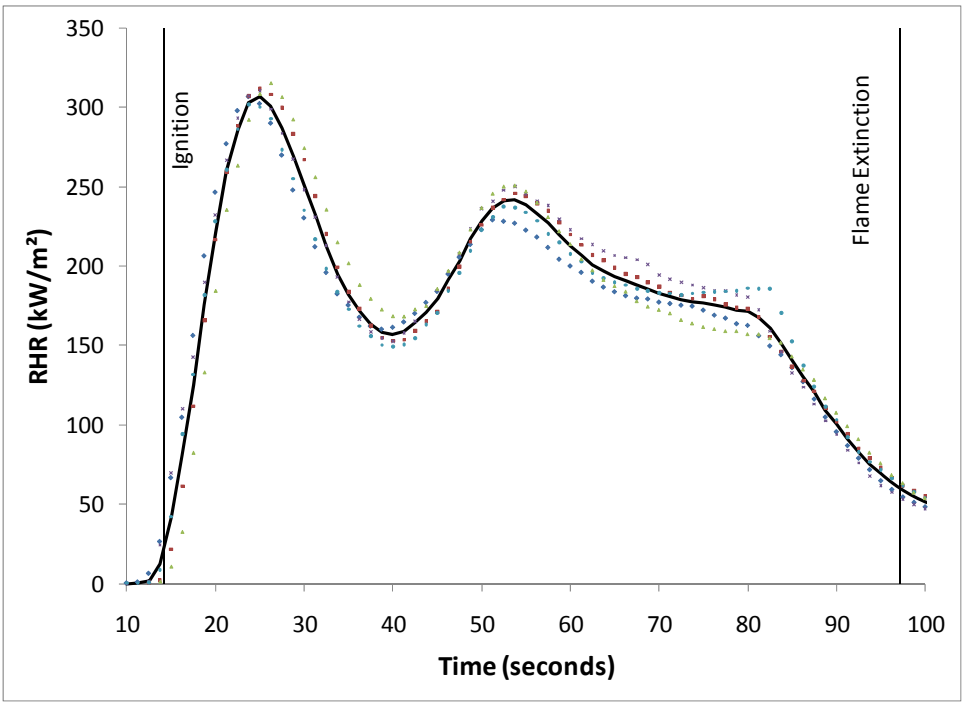

(b)

Figure 3-2: Data Collected from the Cone Calorimeter at an Incident Heat Flux of 40 kW/m2 : (a) Mass Loss Rate Curve (b) Rate of Heat Release Curve

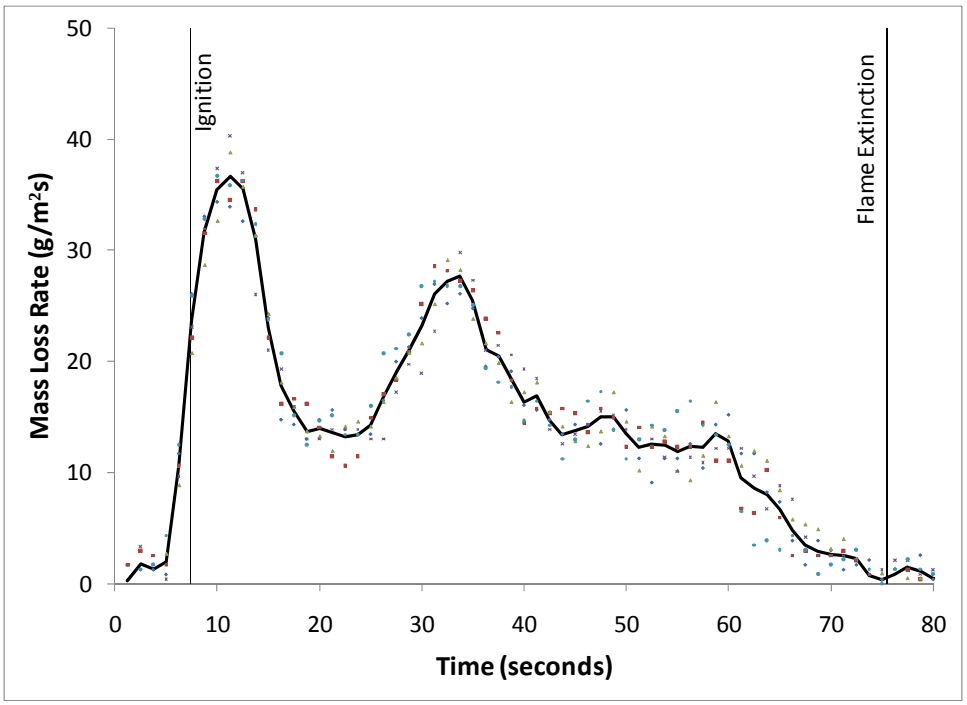

(a)

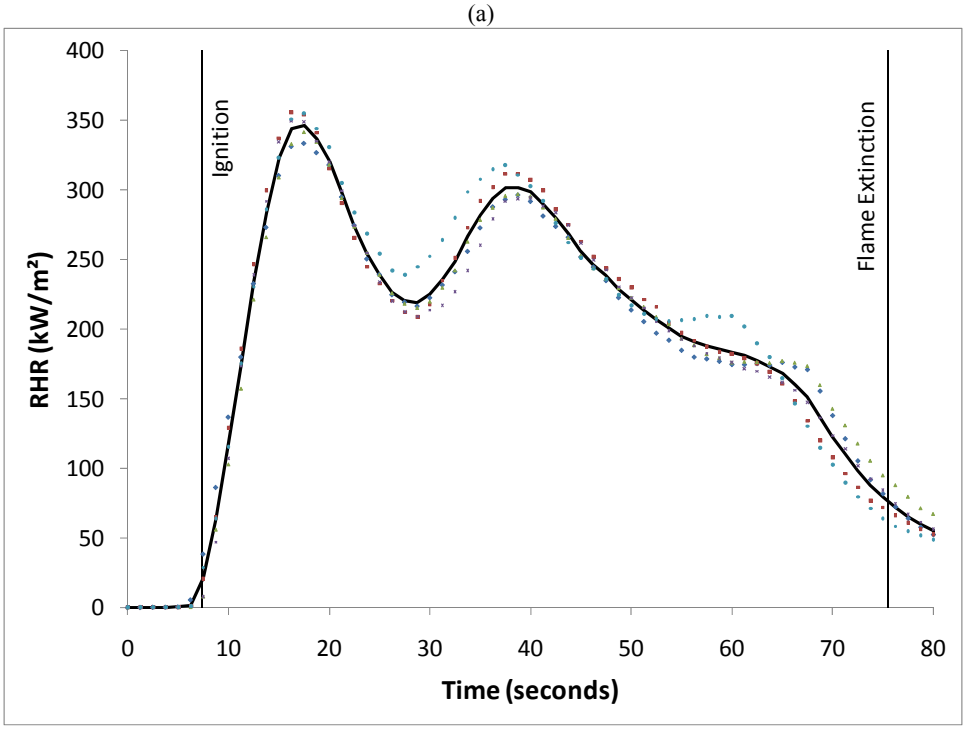

(b)

Figure 3-3: Data Collected from the Cone Calorimeter at an Incident Heat Flux of 60 kW/m2 : (a) Mass Loss Rate Curve (b) Rate of Heat Release Curve

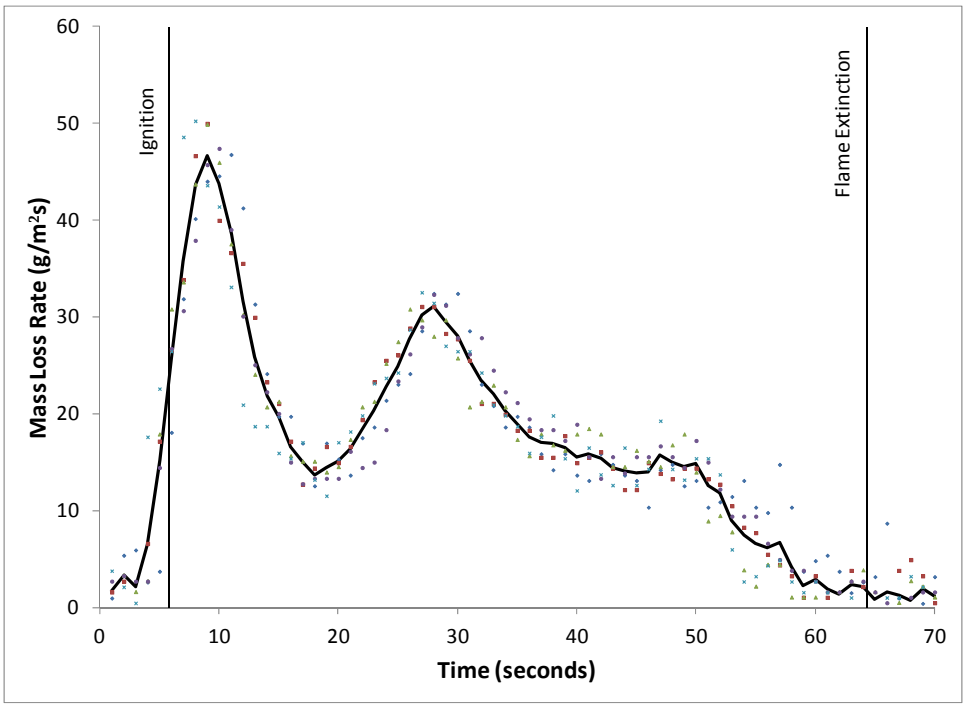

(a)

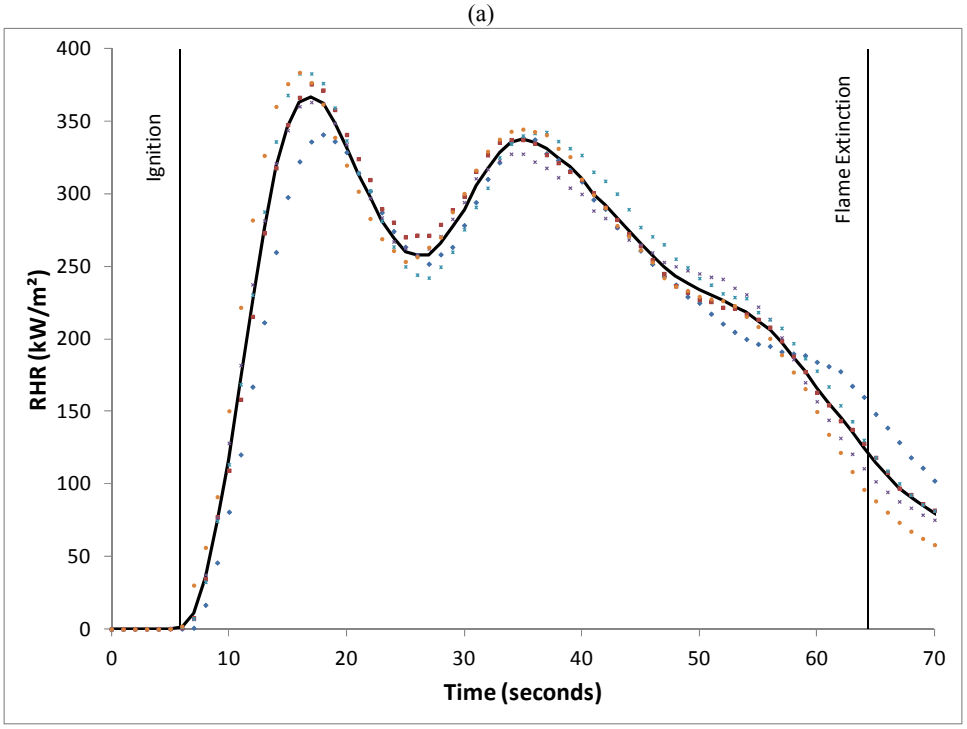

(b)

Figure 3-4: Data Collected from the Cone Calorimeter at an incident Heat Flux of 80 kW/m2 : (a) Mass Loss Rate Curve (b) Rate of Heat Release Curve

The rate of heat release at each heat flux demonstrates similar trends. The heat release rate data collected while the sample was flaming contains three distinct peaks or shoulders, likely caused by the three layers of linerboards, with each peak or shoulder

reaching a lower heat release rate than the previous peak. It is clear from comparing the mass loss rate curves to the heat release rate curves at each heat flux that the curves are qualitatively similar. Combustion theory defines the effective heat of combustion as the proportion of the heat release rate to the mass loss rate, as depicted in Equation 1.

$$HRR = \Delta h_c \dot{m}_f{}'' \tag{1}$$

The effective heats of combustion at each heat flux were calculated based on the integrals of the heat release rate curve and the mass loss rate curve for flaming combustion, smoldering combustion, and for the entire process from the data collected in the cone calorimeter tests. The calculated values are displayed in Table 3-1. It is noteworthy that the heat of combustion during smoldering at each heat flux was approximately three times higher than the heat of combustion during flaming.

Several parameters were extracted from the data collected in the cone calorimeter tests or observed during testing. The time to sustained ignition, the time until approximately half the surface of the sample was flaming, and the time from the beginning of the test when the sample was observed to stop flaming were recorded independently of the data acquisition system. Peak rates of heat release and mass loss rates and the time from the beginning of the test until each of these milestone events occurred were examined and compared at each external heat flux. These calculated and observed values are presented in Table 3-1 where the uncertainties are defined as two standard deviations of the mean.

Table 3-1: Characteristic Values Calculated and Observed in Cone Calorimter Tests

Experimental Value	20 kW/m²	40 kW/m²	60 kW/m²	80 kW/m²
Time to Ignition [seconds]	56.2 ± 3.4	14.2 ± 1.8	7.3 ± 0.6	5.8 ± 0.6
Time to 1/2 Flaming [seconds]	123.4 ± 9.3	69 ± 13	60.7 ± 8.3	56.7 ± 3.0
Time to Flame Extinction [seconds]	158.2 ± 9.1	97.1 ± 3.9	75.5 ± 3.0	64.3 ± 2.7
Time to Peak HRR [seconds]	68.3 ± 2.9	24.8 ± 2.0	17.0 ± 1.4	16.8 ± 0.7
Peak HRR [kW/m²]	241 ± 16	309 ± 10	347 ± 19	369 ± 16
Time to Second HRR Peak [seconds]	108.0 ± 4.5	53.0 ± 2.2	38.5 ± 2.1	35.0 ± 1.1
Second Peak HRR [kW/m²]	183.2 ± 8.6	243 ± 18	303 ± 21	338.1 ± 5.9
Peak Mass Loss Rate [g/m²s]	24.1 ± 1.0	32.6 ± 2.0	37.3 ± 4.6	48.9 ± 1.5
Time to Peak MLR [seconds]	59.3 ± 2.9	18.5 ± 1.1	10.5 ± 1.4	9.4 ± 1.0
Second Peak Mass Loss Rate [g/m²s]	15.1 ± 0.7	21.4 ± 0.7	28.3 ± 1.1	31.8 ± 0.7
Time to Second Peak MLR [seconds]	98.8 ± 2.5	47.8 ± 1.9	32.0 ± 1.0	27.4 ± 0.8
Effctive Heat of Combustion for Flaming [kJ/g]	14.8 ± 0.3	14.3 ± 0.4	14.1 ± 0.2	13.2 ± 0.3
Effective Heat of Combustion for Smoldering [kJ/g]	40.5 ± 4.1	43.6 ± 4.8	40.3 ± 4.1	50.9 ± 2.0
Total Effective Heat of Combustion [kJ/g]	19.9 ± 0.8	19.5 ± 1.0	18.3 ± 0.7	18.9 ± 0.3

3.1.2 Internal Temperatures

The temperature distribution data collected in modified cone calorimeter tests conducted on samples instrumented with thermocouples are displayed in the following figures. The thermocouple data collected at an incident heat flux of 20 kW/m^2 are provided in Figure 3-5 and the data collected at an incident heat flux of 60 kW/m^2 are provided in Figure 3-6. The data collected from the thermocouples is only presented for the period of time from the beginning of the test until the flame above the sample was observed to self-extinguish. The error bars in the figures correspond to two standard deviations of the mean.

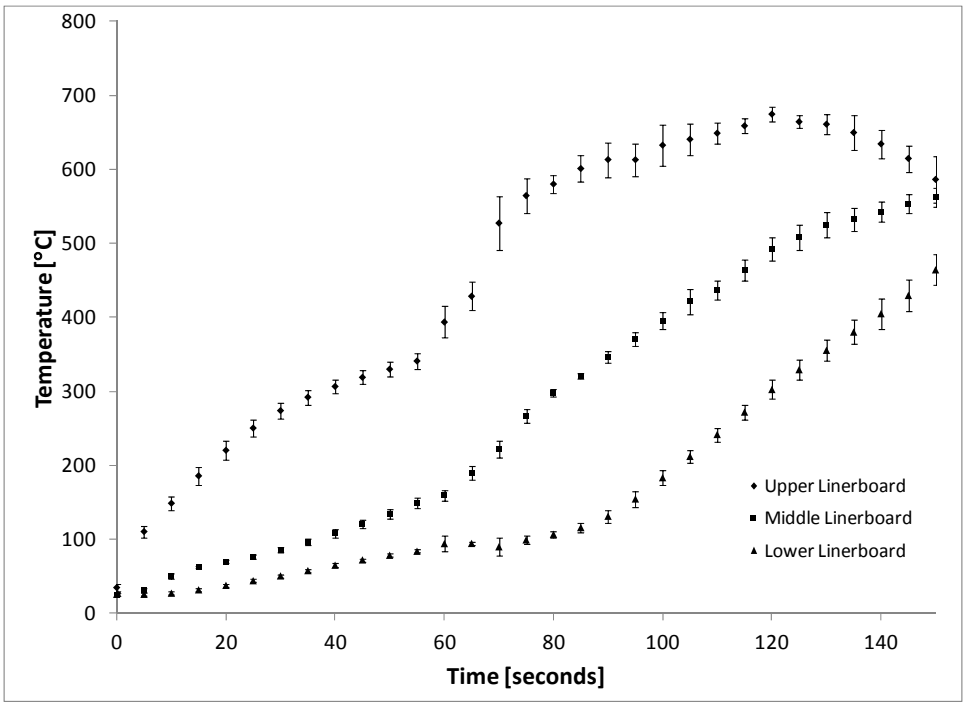

Figure 3-5: Temperature Profile of Corrugated Cardboard Sample Subjected to a Heat Flux of 20 kW/m^2

The temperature profile data displayed in Figure 3-5 and Figure 3-6 were collected at a rate of 1 Hz and are presented at a rate of 0.2 Hz. Each data point displayed in the figures was averaged with the data point preceding by 1 s and following by 1 s to minimize the variations from random noise. The mean data points from five tests are displayed in Figure 3-5 and the mean data from four tests are displayed in Figure 3-6. Each of the error bar magnitudes was calculated including the three consecutive measurements in time for each of the five tests for the data collected at an incident heat flux of 20 kW/m^2 and four tests conducted at a heat flux of 60 kW/m^2.

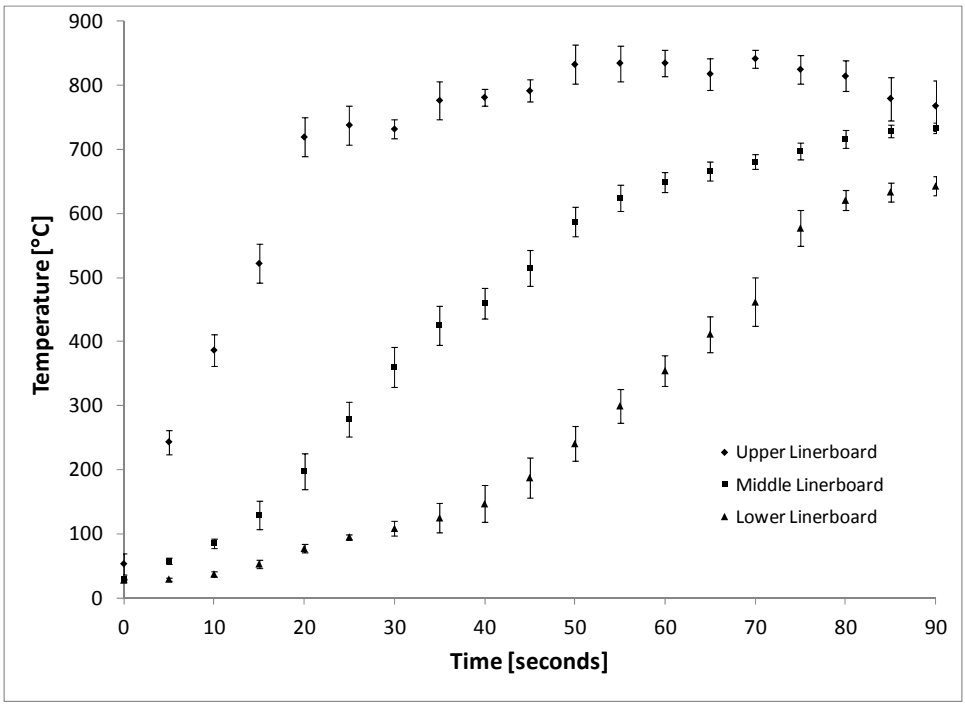

Figure 3-6: Temperature Profile of Corrugated Cardboard Sample Subjected to a Heat Flux of 60 kW/m^2

It was observed that the uncertainty of the locations of the thermocouples in the modified cone calorimeter tests increased as the material degraded, resulting in larger uncertainties in the temperature measurements as the test progressed, as evidenced by the increasing magnitude of the error bars in Figure 3-5 and Figure 3-6. The decay in structural stability of the linerboard layers was most prominent at the upper linerboard because of the proximity of the heater and was observed to be less prominent in the lower linerboards. As the cardboard sample degraded to char and subsequently oxidized to form ash, the structural stability of the sample was compromised. Several times the uppermost thermocouple was observed to shift position such that it was out of the sample shortly after flame extinction. The locations of the thermocouples were required to be constant and well-known throughout the test for an accurate comparison to the model prediction. Based on these observed movements of the uppermost thermocouple, it was concluded that the thermocouple readings became inaccurate above approximately 500°C

and the thermocouple data collected while the sample was flaming were considered not as reliable as the data collected during the pre-ignition heating period.

Temperature profile data were also collected with thermocouples that were pulled in tension through the sample. Measuring the temperatures in this way allowed the locations of the thermocouples to be fixed in space and well-defined. The drawback to this method was the thermocouples did not always make contact with the corrugated cardboard material. The temperature profile data collected from thermocouples inserted in the linerboards were used for all fitting and presentation of data because the data was more consistent and more tests were completed.

The temperature profiles collected at each heat flux are qualitatively similar with the test conducted at a heat flux of 60 kW/m^2 exhibiting higher temperatures and more rapid heating to the peak temperatures. There is a trend in both sets of data that the rate of increase of the temperature was largest for the thermocouple inserted in the upper linerboard and decreased for each of the lower linerboards. The thermal inertia of the corrugated cardboard material was responsible for the delayed propagation of the thermal wave evident in the temperature profile data. Parameters that describe the thermal properties of the corrugated cardboard can be derived from the temperature profile data presented in the preceding figures. The observation that a thermal wave must propagate through the material leads to the confirmation that corrugated cardboard should be treated as a thermally thick material.

The temperature profile data collected with the corrugated cardboard sample with a surface emissivity of 0.95 at a heat flux of 20 kW/m^2 are displayed in Figure 3-7. The

data was collected at a rate of 1 Hz and is displayed at a frequency of 0.2 Hz. The temperature profiles are qualitatively similar to the temperature profiles of the unaltered material. The data collected with a surface emissivity of 0.95 is characterized by a more rapid temperature increase before ignition than the temperature change observed in the unaltered samples at 20 kW/m^2 incident heat flux. The increase in the rate of change of temperature in the upper linerboard is due to more radiant energy being absorbed by the sample because of the higher surface emissivity.

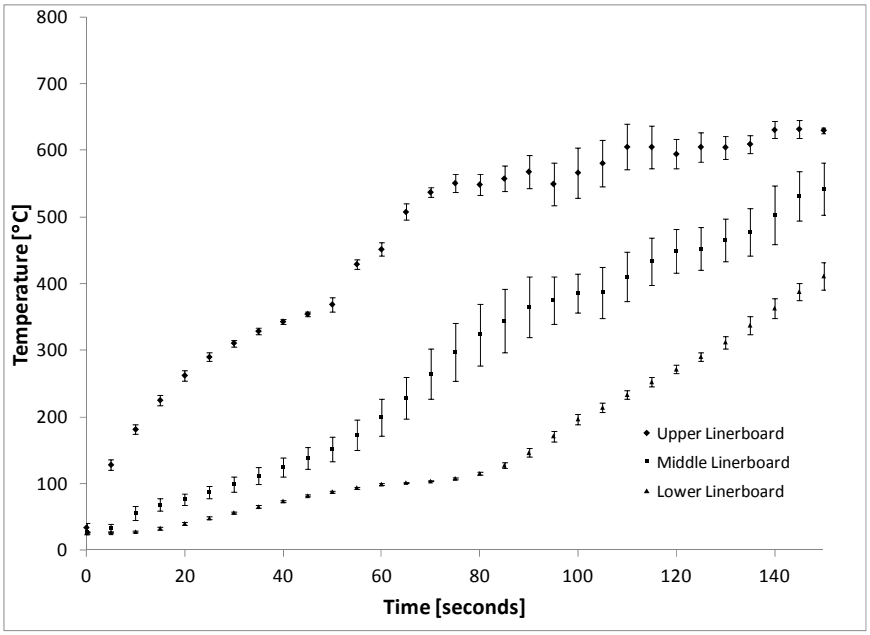

Figure 3-7: Temperature Profile of Corrugated Cardboard Sample with Surface Emissivity of 0.95 Subjected to a Heat Flux of 20 kW/m^2

It is interesting that the peak temperature of the material with a surface emissivity of 0.95 is lower than the unaltered material. A lower peak temperature could possibly be explained by the paint binding the cardboard together such that the structural changes observed in tests on unaltered samples did not occur. The upper thermocouple generally did not shift an observable distance in the tests with the black surface and the thermocouple was obstructed from the heater by the intact upper linerboard. As a result,

the temperature measured by the upper thermocouple did not reach the peak temperatures measured in the unaltered samples.

3.1.3 Flame Heat Flux

An average curve for the total heat flux incident on the sample surface as a function of time was generated. The steady incident heat flux measured before ignition was subtracted from the heat flux evolution profile to obtain the contribution of the flame heat flux to the total heat flux. The evolution of the average flame heat flux over the period of time when the sample was flaming is plotted in Figure 3-8 for 20 kW/m^2 and in Figure 3-9 for 60 kW/m^2.

The data collected with the heat flux gauge in the off-center position was consistent with the data collected at the center position for the tests conducted with an incident heat flux of 20 kW/m^2. The data collected with the heat flux gauge in the off-center position was included in the averaging of the data collected with the heat flux gauge at the center of the sample for 20 kW/m^2 incident heat flux. The off-center data did not agree with the data collected with the heat flux gauge at the center of the sample for the tests conducted at a heat flux of 60 kW/m^2. It was observed that the heat flux gauge was partially obscured due to material deformation during the off-center heat flux gauge tests conducted at 60 kW/m^2. Obscuration of the heat flux gauge led to the disagreement between the tests conducted with the heat flux gauge positioned at the center and off-center locations. It is noteworthy to mention the case of the heat flux gauge becoming obscured due to partially exfoliated material because it presents the possibility that all the heat flux gauge data are unreliable.

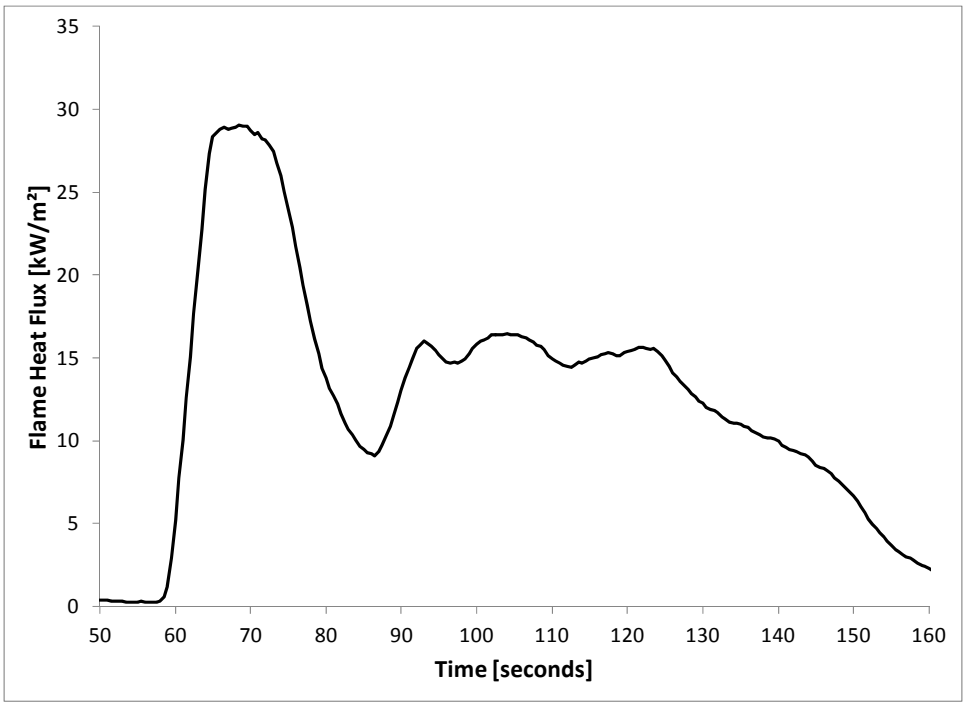

Figure 3-8: Mean Flame Heat Flux Evolution with 20 kW/m^2 Incident Heat Flux

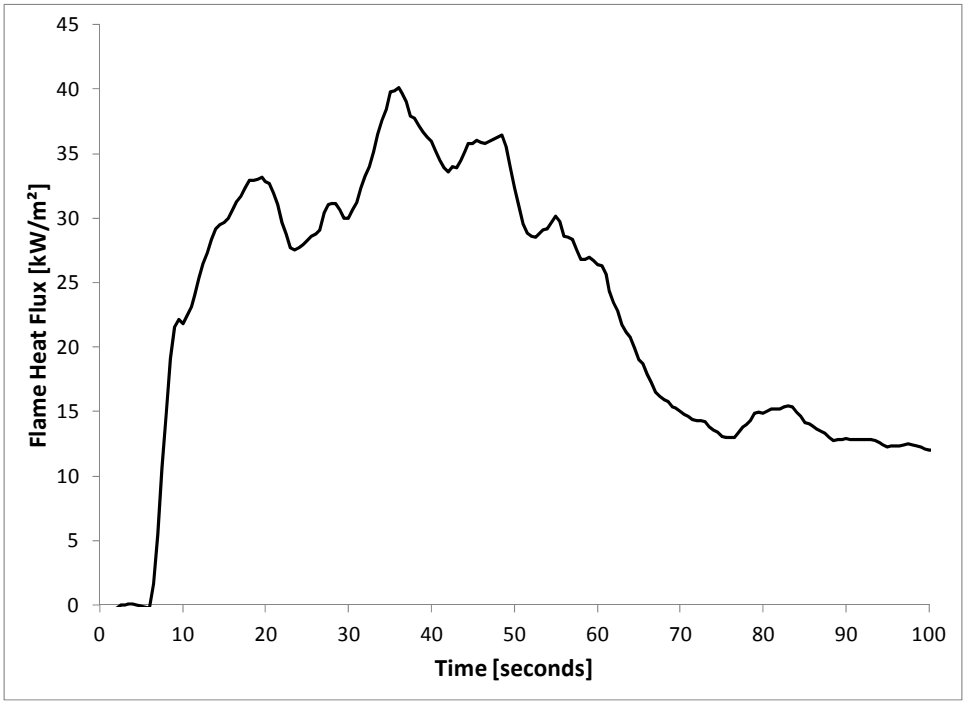

Figure 3-9: Mean Flame Heat Flux Evolution with 60 kW/m^2 Incident Heat Flux

The flame heat flux evolution data collected at each incident heat flux do not follow a similar obvious trend. Each set of data contains a gradual increase to the first

peak as well as a relatively steady period further in to the test, though the initial rate of increase and the magnitude of the heat flux over the steady period are different for each incident heat flux.

It was observed that the heat flux gauge reading did not return to the pre-ignition mean value for tests at either incident heat flux after the flame self-extinguished. The residual heat flux decayed over a prolonged period of time after the flame was extinguished. During the tests conducted at 60 kW/m^2 incident heat flux, there was a possible gas phase reaction that was observed above the sample after the flame had extinguished. It is also likely that the residual heat flux was produced, in part, by convection currents transferring heat from the surrounding hot surface to the cold heat flux gauge surface. The surface of the smoldering char was approximately 900°C and the heat flux gauge surface was approximately room temperature. The theoretical convective heat flux due to this temperature difference is of the order of the residual heat flux measurements.

The flame heat flux measurements collected in the modified cone calorimeter tests were analyzed to determine the most realistic representation of the heat flux from the flame. The average flame heat flux curves collected at 20 and 60 kW/m^2 did not follow a common trend, and it was determined that a mean value would be the best representation of the flame heat flux.

The thermocouple inserted in the upper linerboard behaved similar to a heat flux gauge in the initial heating of the sample. The heat transfer from the upper linerboard in-depth to the material was negligible in the beginning stages of heating, so the initial

temperature measurement provided an accurate representation of the energy from the flame. The measurements conducted with the heat flux gauge were independent of the thermocouple measurements. The thermocouples used in this investigation were adequately thin to show an instantaneous temperature response and the heat flux gauge had a comparatively large response time. A compromise was generally required between the measured temperature profiles and the heat flux gauge measurements which led to uncertainty in the treatment of the heat flux contribution of the flame. There was a transient period between ignition and the observation of the peak heat flux from the flame on the order of ten seconds.

Based on the limitations of the Thermakin program to describe the heat flux from the flame and because of the uncertainty in the fluctuations in the measurement of the flame heat flux, an approximate mean value for the flame heat flux was determined. A threshold value of 50% of the maximum flame heat flux was used to define the limits of the averaging used to describe the mean flame heat flux for the data collected at each incident heat flux. The maximum flame heat flux measured for the cone calorimeter tests conducted at 20 kW/m^2 was 29.0 kW/m^2. The mean flame heat flux measured at 20 kW/m^2 incident heat flux was 17.2 kW/m^2. The maximum flame heat flux measured in the tests with an incident heat flux of 60 kW/m^2 was 40.1 kW/m^2 and the mean flame heat flux was 29.9 kW/m^2. The flame heat flux was simplified from these values to an approximate steady value of 30 kW/m^2.

Observations of the flame during cone calorimeter tests led to the conclusion that the flame should be represented in the Thermakin bench-scale model by an addition of radiative heat flux. The flame was observed as non-transparent and was lifted from the

sample surface a distance to sufficiently assume the contribution of flame heat flux from convection was negligible compared to the radiative flame heat flux contribution. The flame representation adopted for the bench-scale model applied an updated heat flux boundary condition with an additional 30 kW/m^2 of radiation after the critical mass flux for ignition was achieved. The transient growth of the flame was represented by a linear ramp with a duration of 10 s as shown in Figure 3-10.

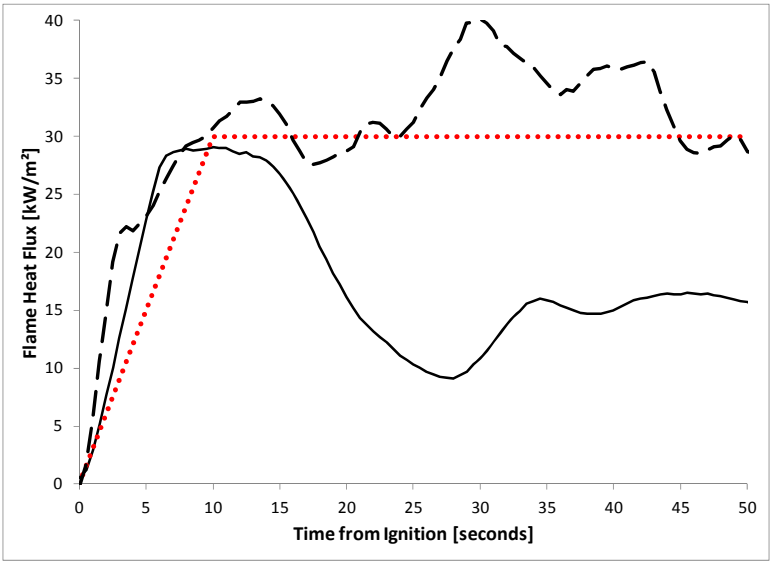

Figure 3-10: Flame Heat Flux Measurements Collected with a Heat Flux Gauge Compared to the Flame Heat Flux Representation in the Model

Observations of the flame in the cone calorimeter tests with an incident heat flux of 20 kW/m^2 led to the conclusion that the heat flux gauge data did not accurately portray the flame above the sample surface. There was no observable change in the nature of the flame to explain the decrease in measured heat flux for the 20 kW/m^2 case and it was assumed the flame heat flux profile measured with the cone calorimeter with an incident heat flux of 60 kW/m^2 was more representative of the general trend. The representation of the heat flux contribution from the flame for the model did not deviate considerably from the mean flame heat flux profile measured with the heat flux gauge. The increase of

the heat flux was characterized according to the heat flux gauge and temperature measurements, but the steady values of the heat flux and the initial rate of change of the heat flux represent the best approximations from observations and independent test data.

The flame heat flux approximation adopted for the model is based on the observations of specific tests conducted during this investigation and was limited by the functionality of the Thermakin program. The Thermakin program produces condensed phase models and was not programmed with the intention of representing a complicated flame heat flux profile. The pyrolysis model was constructed to contribute to a full-scale CFD model. It is likely that the CFD model would calculate the flame heat flux contribution and total heat flux incident to the material surface with a gas-phase model. It is important to note the results obtained during this investigation are dependent on the assumptions and approximations made during construction of the pyrolysis model that would not necessarily be made if the pyrolysis model was coupled to a gas-phase combustion model.

The bench-scale model was constructed to simulate the period of time when the sample surface was covered with flame. The heat flux was increased along the ramp detailed above when the critical mass flux was achieved and remained constant after the ramp for the remainder of each simulation.

It was determined from the tests in which the linerboard was passed between the heater and the heat flux gauge that the linerboard material was optically opaque. The initial heat flux measurement beneath the linerboard was approximately equal to the measurement beneath the Kaowool insulation. The Kaowool insulation and all cardboard

components were defined with absorption coefficients sufficiently high to ensure all the radiation was absorbed by the cardboard material components.

3.2 Milligram-Scale Testing

3.2.1 Mass Loss Rates

Thermogravimetric data resulting from three tests conducted in a pure nitrogen atmosphere with a heating rate of 10 K/min are provided in Figure 3-11 as mass loss rate and normalized total mass data. The data is consistent between tests and all variations between the tests appear to be random noise partially amplified by the numerical differentiation of the total mass data to produce the mass loss rate plots.

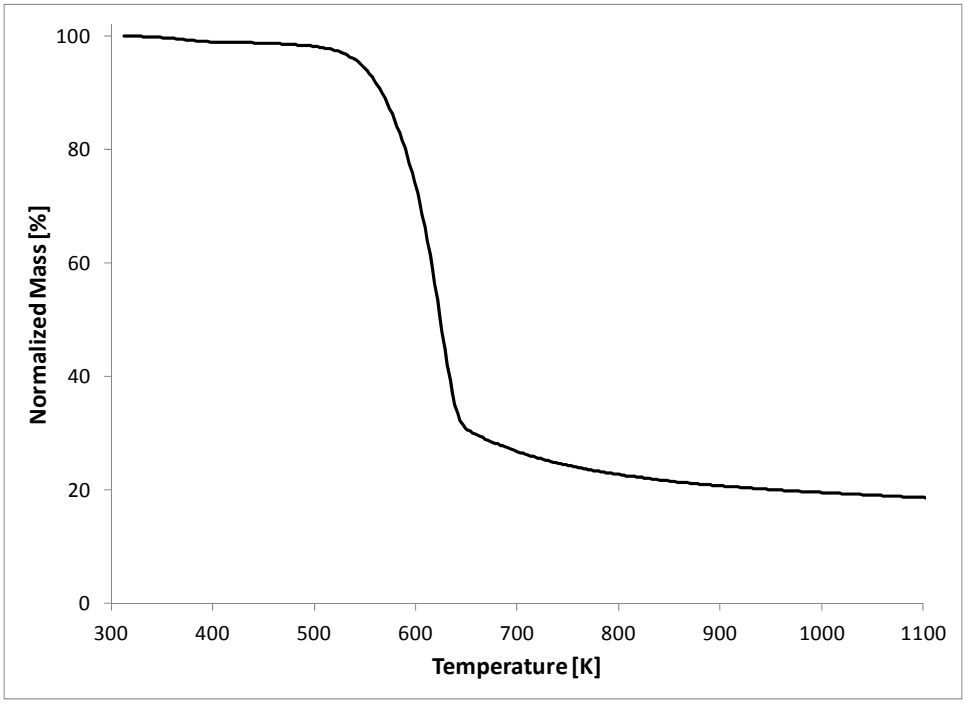

(a)

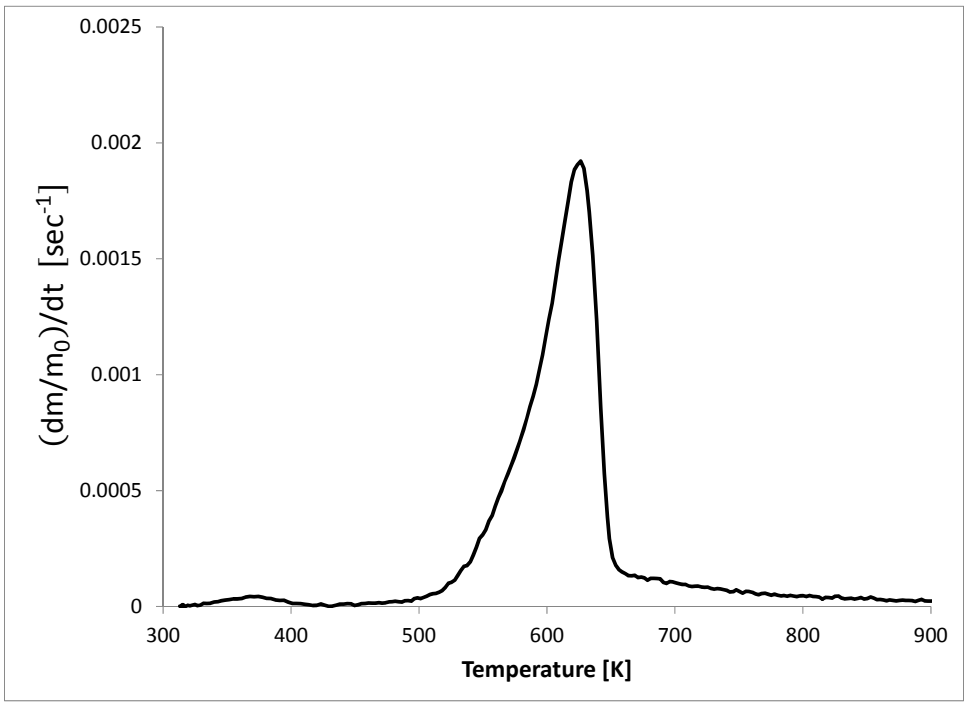

(b)

Figure 3-11: Thermogravimetric Data Collected with a Heating Rate of 10 K/min Displayed as: (a) Average Normalized Total Mass from Three Tests (b) Mean Mass Loss Rate Curve from Three Tests

Three distinct processes can be observed in the degradation of corrugated cardboard powder displayed in Figure 3-11. The first occurred in the range 325-385 K and is attributed to the evaporation of moisture from the sample. The second process was evidenced by the large peak ranging 500-650 K when the majority of the mass of the sample was degraded. The final process started at approximately 650 K and finished at approximately 850 K, generating a tail that slowly approached zero as the sample pyrolyzed to yield a final char in the amount of approximately 18.5% of the original mass.

The mass loss rate data collected in three TGA tests conducted on corrugated cardboard powder in a pure nitrogen atmosphere with a heating rate of 5 K/min are provided in Figure 3-12. The mass loss rate data presented in Figure 3-12 had more variation from noise than the data displayed in Figure 3-11. To minimize the variations

from noise in the presentation of the data, a 66-second (11 data points) moving average has been applied to the curve.

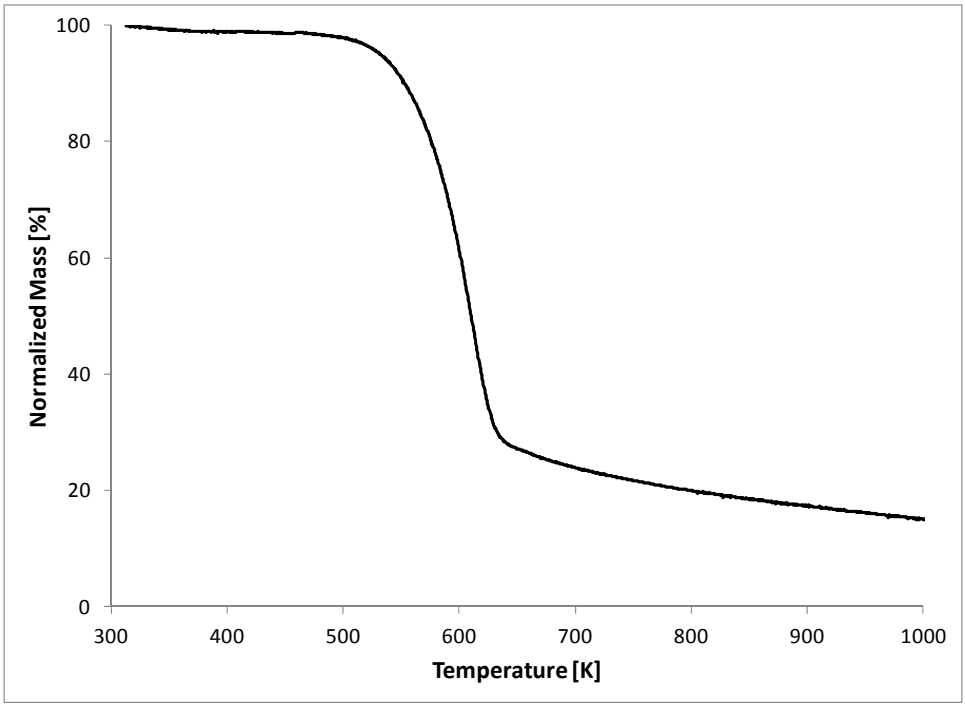

(a)

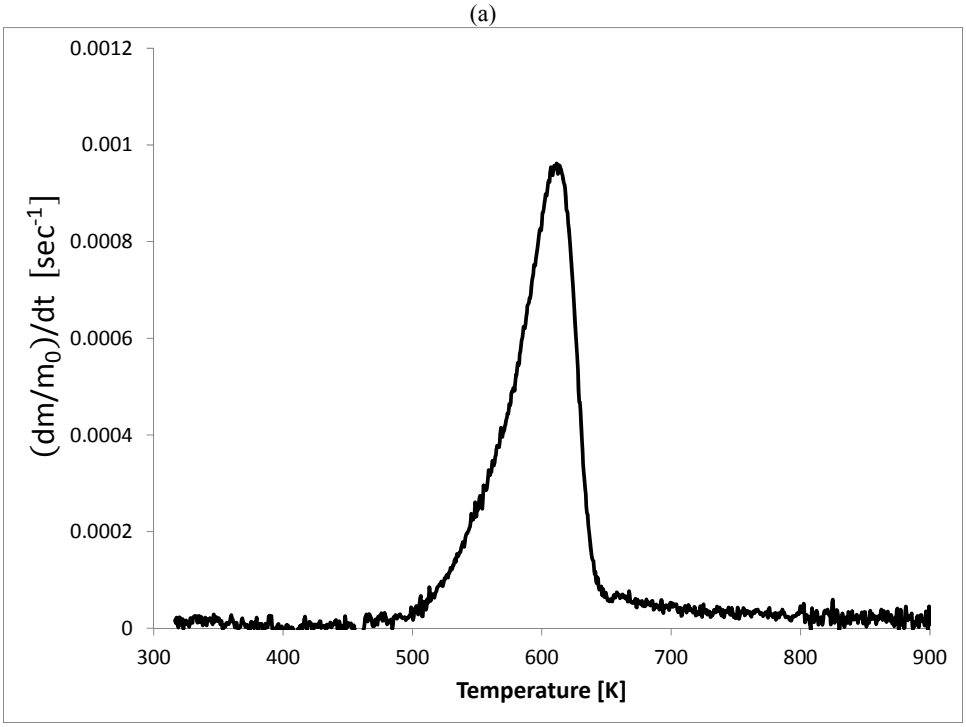

(b)

Figure 3-12: Thermogravimetric Data Collected with a Heating Rate of 5 K/min Displayed as: (a) Average Normalized Total Mass from Three Tests (b) Mean Mass Loss Rate Curve from Three Tests Smoothed with a 66-Second Moving Average

The high frequency variations in the data are likely attributable to several changes in the procedure for the tests conducted at each heating rate. The tests conducted at a heating rate of 5 K/min were completed with a different STA apparatus than the tests conducted with a heating rate of 10 K/min. The sample masses for the tests conducted with a heating rate of 5 K/min were in the range 4-7 mg whereas the sample masses for the tests conducted with a heating rate of 10 K/min were in the range of 6-10 mg. It has been observed in these and previous TGA tests that smaller sample masses produce comparatively more variations in the total mass and mass loss rate measurements.

The mass loss rate data collected at a heating rate of 5 K/min has the same qualitative shape as the data collected at a heating rate of 10 K/min. The magnitude of the mass loss rate data collected at a heating rate of 5 K/min is approximately half the magnitude of the mass loss rate data collected at a heating rate of 10 K/min. It is important to note the moving-average smoothing operation that was performed on the data collected at a heating rate of 5 K/min decreased the magnitude of the maximum by approximately 9%.

The heating rate also had a marked effect on the final char yield and the temperature corresponding to the maximum mass loss rate. The average final char yield in the tests conducted with a heating rate of 10 K/min was 18.5% of the initial mass and the average final char yield in the tests conducted with a heating rate of 5 K/min was 14.6%. The temperature corresponding to the peak mass loss rate for the data collected with a heating rate of 5 K/min was 609 K and 626 K for a heating rate of 10 K/min. These observations are consistent with observations noted in the literature [7][12].

The data collected in TGA tests conducted on samples from the three different layers of the corrugated cardboard are provided in Figure 3-13 with a comparison to the TGA data collected for the composite material. The fluted materials have been identified by each flute designation. The C-flute material is the corrugated material in the thicker fluted section with fewer flutes per meter and the B-flute material is the material in the thinner fluted section.

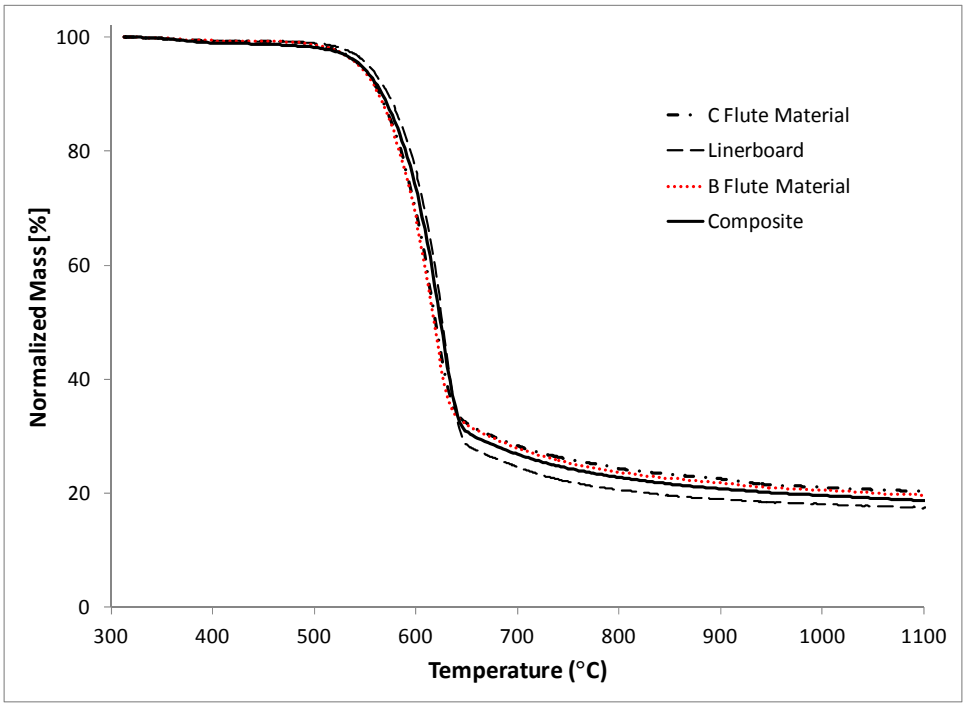

(a)

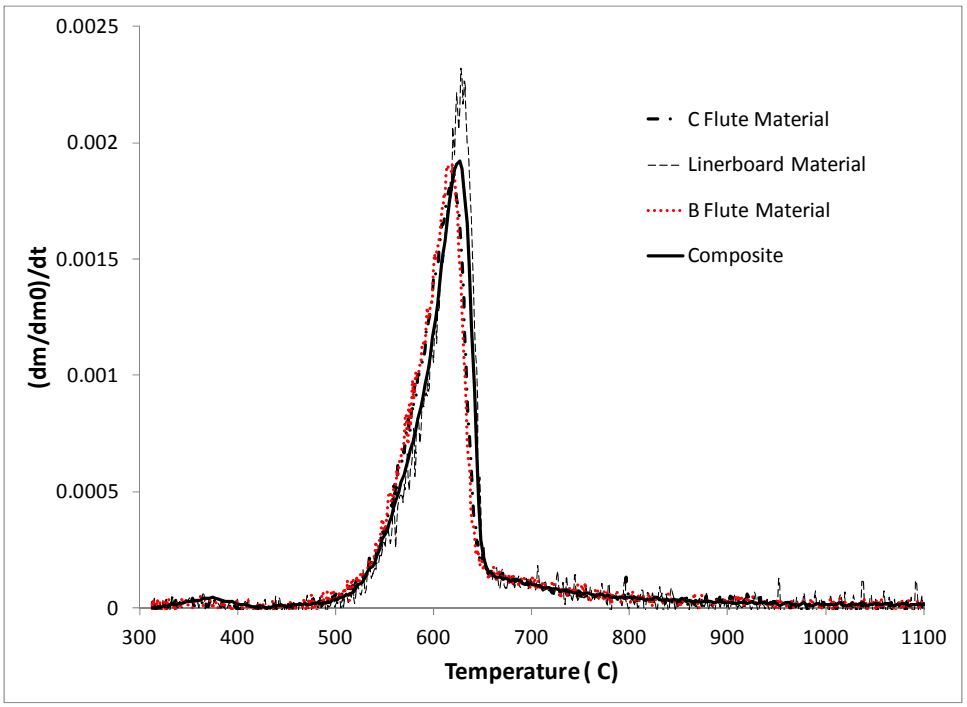

(b)

Figure 3-13: Thermogravimetric Data for the Corrugated Cardboard Component Layers Collected with a Heating Rate of 10 K/min Displayed as: (a) Average Normalized Total Mass from Three Tests (b) Mean Mass Loss Rate Curve

The mass profile and the mass loss rate profile for each component layer are within the limits of error of the composite material. It can be assumed that each layer has approximately the same composition and a single reaction mechanism can describe the mass loss rate of all the components. It is interesting that the maximum mass loss rate of the linerboard profile is larger than the maximum of the composite material mass loss rate profile. The linerboard makes the largest contribution to the composite material by mass. The assumption follows that the linerboard mass loss rate profile would be most similar to the composite material mass loss rate profile, though that is not the case.

3.2.2 Thermodynamics

The heat flow data collected in five DSC tests conducted on corrugated cardboard powder are provided in Figure 3-14. There is considerable scatter in the heat flow data that is likely partially attributed to deformation of the sample as the sample degraded. It

has been hypothesized that contact between the material and the crucible was affected by changes in the sample structure. Poor contact with the bottom of the sample crucible resulted in an unrealistic measurement of sample temperature. The DSC signal is dependent on the sample temperature. The deformation of the sample is likely to lead to uncertainty and scatter in the DSC signal. The scatter in the signal is also attributed to the reduction in the sensitivity of the heat flow measurements at high temperatures.

In this investigation the convention that has been adopted is negative heat flow values correspond to endothermic processes and positive values correspond to exothermic processes. It is clear from Figure 3-14 that the pyrolysis of corrugated cardboard is an endothermic process because the data points correspond to negative heat flow values. These measurements agree with theory that states a net absorption of energy by the material is required to thermally degrade the condensed phase fuel to the products of pyrolysis.

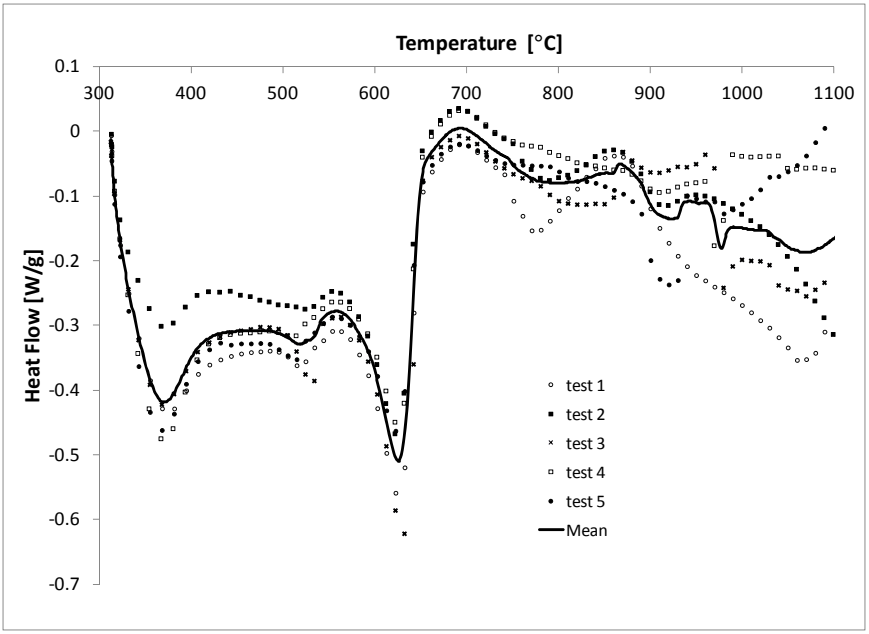

Figure 3-14: DSC Data Presented Displayed as Heat Flow as a Function of Temperature

The heat capacities for the initial dried material and the char components were calculated from DSC data collected with the procedure described previously. The DSC data were presented in units of mW/mg. The heat capacity [J/g/K] was calculated by dividing the DSC signal [mW/mg] by the true heating rate [K/s]. The heating rate set point could not be used in the heat capacity calculation because there was a transient period while the heating rate increased from zero for the isothermal phases to the set heating rate. During these transient periods the true heating rate deviated from the set heating rate. The true heating rate was calculated by the simple differentiation described in Equation 2.

$$HR = \frac{T_{n+2} - T_n}{t_{n+2} - t_n} \tag{2}$$

A region between the release of moisture and the onset of the first degradation reaction was identified as the most representative period of time to describe the heat capacity of the dried virgin cardboard material. The data could not be accurately described with a linear relationship because the extrapolated values at high temperatures were out of the range of realistic values. The mean value of the five data sets in the range 400 K to 540 K was calculated as 1.8 J/gK and was defined as the heat capacity of the initial cardboard component for all subsequent Thermakin models. The region of the heat capacity curve that was used to determine the heat capacity is displayed in Figure 3-15. The values defined by the heat capacity curve of Figure 3-15 are normalized by the initial mass of the material.

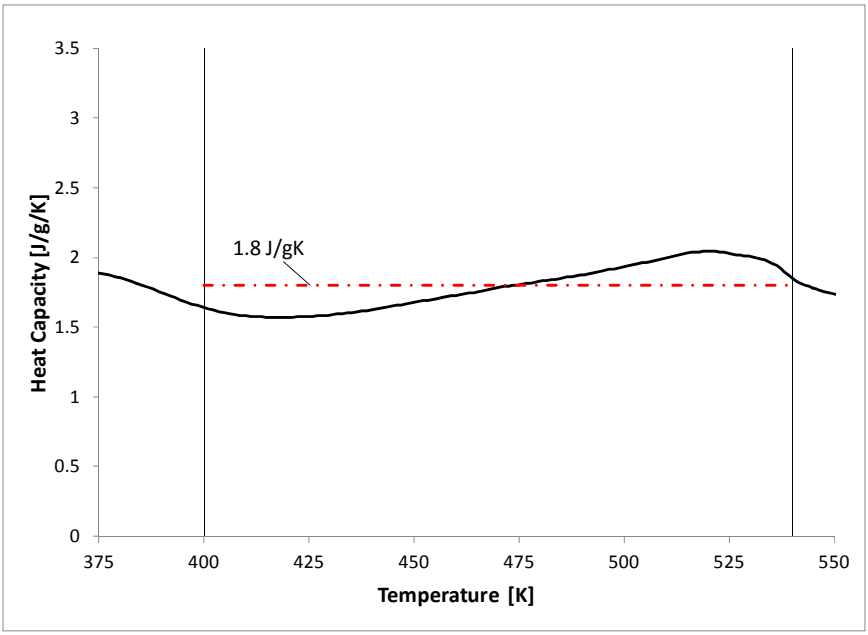

Figure 3-15: Mean Heat Capacity Curve for the Initial Dried Material calculated from DSC Data

The heat capacity for the char was not necessarily accurately depicted by the DSC because the mass of the sample was undergoing a change over the temperature range from 700 K to the end of the test. A non-steady mass indicates one or several reactions were occurring when the char components were present. The energy absorbed in the reaction caused the actual heat capacity of the char to deviate to lower values from the values calculated here.

The heat flow values in the range 700 K – 870 K were considered the steadiest portion of the DSC data when the only the char components were present. The values in this range were identified as the best representation of the heat capacity of the char components. The mean of the five data sets in the range 700 – 870 K was 1.28 J/gK and was defined as the heat capacity of the char components for all subsequent Thermakin models. The heat capacity curve for the char components produced during pyrolysis is presented in Figure

3-16. The heat capacity data in the figure are normalized by the mass of the sample measured at 700 K.

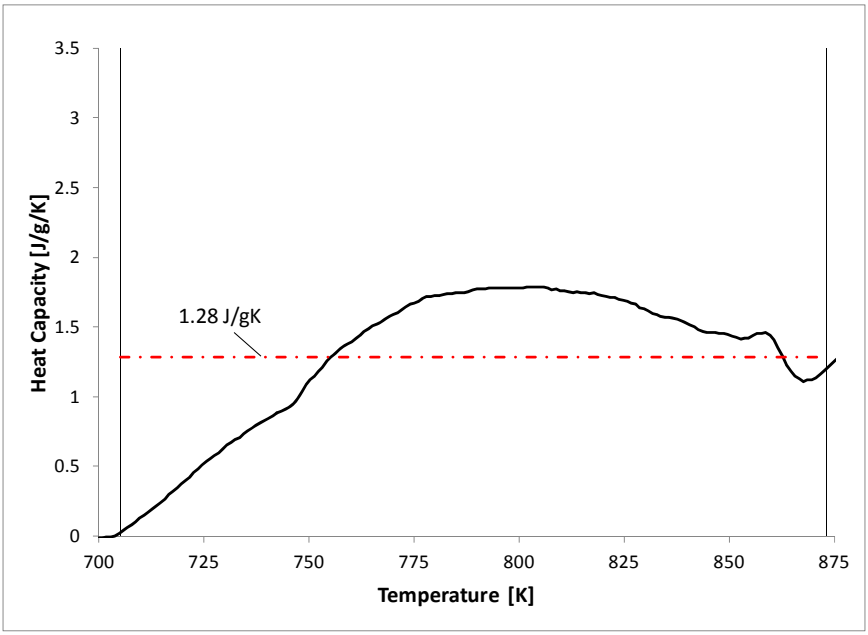

Figure 3-16: Mean Heat Capacity Curve for the Char Components Calculated from DSC Data

The heat capacity of the intermediate species could not be determined from the DSC test data because the intermediate species exists during the part of the pyrolysis process with the largest mass loss rate variations, which makes it hard to separate the heat absorption attributed to the heat capacity of the material from the heat absorption attributed to thermal degradation. It was assumed that the properties of the components evolved in a sequential manner similar to the evolution of the corrugated cardboard components from the initial state to the final char state. The heat capacity of the intermediate species was defined as the mean of the initial material heat capacity and the char heat capacity. The intermediate species heat capacity was calculated as 1.54 J/gK and defined as such in all subsequent Thermakin models.

The thermal conductivity of the gaseous pyrolysis products was the only parameter assigned to the gaseous species that affected the model. The heat capacity of the gaseous pyrolyzate was defined as equivalent to the char heat capacity, 1.28 J/gK.

The mean curve from the data collected in five PCFC tests is presented in Figure 3-17. Though there is some scatter between the tests all the heat release rate profiles show similar trends. A qualitative comparison between the mass loss rate profiles from the TGA tests and the heat release rate profiles from the PCFC tests show agreement in the major features of each data set. The heating rate of the PCFC tests was much higher than the heating rate for the TGA tests. The temperature of the peak heat release rate appears to be shifted higher than the temperature of the peak mass loss rate.

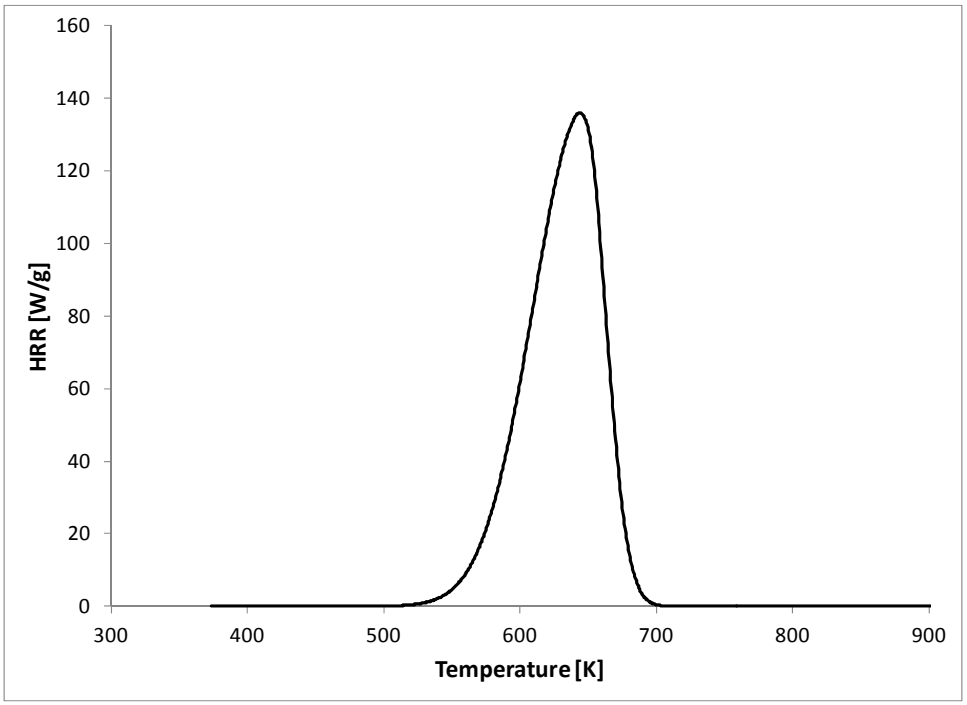

Figure 3-17: Mean Curve of Micro-Combustion Calorimeter Data Collected for Corrugated Cardboard

One conclusion that can be made regarding the MCC data is that the first reaction in the four reaction mechanism is not associated with a heat release rate due to a

combustion process. The lack of a heat release rate confirms that the first peak in the mass loss rate data curve does not involve the gaseous volatiles from the corrugated cardboard and only involves the evaporation of moisture from the sample.

4. Modeling

4.1 Milligram-Scale Modeling

The milligram-scale experiments were simulated with Thermakin in the thermally thin mode, as discussed in an earlier section. The top and bottom boundary conditions for the simulations conducted in the thermally thin mode were defined such that the temperature at the boundary followed the same idealized linear heating rate profile as the physical test heating rate set program. The convection coefficient for both boundary conditions was defined as 100,000 W/m^2K. This convection coefficient and the ambient temperature program led to the temperature throughout the simulated sample to be uniform and equal to the outside temperature. The mass flow boundary condition at the upper surface was defined with a linear equation to remove the gases evolved during pyrolysis of the solid sample. The bottom boundary condition was defined such that no mass was transferred in to or out of the sample.

4.1.1 Pyrolysis Kinetics Modeling

The thermogravimetric data collected in a pure nitrogen atmosphere were used as the basis for a corrugated cardboard pyrolysis model constructed with the Thermakin program. The parameters in the Thermakin program were defined to eliminate the effects of heat transfer and mass transport. Under the conditions defined for the milligram-scale model, the material properties of the sample did not affect the prediction. The mass loss rate curve was initially fit with a single reaction mechanism for simplicity, but it was determined that a single reaction could not accurately depict the processes involved in the thermal degradation of the cardboard sample. A four reaction mechanism was found to be the simplest curve that could encompass all the features of the curve. It is important to

note that the reaction mechanism and the components included in the mechanism are not necessarily physically significant. The mechanism is intended to mathematically mimic the mass loss rate data in the simplest form possible and relies on model-specific kinetics that can reproduce the experimental curve.

The mass loss rate data collected during the TGA tests was fit with an apparent reaction mechanism that consisted of four Arrhenius-type first-order reactions presented in Table 4-1. The reaction scheme is provided in the diagram in Figure 4-1, where k_i denotes the reaction rate constant for reaction number i. Arrhenius reactions and the reaction rate constant are defined later in this section.

Table 4-1: Pyrolysis Reaction Mechanism

#	Reaction Equation	A (sec^{-1})	E_a (J/mol)
1	$H_2O_\ell \rightarrow H_2O_g$	6.14	2.35×10^4
2	$CB_a \rightarrow 0.9CB_b + 0.1CB_{volatiles}$	7.95×10^9	1.3×10^5
3	$CB_b \rightarrow 0.37CB_{char,1} + 0.63CB_{volatiles}$	2.0×10^{11}	1.6×10^5
4	$CB_{char,1} \rightarrow 0.59CB_{char,2} + 0.41CB_{volatiles}$	2.61×10^{-2}	1.7×10^4

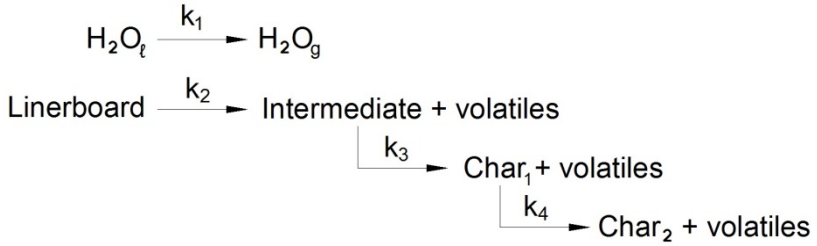

Figure 4-1: Reaction Scheme for Corrugated Cardboard Pyrolysis

The best agreement between the prediction and the data required the initial corrugated cardboard sample to contain 98% of component CB_a and 2% of H_2O_ℓ. The

water was assumed to be bound in the components of the material and was defined as a solid in the model to avoid unnecessary complication. The first reaction corresponds to the drying and liberation of bonded water in the virgin material and does not contribute considerably to the mass loss. Reactions 2-4 represent cardboard decomposition as a sequential process. Reactions 2 and 3 describe the large peak in the mass loss rate curve. The material resulting from each of these two reactions are describe by generic intermediate species between the dried virgin material and the final residual carbon char, depicted in the table as CB_b and $CB_{char,1}$. Reaction 4 corresponds to the gradually decreasing tail of the mass loss rate curve. The first and fourth reactions are considerably slower than the other two reactions, resulting in considerably lower pre-exponential factors. The experimental TGA data is provided with the simulated TGA mass loss rate profile along with the contributions due to single reactions in Figure 4-2.

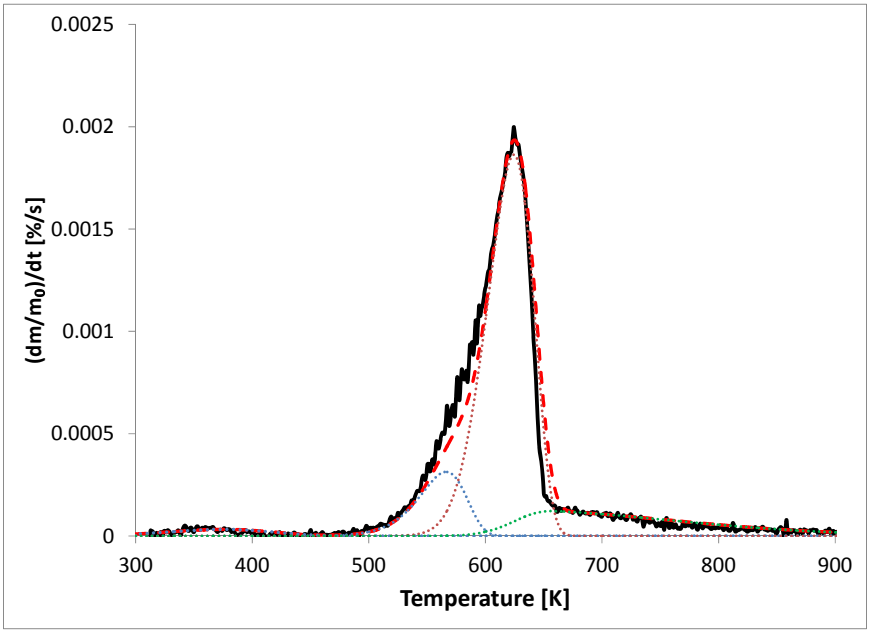

Figure 4-2: Thermogravimetric Data Collected in a Pure Nitrogen Atmosphere Plotted with the Curve Predicted by the Thermakin Program and the Contributing Reactions

The average experimental data is depicted in the figure as the thick black line. The thick dashed line corresponds to the total simulated mass loss rate based on the reaction mechanism outlined in Table 4-1. The dotted lines indicate the contribution of each reaction in the mechanism to the total mass loss rate, with each subsequent reaction corresponding to a higher temperature peak mass loss rate.

The reaction mechanism is described as an apparent reaction scheme because an attempt has not been made to describe the actual reaction scheme and identify the actual components of the cardboard material. In fact, there are likely hundreds of reactions involving dozens of species in the actual thermal degradation of corrugated cardboard. No study has successfully identified all species present or all of the reactions taking place in the thermal degradation of a lignocellulosic material and such an analysis is clearly beyond the scope of this work.

Arrhenius reaction rate constants, k, are mathematically described by Equation 3. In the equation, A is the pre-exponential factor with units of frequency [sec^{-1}]. E_a is the activation energy with units [J/mol] and is defined as the minimum amount of energy required for the reaction to be initiated. R is the universal gas constant. For a single-reaction mechanism, the temperature T corresponds to the pyrolysis temperature, but in a multiple reaction scheme, like the one devised for this investigation, T corresponds to a representative temperature for the reaction taking place. The reaction rate constant is left as a function of temperature to make the reaction rate and, in effect, the production of volatile species a function of temperature.

$$k = A \exp\left[\frac{-E_a}{RT}\right] \tag{3}$$

The reaction kinetic mechanism that was fit to the TGA data evolved from a single reaction, global scheme to a multi-step semi-global scheme. The single reaction scheme was initially used in an attempt to minimize the number of unknown parameters that required measurement or fitting. It was clear from analysis of the single-reaction scheme and comparison to the TGA data that a more representative fit could be determined with the inclusion of more reactions. The resulting multi-step, semi-global scheme consisted of four first order reactions.

All the gaseous volatiles liberated from the condensed phase cardboard have been grouped into a single simplified form in the pyrolysis mechanism and are described in Table 4-1 as $CB_{volatiles}$. The formation of high molecular mass volatiles (tars) and subsequent cracking were not considered during the formulation of this reaction scheme. It is assumed that those processes are grouped into the intermediate reactions in the current reaction mechanism. This was done to decrease the number of unknown parameters in the model that required measurement or fitting and improve the simplicity of the model by eliminating degrees of freedom.

The properties of the gaseous volatiles had little impact on the model because the mass of the solid phase components was much larger than the mass of the gases. The heat transfer due to advection of gases through the fuel was effectively neglected by assuming the gases exited the computational domain instantaneously. The heat capacity of the representative gas was the only factor that was found to affect the model. The determination of the heat capacity of the gaseous volatiles was discussed in an earlier section.

Initially a single reaction mechanism was attempted and the curve fitting was focused on the main peak. The procedure for fitting the thermogravimetric data to determine the kinetic parameters A and E_a required the determination of the pyrolysis temperature and the maximum mass loss rate from the mass loss rate data. The pyrolysis temperature was considered the temperature at which the peak mass loss rate occurred. A generic value of 2.0 x 10^5 J/mol was used as the initial value for the activation energy. The Arrhenius reaction rate equation was manipulated in the following steps. The definition of the reaction rate in the Equation 4 was used to describe the rate of change of the total mass of the sample by the reaction rate constant and the total mass of the sample. All reactions were assumed to be of first order (n=1)

$$\frac{dm}{dt} = k[m]^n \tag{4}$$

The definition of the reaction rate was manipulated to get an expression for the reaction rate constant.

$$k = \frac{dm}{dt}/[m] \tag{4a}$$

Combining the definition of the reaction rate constant from Equation 3 with the definition from Equation 4a yields Equation 5.

$$\left(\frac{dm/dt}{[m]}\right) = A \exp\left[\frac{-E_a}{RT}\right] \tag{5}$$

The method defined by the equations above was only suitable for a single reaction mechanism. The peak mass loss rate, the temperature that corresponded to the peak mass

loss rate, and the total mass of the sample at the peak mass loss rate were easily determined from the data. The manipulated Arrhenius equation related the pre-exponential factor to the activation energy through several parameters that were constant at the peak mass loss rate. A, E, and, to a lesser extent T, were varied to find a suitable fit. Upon determining the kinetic parameters that provided the most representative fit, it was evident that gradual increase of the mass loss rate to the first peak and the slow decay of the mass loss rate in the tail of the curve could not be adequately represented by a single reaction mechanism.

The three distinct processes that were identified in the mass loss rate curve led to the conclusion that a minimum of three reactions would be required to mathematically describe the thermogravimetric data. The peak of the mass loss rate curve was identified as the most important feature of the curve and, as a result, the first target for fitting. The kinetic parameters identified through fitting the data with a single reaction scheme were adjusted in combination with the inclusion of a second reaction to describe the gradual increase in mass loss rate. An adequate fit was determined for the peak with two reactions.

The slow decay of the mass loss rate in the tail of the mass loss rate curve was identified as the second target for fitting. It was evident early in the fitting process that the reaction describing the tail of the curve would occur partially simultaneously with the reactions describing the peak, and the reaction describing the peak was adjusted simultaneously with the reaction describing the tail of the curve. Three reactions were found to accurately describe the main peak and the gradual decay in the tail of the mass loss rate curve.

The first maximum in the mass loss rate curve was the final feature of the thermogravimetric data that was fit with kinetic parameters. The first maximum was independent of the other features in the thermogravimetric data for the pyrolysis of corrugated cardboard. The kinetic parameters that were already fit to the data were unaffected by the kinetic parameters for the first reaction and required no modifications.

The kinetic parameters that define the reaction mechanism are dependent on the testing conditions for the TGA tests conducted to determine the mass loss rate profile. The reaction mechanism that was fit to the data collected with a heating rate of 10 K/min was tested against the TGA data collected with a heating rate of 5 K/min. The mass loss profile collected in the tests conducted with a heating rate of 5 K/min is provided in Figure 4-3 with the corresponding predicted mass loss rate profile generated with the Thermakin program This comparison was made to investigate the sensitivity of the reaction mechanism to the heating rate in the thermogravimetric tests.

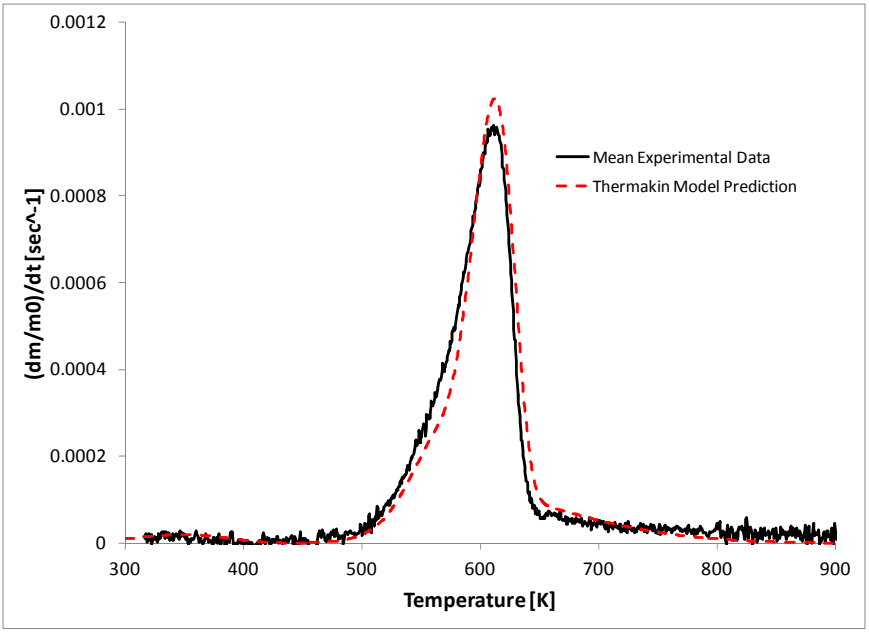

Figure 4-3: Thermogravimetric Data Collected in a Pure Nitrogen Atmosphere with Heating Rate of 5 K/min Presented with a 66-Second Moving Average Compared to the Thermakin Model Prediction

The Thermakin prediction that applies the reaction mechanism determined from the data collected at a heating rate of 10 K/min to the testing conditions with a heating rate of 5 K/min appears consistent with the thermogravimetric data collected at a heating rate of 5 K/min. It can be concluded that the reaction mechanism used for all the models in this investigation is not sensitive to small magnitude variations in the heating rate.

4.1.2 Pyrolysis Thermodynamics Modeling

The effective heat of reaction for the pyrolysis of corrugated cardboard was calculated from the DSC heat flow data. A baseline curve was constructed to represent the energy absorbed by the sample to raise the temperature of the material. The baseline accounted for the change in the heat capacity of the sample material as the material degraded. The contribution of each component to the total mass of the sample was calculated with the Thermakin milligram-scale model using the reaction mechanism determined from the thermogravimetric data. The composite heat capacity was assumed to be additive and each species contributed to the composite heat capacity an amount proportional to the mass fraction of that species. The average heat flow curve collected in the DSC tests is plotted in Figure 4-4 with the calculated heat flow baseline. The baseline was calculated assuming adherence to the ideal heating rate defined as the set program in the DSC tests.

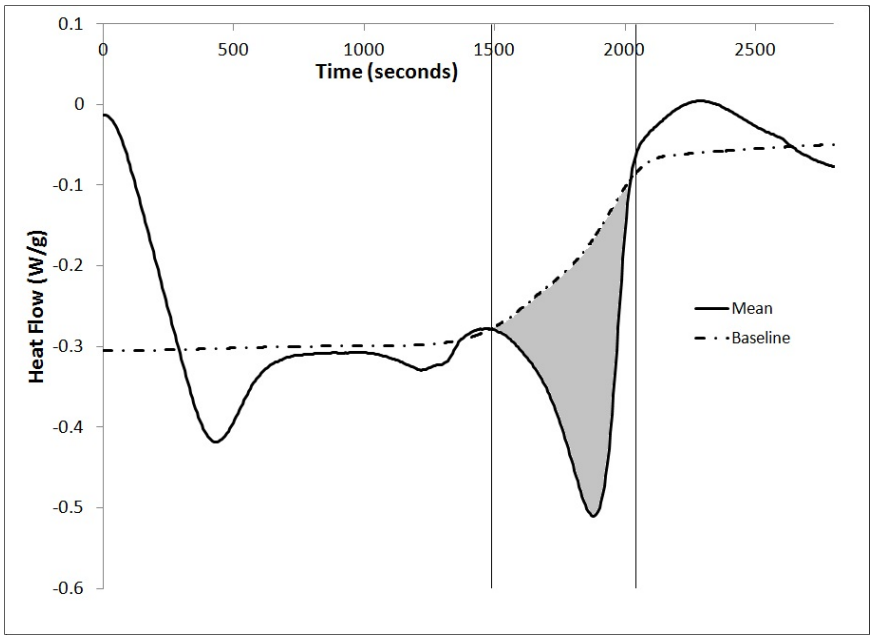

Figure 4-4: Average Heat Flow Curve Plotted with the Heat Flow Baseline Accounting for the Heat Capacity of the Components

The effective heat of reaction for the pyrolysis process was defined as the integral of the difference between the DSC signal curve and the baseline. The range of the integration was from approximately 560 K to 650 K, which corresponded to 1488 seconds and 2040 seconds, respectively. This range corresponded to the largest peak in the DSC data and the largest magnitude mass loss in the TGA data. The other variations in the heat flow curve were attributed to changes in the sample heat capacity, sample structure, actual heating rate, or to insignificant reactions and were neglected. The effective heat of reaction determined through the integration of the heat flow data was -113.4 J/g. The effective heat of reaction was calculated according to the initial mass of the sample and was normalized by the fraction of the initial mass remaining when the reaction occurred. The effective heat of reaction was corrected to -126 J/g.

The reaction corresponding to the evaporation of moisture was assigned a heat of reaction equal to the enthalpy of vaporization [37]. The effective heat of reaction for the

pyrolysis process was assigned entirely to the reaction associated with the largest mass loss and mass loss rate (reaction 3). The heat flow data curve collected in the DSC tests is plotted in Figure 4-5 with the heat flow curve predicted by the Thermakin program. The heat flow curve generated by the Thermakin program was parameterized with the reaction mechanism, heat capacities for each component, and the heats of reaction for the first and third reactions. The major deviations from the experimental data were caused by variations in the heating rate and a decay in the sensitivity of the measurement at high temperatures. The agreement between the experimental data and the prediction is good considering the simplifications made.

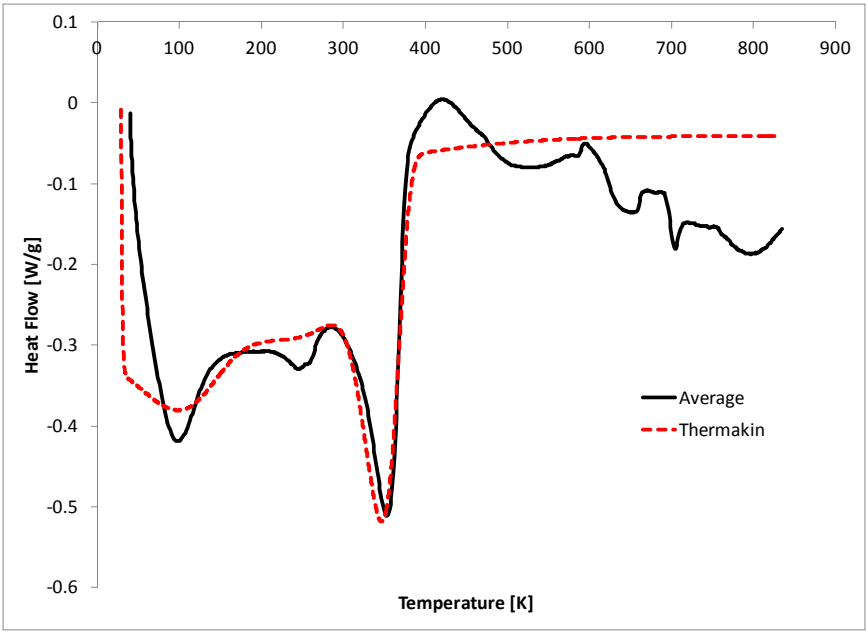

Figure 4-5: Mean Heat Flow Curve Collected in DSC Tests Plotted with the Heat Flow Curve Predicted with the Thermakin Program

4.1.3 Comparison to Other Studies

The kinetic mechanism that was fit to the thermogravimetric data collected at a heating rate of 10 K/min was a four reaction mechanism. No similar four reaction mechanisms that accounted for the release of moisture could be found in the literature for any lignocellulosic material. Bryden et al. and Hagge et al. developed one step parallel

reaction models that accounted for the production of moisture although the reaction predicted by the investigators was considerably faster than the moisture vaporization reaction determined in the current study with A = 7.38e5 sec^{-1} and E_a = 1.065e5 J/mol [11]. Salvador, et al. accounted for moisture in a bench-scale model with kinetic parameters A = 1.46e5 sec^{-1} and E_a = 6.013e4 J/mol [24]. In both studies that accounted for drying kinetics, the reactions were much faster and required a higher activation energy than the drying reaction determined in the current study. These difference could be attributed to test conditions or different characteristics of the samples.

The kinetic parameters fit to thermogravimetric data available in the literature were reviewed considering the sample material, test method, reaction scheme, and heating rate. None of the available reaction mechanisms, regardless of test conditions, included a reaction describing char pyrolysis similar to the reaction determined in the current study. The char pyrolysis reaction determined in this study was considerably slower than any reaction found in the literature [12] [11].

Few researchers employed multiple consecutive reactions in a single reaction pathway to describe the pyrolysis of lignocellulosic materials [8] [9] [21]. David et al. performed a similar thermogravimetric study on cardboard to determine a reaction mechanism for the data collected at a range of heating rates [8]. The study fit the thermogravimetric data with an optimization algorithm assuming six different reaction schemes.

There were two reaction mechanisms assumed by the investigators that resembled the reaction mechanism determined in the current study. The reaction mechanism that

was accepted in the study had two reactions, and the reaction scheme that was rejected had three reactions. The reaction mechanisms with kinetic parameters fit to the data collected at 10 K/min are provided in Table 4-2 and Table 4-3, respectively.

Table 4-2: Two Reaction Mechanism Fit to TGA Data for Cardboard - Adapted from [8]

#	Reaction Equation	A (sec^{-1})	E_a (J/mol)
1	$C \rightarrow 0.42I_1 + 0.58G$	3.98×10^8	1.074×10^5
2	$0.42I_1 \rightarrow 0.34\text{Char} + 0.66G$	3.80×10^5	6.95×10^4

Table 4-3: Three Reaction Mechanism Fit to TGA Data for Cardboard - Adapted from [8]

#	Reaction Equation	A (sec^{-1})	E_a (J/mol)
1	$C \rightarrow 0.13I_1 + 0.87G$	7.53×10^8	1.102×10^5
2	$0.13I_1 \rightarrow 0.35I_2 + 0.65G$	42.0	2.27×10^4
3	$0.35I_2 \rightarrow 0.33\text{Char} + 0.67G$	5.03×10^3	3.27×10^4

The reaction mechanisms determined by David et al. appear to be closest to the reaction mechanism determined in the current investigation although the kinetic parameters and stoichiometric coefficients do not align with those determined in the current investigation. The two reaction mechanisms determined by David, et al. are provided in Figure 4-6 along with the experimental data collected at a heating rate of 10 K/min and the kinetic mechanism used in the current investigation.

The mass loss rate curves predicted by the kinetics developed by David, et al. are shifted to lower temperatures. Neither mechanism predicts the char pyrolysis in the gradually decreasing tail of the curve that was observed in the TGA tests.

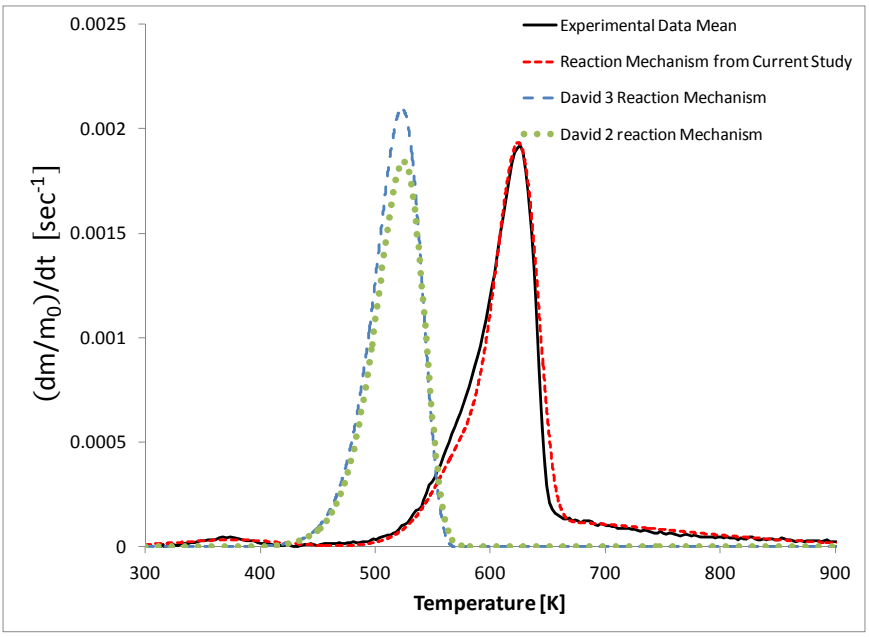

Figure 4-6: Comparison of Mass Loss Rate Data Predicted by Kinetics Determined by David, et al. to Mass Loss Rate Data Predicted by the Kinetic Mechanism for the Current Study

The kinetic parameters determined by Gupta and Müller based on thermogravimetric data for cardboard tested with a heating rate of 10 K/min in argon were not similar to the kinetic parameters determined in the current study. The gas flow rate for the TGA tests conducted by Gupta and Müller was 5 mL/min, though the investigators concluded the effect of the flow rate was negligible. Gupta and Müller fit parameters for two successive reactions to describe the pyrolysis of cardboard, but the discrepancy between the parameters determined in the current study and in that study was several orders of magnitude [9]. The residual masses resulting from the tests conducted in that study were smaller in inert atmospheres than for oxidative atmospheres. This result is counter to the results and conclusions obtained in the current study.

Wu, et al. conducted thermogravimetric analyses on mixed papers prevalent in municipal solid waste. The TGA tests were conducted at a heating rate of 5 K/min in an inert atmosphere. The investigators used a two reaction scheme to describe the pyrolysis

process for several paper products. A representative reaction mechanism is provided in Table 4-4.

Table 4-4: Representative Two Reaction Mechanism Determined by Wu et al. - Adapted from [21]

#	Reaction Equation	A (sec^{-1})	E_a (J/mol)	n (sec^{-1})
1	$P \rightarrow I + gases$	1.1×10^{12}	1.72×10^{5}	1.6
2	$I \rightarrow C + gases$	1.1×10^{9}	1.71×10^{5}	1.8

The kinetic parameters predicted by Wu and et al. were generally similar to the kinetic parameters determined in the current study. The reaction mechanism for the current investigation was constructed under the assumption that all reactions were of the first order. The most significant deviation from the current study by the mechanisms used by Wu, et al. was the use of reaction orders ranging from 1.14 to 2 [21].

4.2 Bench Scale Modeling

The bench-scale model was constructed under the assumption that the pyrolysis process for flaming combustion was non-oxidative. This assumption proved to be valid under the circumstances and orientations tested. This assumption was based on the theory pertaining to diffusion flames and the oxygen concentration on the fuel-rich side of the diffusion flame. Experimental data also suggested that the oxygen did not react with the sample while the flame covered the sample surface.

The average temperature throughout the sample for the cone calorimeter tests at the point when the sample transitioned from fully flaming to approximately half the sample covered with the flame was determined from thermocouple data. The temperatures ranged from 500°C at 20 kW/m^2 to 620°C at 60 kW/m^2. The mass

remaining in the cone calorimeter was 31.4% on average in the 20 kW/m^2 tests and 21.3% on average in the 60 kW/m^2 tests. The total mass data collected in TGA tests conducted in nitrogen were compared to the total mass data at the average temperatures of the samples in the cone tests. The residual mass was approximately 23.5% of the initial mass at 500°C and 20.9% of the initial mass at 620°C in the TGA tests. The reactions observed in the TGA tests conducted in air were completed by 500°C and the residual mass was steady at 4% of the initial mass. It is likely that if oxygen was allowed to react with the charred fuel in considerable quantities, the mass data collected in the cone calorimeter tests would be lower than the masses from the TGA tests conducted in pure nitrogen because the oxidation reaction is much faster than inert pyrolysis at the temperatures observed. The data collected from the TGA tests conducted in oxidizing atmospheres are provided in Appendix I - Oxidative Pyrolysis.

In the construction of a bench-scale model for burning, the physical properties of the tested material must be established as input parameters. These parameters include emissivity, thermal conductivity, and absorption coefficient for all components as well as the critical mass flux for ignition, heat flux from the flame, and information about the geometry of the sample. It has been noted in several investigations that these properties are not widely available in the literature, and, in the case of a composite material, the literature values that are obtained may not accurately describe the material of interest. A detailed description of the tested material is crucial to the process of understanding its burning characteristics including time to ignition, time to flaming, and time to flame extinction as well as the temperature distribution throughout the material as a function of time.

The model was parameterized according to a linear evolution in which the complexity of the model was increased to make the model predictions more consistent with experimental data at each phase. In each phase, assumptions were made to simplify the model such that a single input parameter was changed to improve the fit between the model and the target data. This fitting procedure was repeated with several sets of data to determine the unknown parameters that were not directly measured. Each successive phase of the model development built on the preceding phase by improving the definition of a single parameter. Each phase of the model development is present here as a logical progression of phases with increasing complexity.

4.2.1 Boundary Conditions

The boundary condition for the top surface was defined with a radiative heat flux according to the heat flux set point for the cone calorimeter tests. The convective heat transfer coefficient at the upper surface was defined as 10 W/m^2K and the ambient temperature was defined as 300 K to allow convective cooling from the surface as the simulated incident heat flux caused the temperature of the sample to increase prior to ignition. A mass transport relationship was defined at the upper surface to provide no impedance to the escape of pyrolyzate gases and water vapor.

A flame was assumed to cover the entire surface of the sample after a critical mass flux of volatile gases was achieved. The flame was defined as part of the top surface boundary conditions and the details concerning the flame heat flux boundary conditions were discussed in an earlier section. After ignition, the convective heat transfer coefficient at the upper surface boundary was defined as zero because convective cooling does not occur in the presence of the flame.

Ignition is treated as a change in the heat flux boundary condition at the upper surface of the simulated sample in Thermakin. The change in the boundary condition is triggered by a critical mass flux of the gaseous volatiles evolved from the pyrolysis process. The existence of a critical mass flux for sustained ignition is based on physical theory and corresponds well to experimental observations. The critical mass flux was converted to a heat release rate with Equation 6 using the effective heat of combustion approximated from the cone calorimeter data as presented in Table 3-1. The critical heat release rate was considered acceptable in the range 10-20 kW/m^2 [28] [27]. The average value of 15 kW/m^2 was used for the critical heat release rate for the bench-scale model.

$$\dot{q}''_{crit} = \Delta H_c \dot{m}''_{crit} \quad (6)$$

The bottom boundary of the corrugated cardboard sample was insulated in the cone calorimeter tests with 30 mm of Thermal Ceramics Kaowool PM Low Temperature Board. Chaos, et. al. found heat loss from the back boundary can significantly affect the results predicted by a bench-scale model [31] [30]. It is important to accurately characterize the back boundary condition in the model. The insulation was simulated in the Thermakin model with a 15 mm layer with the thermal properties reported for Kaowool PM by the manufacturer and listed in Table 6. A sensitivity analysis on the thickness of the insulation was conducted and it was determined that a 15 mm thick simulated layer was sufficient. The thermal conductivity of Kaowool was approximated by the cubic polynomial shown in Figure 4-7. The properties presented for Kaowool were adopted for all models in this investigation.

Table 4-5: Thermal and Material Properties for Kaowool PM

Density	256 kg/m3
Specific heat capacity	1.07 kJ/kgK (980°C)
Thermal conductivity (W/m-K)	0.0576 (at 260°C)
	0.085 (at 538°C)
	0.125 (at 816°C)
	0.183 (at 1090°C)

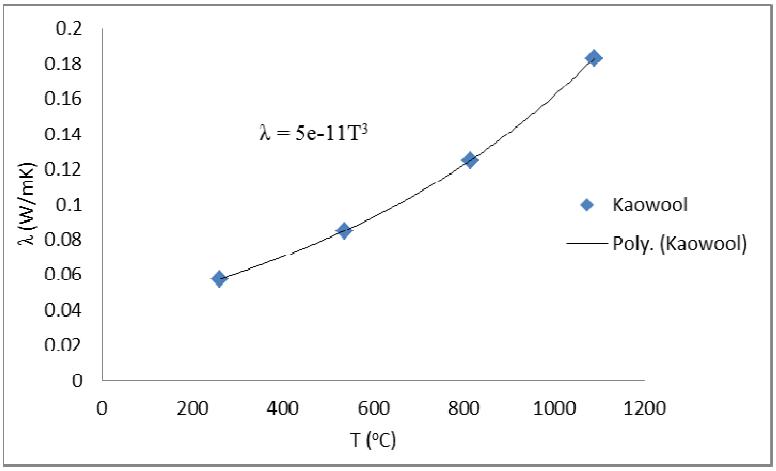

Figure 4-7: Curve Fit of the Temperature-Dependent Thermal Conductivity of Kaowool PM

The properties of Kaowool PM board were validated by cone calorimeter tests conducted with thermocouples inserted directly beneath the corrugated cardboard sample, under the top sheet of Kaowool, and under the second sheet of Kaowool. The temperature profile at each of these locations was extracted from the Thermakin prediction and plotted against the experimentally collected data. The temperature profiles at all locations below the sample and in the insulation predicted by the Thermakin model agreed with the collected temperature data. These data are presented in a later section.

4.2.2 Thermal Conductivity of Initial Material

4.2.2.1 Homogeneous Model

The thermal conductivity of the corrugated cardboard was evaluated as one of the most important physical properties in fire modeling particularly with respect to the time to ignition [29]. A homogeneous model of the corrugated cardboard with a single component that had a single density and a single thermal conductivity was considered and developed in parallel with a non-homogeneous model to assess the ability of the assumptions in each model to describe the physical situation of interest. The models were constructed to provide a comparison against the temperature distribution data collected before ignition with the surface of the sample painted black at a heat flux of 20 kW/m^2. The only parameter that was adjusted in these models to improve the agreement between the prediction and the experimental data was the thermal conductivity of the initial components.

Temperature data collected before ignition with the sample surface painted black with an incident heat flux of 20 kW/m^2 were used as the target for fitting the model prediction by varying the thermal conductivity of the virgin species. The emissivity of the paint used to cover the sample was specified as 0.95 by the manufacturer. The thermal conductivity was adjusted and the temperature profile predicted by the model was compared to the experimental data.

The homogeneous model could not accurately predict the experimental temperature distribution with a single, constant thermal conductivity. The physical non-homogeneous structure likely caused the inaccuracy of the homogeneous model. The

largest volumetric component in the sample was air, which is a relatively poor thermal conductor, but acts as a good medium for radiative heat transfer. An effective method to simulate this possible radiative heat transfer was the radiation-diffusion approximation. The radiation-diffusion approximation consisted of defining the thermal conductivity as a function of temperature to include the contribution from radiation along with the contribution. The contribution from radiation was included along with the contribution from conduction. The details of this approximation are explained later in this chapter.

The thermal conductivity that provided the most consistent agreement between the model prediction and the experimental data was $0.09 + 5e\text{-}11\ T^3$. The model prediction for the temperature distribution during the pre-ignition heating is provided in Figure 4-8 with the experimental data collected with the surface of the sample painted black. The uncertainty in the position of each thermocouple is indicated by dashed and dotted lines on either side of the solid line denoting the model prediction.

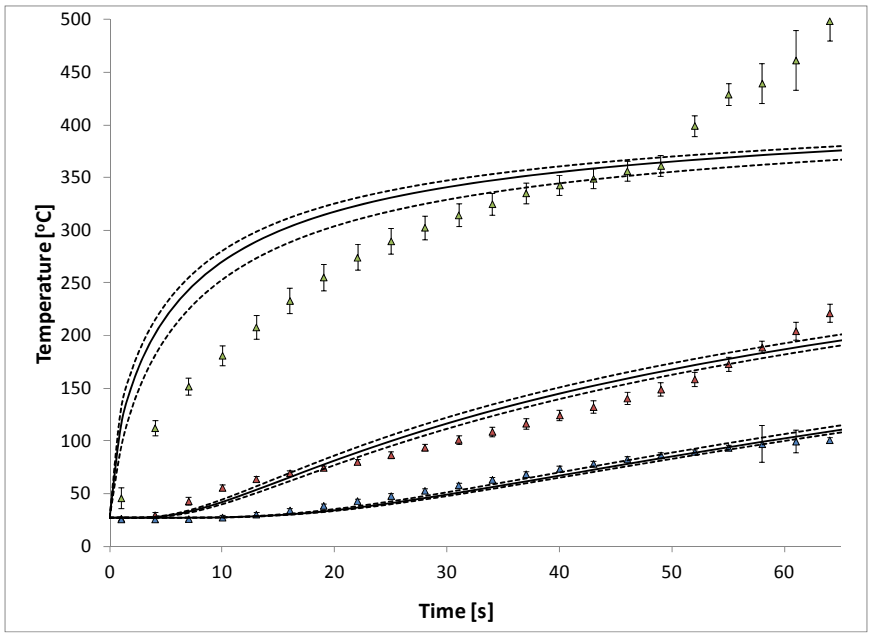

Figure 4-8: Temperature Profile Data Collected with the Surface Painted Black at 20 kW/m2 Presented with the Homogeneous Model Prediction

4.2.2.2 Non-Homogeneous Model

The non-homogeneous bench-scale model consisted of five layers composed of three different materials, similar to the structure of the actual corrugated cardboard sample. The linerboard layers were simulated by a material with a density equal to the measured density of the linerboards. The densities of the fluted medium sections were defined as the mass of the flute material normalized by the volume of the entire section

Each initial component was assigned the density determined for that component as explained in an earlier section. The non-homogeneous model was constructed with a single, constant thermal conductivity to describe all the initial components. The thermal conductivity was adjusted and the predicted temperature profile was compared to the temperature profile measured during the preheating of the material before ignition.

The thermal conductivity in the non-homogeneous model that provided the most consistent agreement between the model prediction and the experimental temperature

profiles was 0.1 W/mK. The non-homogeneous model prediction for the pre-ignition heating for the case with all emissivities defined as 0.95 is presented with the experimental data in Figure 4-9.

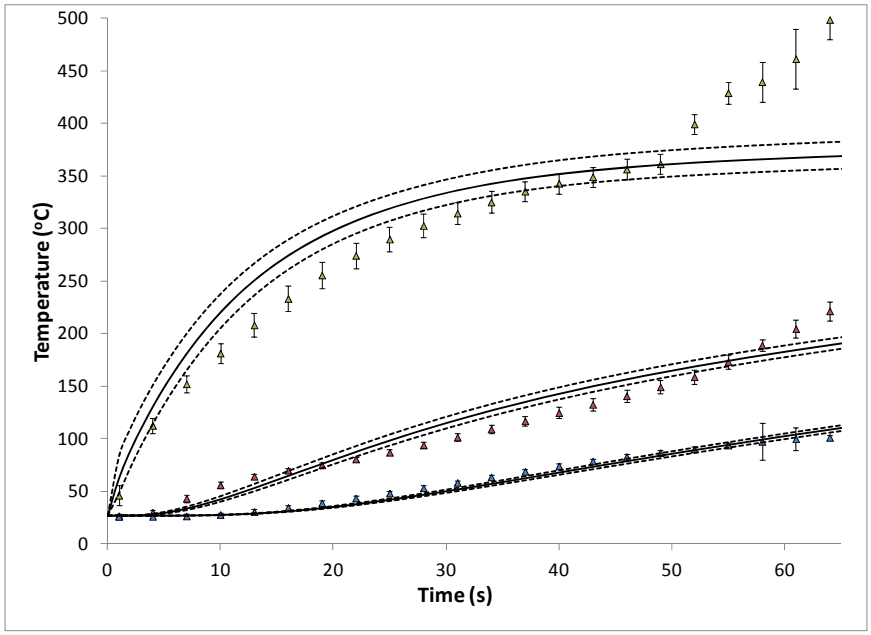

Figure 4-9: Temperature Profile Data Collected with the Surface Painted Black at 20 kW/m2 Presented with the Non-Homogeneous Model Prediction

The agreement between the non-homogeneous model and the collected data was determined to be better than the agreement found with the homogenous model. The simulated curves from the non-homogeneous model were considerably closer to the experimental data than those predicted by the homogenous model. It was concluded that the homogeneous model could not achieve the accuracy desired for this investigation and was disregarded in further phases of the development of a bench-scale model.

4.2.3 Emissivity of All Components

Temperature data collected before ignition with the unaltered corrugated cardboard samples were used as the target for fitting the emissivity of the virgin material components. The thermal conductivity values were set equal to 0.1 W/mK, as

determined in the first phase of the model evolution. With the thermal conductivity defined as a constant value for the virgin material, the emissivity of all layers of the virgin material was varied to minimize the difference between the model prediction and the target experimental data.

The best agreement between the model prediction and the experimental data was achieved with the emissivity of the initial components set to 0.7. The predicted temperature profiles generated with an initial emissivity value of 0.7 are provided in Figure 4-10 presented in comparison with the temperature profiles collected in cone calorimeter tests with unaltered samples at a heat flux of 20 kW/m^2.

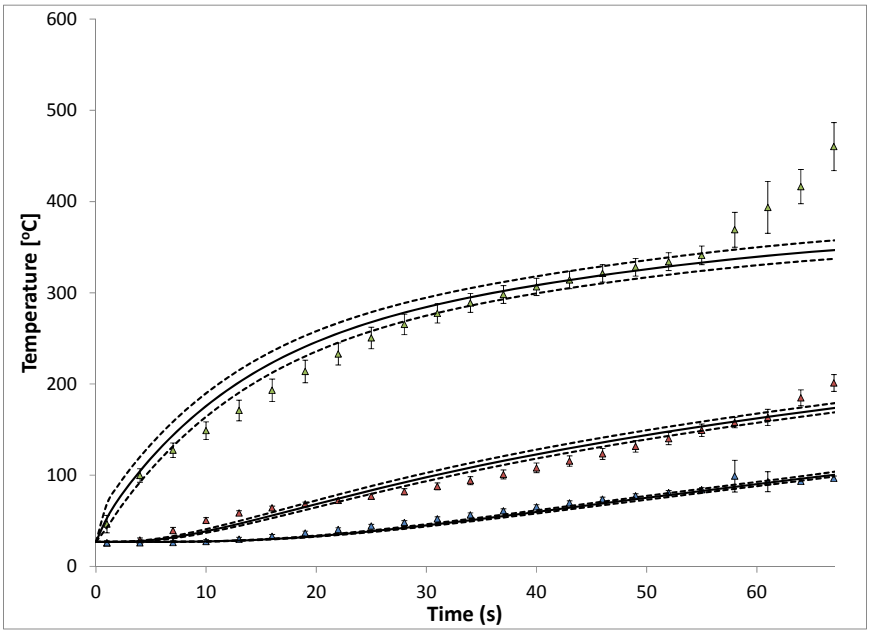

Figure 4-10: Temperature Profile Data Collected in Unaltered Material at 20 kW/m2 Presented with the Model Prediction

A recent study has reported that, for many materials, including lignocellulosic materials, absorptivity (i.e. emissivity) in the 8-10 μm range lies within the range $0.8 < \varepsilon_s < 1$ for both virgin material and char [3]. The value that predicted temperature profiles

that most closely agreed with the experimental data was close to this range of emissivity values and was accepted for all subsequent model curve fits.

4.2.4 Thermal Conductivities of the Char Components

The char components were characterized by a highly porous structure and low densities. The temperatures at which the char was formed and degraded to lower-density char were sufficiently high enough that radiation was the dominating form of heat transfer in the porous char layers. The radiation-diffusion approximation was invoked to describe the radiative heat transfer in terms of an effective thermal conductivity. The radiation-diffusion approximation [38] is stated as the following, where K is an arbitrary constant defined by model-specific parameters, σ is the Stefan-Boltzmann constant, and k' is the effective thermal conductivity.

Fourier's law for conductive heat transfer is defined as Equation 8a and represents the diffusion of energy along a spatial temperature gradient. The spatial gradient of temperature can be approximated as a finite temperature difference over a finite distance instead of the infinitesimal temperature difference for the differential defined in the equation.

$$q'' = -k\frac{\partial T}{\partial x} \approx -k\frac{\Delta T}{\Delta x} \tag{8a}$$

The Stefan-Boltzmann law for radiative heat transfer is provided as Equation 8b. The radiative heat transfer is proportional to the fourth power of the temperature of the radiating surface.

$$q'' = \epsilon\sigma T^4 \tag{8b}$$

By manipulating the Stefan-Boltzmann law and Fourier's law and introducing an effective thermal conductivity, k', to approximate the radiative heat transfer by the conductive heat transfer equation, Equation 9 is yielded.

$$k'\Delta T \approx \epsilon\sigma T^4 \Delta x \tag{9}$$

The effective thermal conductivity that describes the radiative heat transfer with Fourier's law is defined by simplifying Equation 9 and approximating ΔT as T.

$$k' \approx (\epsilon\sigma\Delta x)T^3 = KT^3 \tag{10}$$

It was assumed that the coefficient for the T^3 term of the thermal conductivity for the char components was inversely proportional to the density of each component. This assumption was based on the interpretation that the char material can be treated as a stack of dense layers separated by a low density (gaseous) medium. Higher density chars were considered to have more layers and to provide more resistance to heat transfer in this interpretation. To simplify the relationship between the density and the effective thermal conductivity, the ratio of densities between the linerboards and the fluted sections was assumed to be 10:1 and the ratio of the effective thermal conductivity coefficients was assumed to be 1:10. A similar treatment of the char that considered the radiative heat transfer within the solid was adopted in a recent verification study using the Thermakin program that produced results that agreed with experimental data [28]. The coefficients for the T^3 term of the effective thermal conductivity of the char components that provided the best overall agreement between physical data and the model prediction were 1.5e-10 for the char components corresponding to the linerboards and 1.5e-9 for the char components corresponding to the fluted medium sections.

The thermal conductivity of the intermediate components was assumed to be an average thermal conductivity between the initial components and the char components. The thermal conductivities of the intermediate components were $0.05 + 7.5e\text{-}11T^3$ for the intermediate component corresponding to the linerboards and $0.05 + 7.5e\text{-}10T^3$ for the intermediates corresponding to the fluted medium sections.

4.2.5 Emissivities of Char and Intermediate Components

The char components were assumed to be similar to graphite in composition and structure. This assumption was based on polymer thermal decomposition theory and observations of the experimental tests. The emissivity of graphite was measured at elevated temperatures as approximately 0.85 [39]. The emissivity of the char was defined in the model as 0.85.

The emissivity of the intermediate components was defined as the mean value between the initial material components and the char components. The emissivity of the intermediate components was defined as 0.775.

4.2.6 Sensitivity Analysis

A sensitivity analysis was conducted on the integration parameters, the mass transport parameters in the material and at the boundary for the model, and the heat of reaction assigned to the pyrolysis process in the model.

The cell side length for the bench-scale model was defined as 5e-5 m and the time step was defined as 0.01 seconds. The grid size and the time step were adjusted to provide better resolution for the computational grid. The model prediction was found to be independent of these two parameters because there was no significant change in the resulting predictions. It was found that the mass transport characteristics for the model

did not affect the predicted mass loss rate curves and the assumed values for the gas transport coefficients were considered acceptable. There was uncertainty in the heat of reaction measured with DSC and the value was relatively low in comparison to the heats of reaction for pyrolysis of synthetic polymers. The heat of reaction was increased and decreased by 10% with no noticeable change in the mass loss rate curve or temperature profile predictions. The values of the heat of reaction and its assignment to the third reaction were maintained based on the results of the sensitivity analysis.

4.2.7 Full Model Description

A schematic representation of the geometry of the initial sample defined in the model is provided in Figure 4-11 where the hatching denotes different material components.

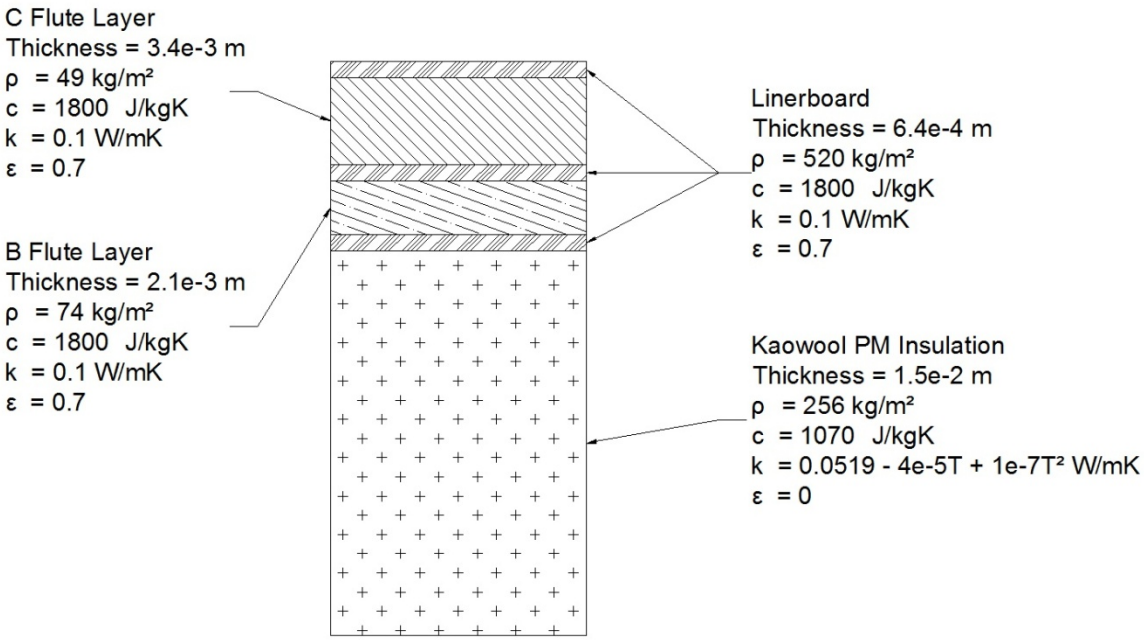

Figure 4-11: Schematic Representation of the Initial Sample Definition in the Bench-scale Model

Schematic representations of the sample defined in the model with the boundary conditions labeled are provided in Figure 4-12 . The figure presents the boundary conditions for the model prior to ignition and after ignition.

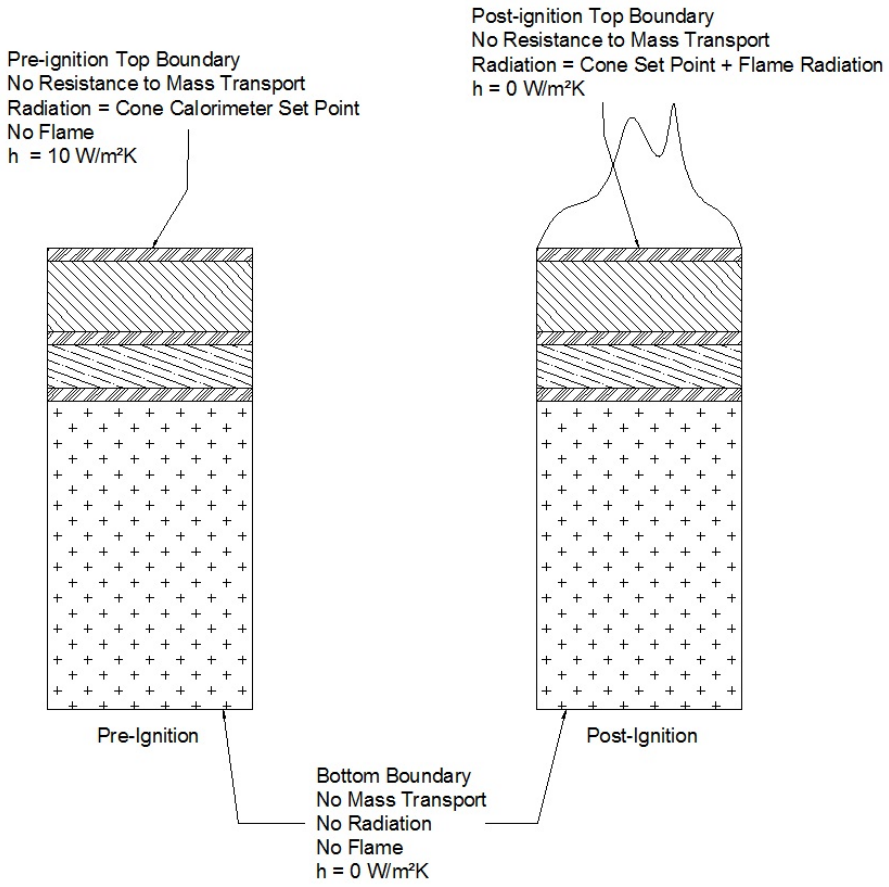

Figure 4-12:Schematic Representation of Pre-ignition and Post-ignition Boundary Conditions

Each layer of the sample was initially defined to be composed of 2% liquid water by mass. The thermal conductivity, gas transport coefficient, emissivity, and absorption coefficient for the water component was chosen to be equal to those properties for the virgin cardboard components. This was done under the assumption that the presence of the water as a component in the initial material did not affect the properties of the initial components.

The density of the components evolved during the simulation in proportion to the stoichiometric coefficients describing the reaction mechanism. By allowing the density of the solid material to evolve in the same ratio as the mass loss of each component during the reactions, the thickness of each layer, and the overall thickness of the entire sample, remained constant throughout the simulation. This was done to agree with the observation that the sample did not tend to swell or contract in the direction of the thickness of the material.

The full reaction scheme with the effective properties of all the pseudo-components and the model parameters that describe the components is provided in Figure 4-13. The set of properties in the upper right corner were assigned to all the representative gaseous pyrolyzate species. Input files for the Thermakin program that define all the variables here are provided in Appendix III - Thermakin Input Files for Bench-Scale Model.

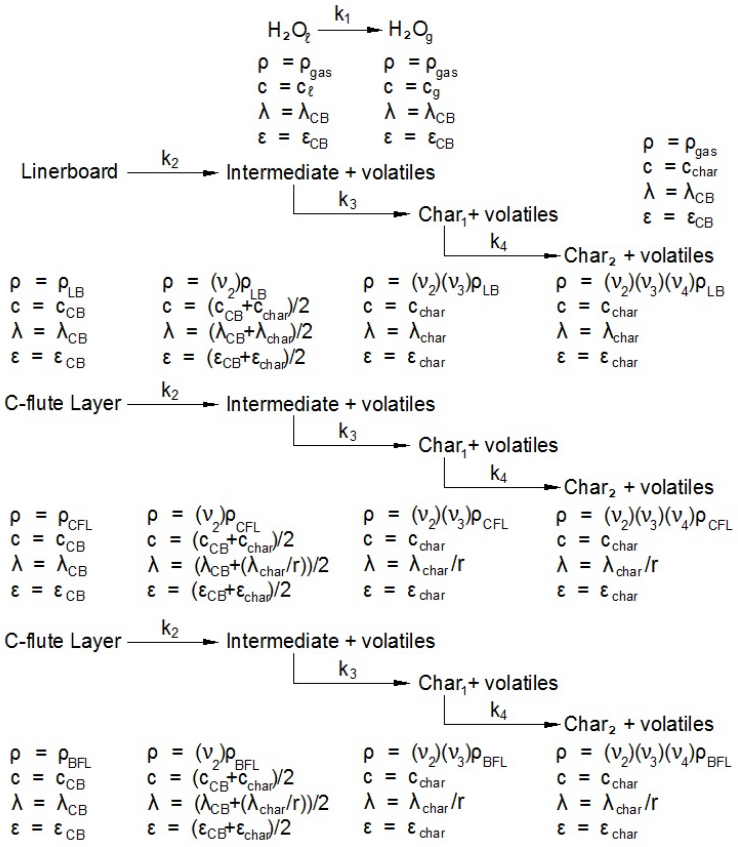

Figure 4-13: Complete Pyrolysis Reaction Mechanism with all Component Material Defined

Table 4-6: Definitions of Symbols used in Figure 4-13

Symbol	Description	Value
ρ_{gas}	Density of gaseous components	10000 kg/m^3
ρ_{LB}	Density of linerboard	520 kg/m^3
ρ_{CFL}	Density of C-flute layer	49 kg/m^3
ρ_{BFL}	Density of B-flute layer	74 kg/m^3
c_ℓ	Heat Capacity of bound water	$5230 - 6.71T + 0.011T^2$ J/kg·K
c_g	Heat Capacity of water vapor	$2398 - 1.16T + 0.0016T^2$ J/kg·K
c_{CB}	Heat Capacity of initial material	1800 J/kg·K
c_{char}	Heat Capacity of char	1280 J/kg·K
λ_{CB}	Thermal conductivity of initial material	0.1 W/m·K
λ_{char}	Thermal conductivity of char	$1.5e-10T^3$ W/m·K
ϵ_{CB}	Emissivity of initial material	0.7
ϵ_{char}	Emissivity of char	0.85
ν_2	Stoichiometric coefficient for solid products in reaction 2	0.9
ν_3	Stoichiometric coefficient for solid products in reaction 2	0.37
ν_4	Stoichiometric coefficient for solid products in reaction 2	0.59
r	Approximate Ratio of fluted medium density to linerboard density	0.1

5. Bench-Scale Modeling Results and Discussion

It was decided that the fit parameters should be determined independent from the resulting mass loss rate curve fit. All processes calculated by the Thermakin program were dependent on the temperatures of the computational cells. It was assumed that by matching the temperature profiles generated with the Thermakin program to the experimental temperature profiles, the Thermakin program would accurately predict the experimental mass loss rate profiles.

The bench-scale model was developed by determining parameters to describe the corrugated cardboard. Some of those parameters were measured directly, while others were determined by fitting data to specific tests conducted to identify single parameters. The temperature profile data used for fitting were collected at heat fluxes of 20 and 60 kW/m^2. The final fits of the temperature profile and mass loss rate data are provided in the following sections.

5.1 Temperature Profile Predictions

The fits of the experimental temperature data were used to inform the parameters that defined the corrugated cardboard material in the model, so the fits to the experimental data presented in the following figures are contrived. The temperature profile data and the curves predicted by Thermakin for a bench-scale cone calorimeter test at 20 kW/m^2 are provided in Figure 5-1.

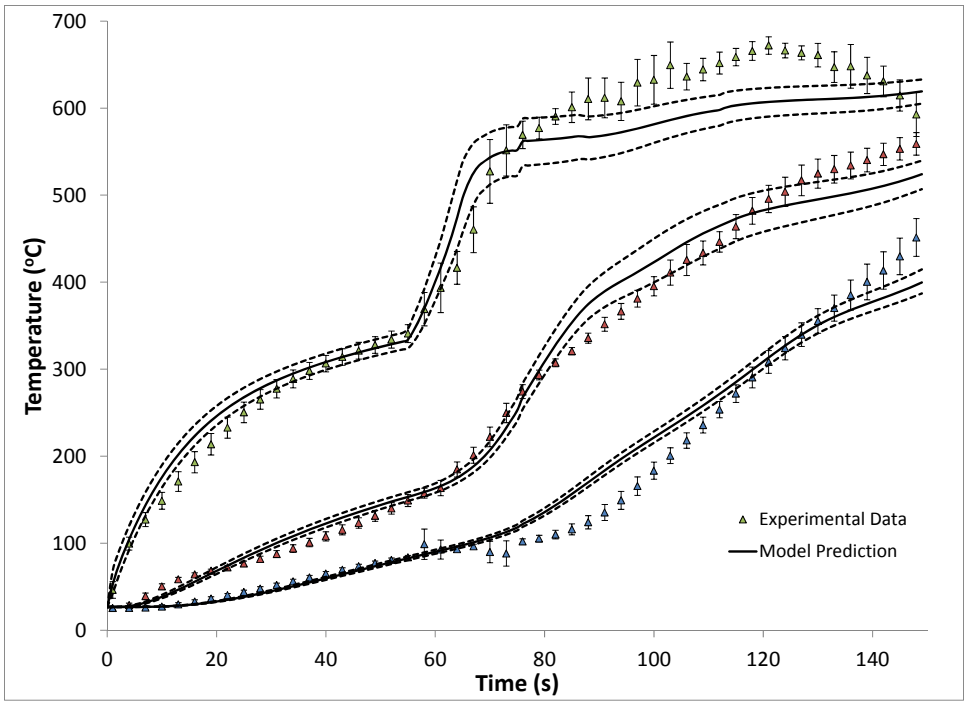

Figure 5-1: Collected Temperature Profile Data Presented in Comparison with the Thermakin Model Predicted Temperature Profiles for 20 kW/m^2

The error bars on the discrete data points correspond to two standard errors and the dashed lines surrounding the solid lines correspond to the uncertainty in the position of the thermocouple. The uncertainty in the position of each thermocouple was defined as ± 0.15 mm. This uncertainty represents approximately half the thickness of the linerboard.

The temperature increases measured in all of the linerboards during the pre-ignition heating phase and the apparent point of ignition, characterized by a change in the temperature curve, were well represented by the Thermakin model for 20 kW/m^2 incident heat flux. There were deviations from the experimental temperature profiles at the middle and lower linerboard in the early stages of flaming, with the temperature predictions higher than the experimental values, though there was no systematic deviation for all simulated thermocouple positions. The thermocouple measurements are

considered less reliable further in to the test, so deviations from the experimental curves late in the tests are likely within the limits of experimental uncertainty of the test data. The temperature profile data collected at 60 kW/m^2 and the related Thermakin-predicted curves are provided in Figure 5-2.

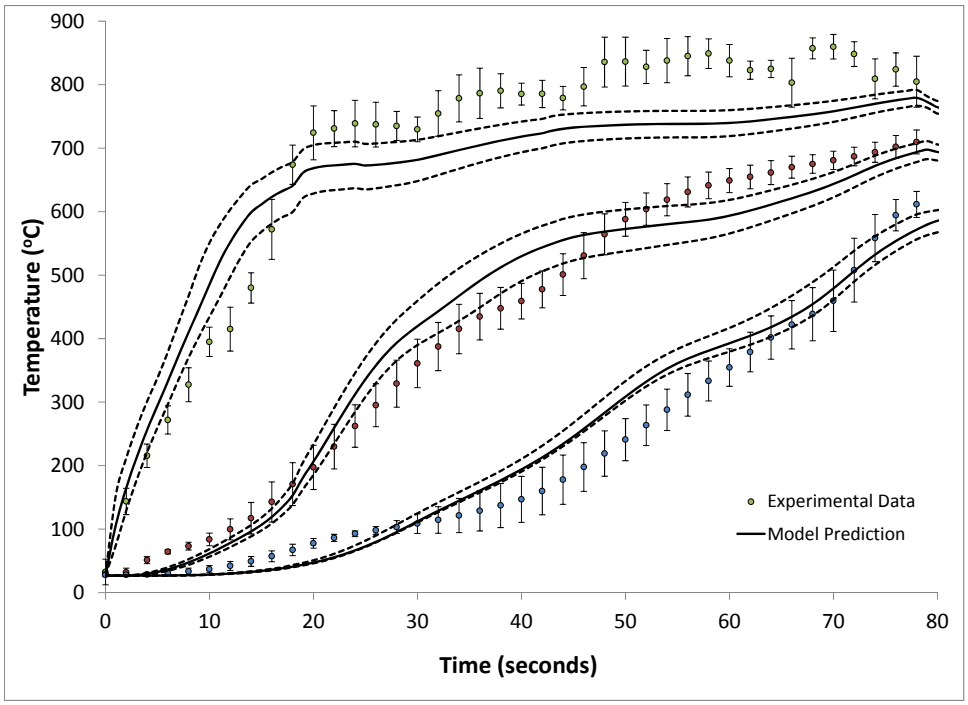

Figure 5-2: Collected Temperature Profile Data Presented in Comparison with the Thermakin model Predicted Temperature Profiles for 60 kW/m^2

The temperature profile predictions for 60 kW/m^2 are consistent with the experimental temperature profile data. Like the predictions for 20 kW/m^2 heat flux, there are no systematic deviations from the experimental data that would point to gross errors in the development of the model and its interpretation of the physical phenomena. At the point the flame was observed to completely extinguish, the model predicted temperature profiles that were lower than the measured temperatures for all the linerboards.

During the curve fitting process, a compromise between the temperature curves collected at external heat fluxes of 20 kW/m^2 and 60 kW/m^2 had to be found to provide

the most representative general fit. The model parameter values were accepted or rejected according to the fit of both temperature profile curves. Though a better fit for the temperature profiles at either heat flux could have been determined, the parameters corresponding to the fit for a single heat flux would likely not have generated a physically realistic set of properties or would not have generated an accurate fit over the required range of heat fluxes. The prediction for the temperature profiles at 20 kW/m^2 appears to agree better with the corresponding experimental data that the prediction at 60 kW/m^2. This is likely due to the thermal conductivity curve fit for the initial material because the thermal conductivity was fit to data collected with the sample surface painted black collected only at 20 kW/m^2.

5.2 Mass Loss Rate Curve Predictions

The predicted mass loss rate curves that correspond to the temperature profile predictions displayed in the previous plots are provided in the following figures with the experimental mass loss rate curves. The Thermakin program calculated the total mass of the sample according to the conservation equations and the mass loss rate curve predictions reflect the evolution of the total mass of the sample in a cone calorimeter test. The mass loss rate prediction and experimental data curve for 20 kW/m^2 are provided in Figure 5-3 and for 60 kW/m^2 in Figure 5-4. The discrete points in each figure correspond to the mass loss rate curves collected in individual tests and the solid black line corresponds to the mean experimental curve for all tests.

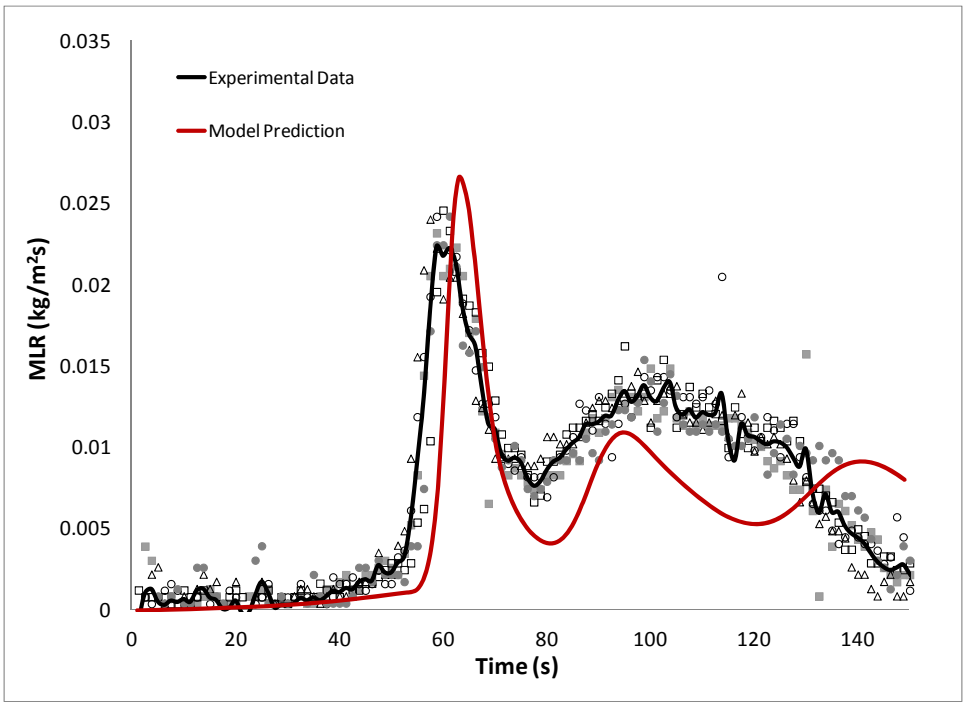

Figure 5-3: Mass Loss Rate Curve Collected with the Cone Calorimeter at an Incident Heat Flux of 20 kW/m^2 Presented with the Curve Predicted by the Final Thermakin Model

The model was constructed to fit primarily to the temperature profile data, resulting in a model prediction that does not correspond directly to the apparent ignition time on the mass loss rate curve collected at an incident heat flux of 20 kW/m^2. The ignition time for 20 kW/m^2 was observed to be 56.2 ± 3.4 seconds and the ignition time predicted in the model, according to the ignition criteria defined in the development of the model, was approximately 55 seconds. The model predicted the main features of the experimental curve with acceptable agreement although the prediction of the amount of time the sample was covered with the flame was larger than the actual duration of flaming.

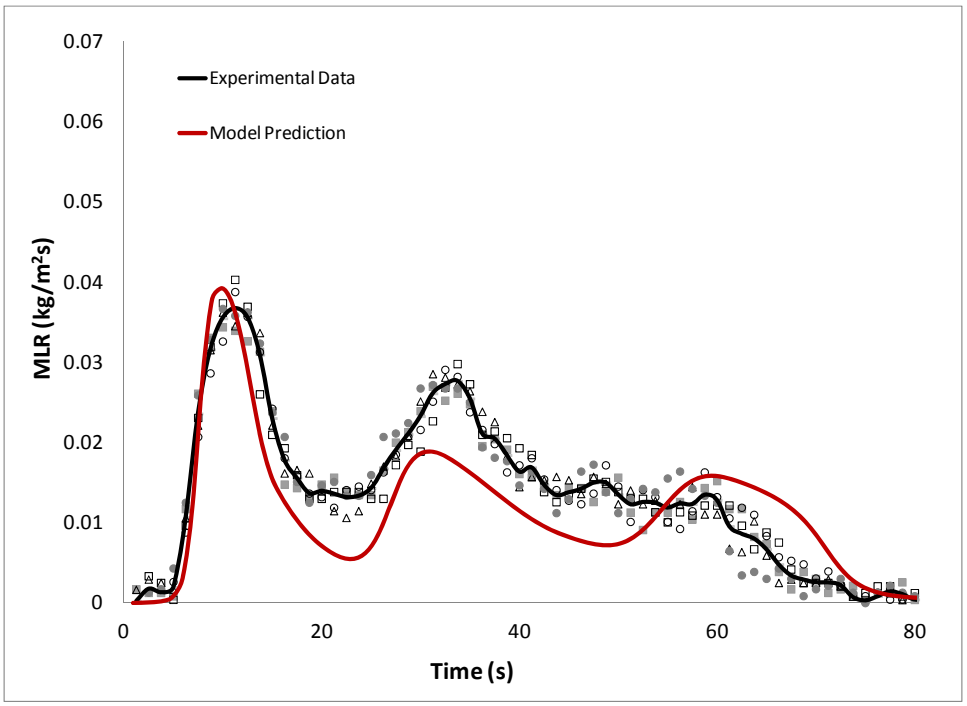

Figure 5-4: Mass Loss Rate Curve Collected with the Cone Calorimeter at an Incident Heat Flux of 60 kW/m^2 Presented with the Curve Predicted by the Final Thermakin Model

The agreement between the predicted curve and the experimental curve for 60 kW/m^2 incident heat flux appears to be better than the agreement between the prediction and experimental curve at 20 kW/m^2. The first peak of the predicted curve had a larger magnitude than the experimental curve although the time to ignition and rate of change of the predicted curve are similar to those characteristics for the experimental curve. The duration of flaming was overpredicted by the Thermakin model by approximately seven seconds. Based on the relative complexity of the model, it is hard to associate the deviations in the prediction to the model parameters or physical processes that cause the deviations.

The deviation of the predicted curve from the experimental curve could be due to an invalid assumption in the heat transfer parameters for one of the intermediates or chars. The error in the predicted mass loss rate curves might also be attributed to the

heating rate at which the TGA data was collected to determine the reaction mechanism. It has been demonstrated that the kinetic parameters are affected by the heating rate and an inaccurate reaction mechanism could prescribe an inaccurate rate of production of volatile gases.

The predicted curves are stretched in time further than the experimental curves. This systematic overprediction of the duration of burning is likely caused by oxygen reacting with the sample that was not taken into account for the model. There was a short period of time when the flame covered approximately half the surface of the sample and the assumption was not valid that the oxygen concentrations near fuel were low. During this period, it is possible that fast oxidation reactions occurred that sped the pyrolysis process.

The bench-scale model was constructed as a tool used to predict the processes occurring during the inert pyrolysis of corrugated cardboard and, ultimately, to predict the mass flux evolution of volatile gases from the solid material as a function of time and incident heat flux [23]. One of the best metrics to determine the appropriateness of the model as a predictive measure is assessing the accuracy of the predicted mass loss rate curves at heat fluxes that were not considered during the parameter determination process. Mass loss rate curves for external heat fluxes of 40 and 80 kW/m^2 were generated independent of the fitting procedures used to determine the parameters for the model. The mass loss rate curves collected in the cone calorimeter tests are plotted against the mass loss rate curves predicted by the model in the following figures. The experimental and predicted mass loss rate curves for 40 kW/m^2 are provided in Figure 5-5 and for 80 kW/m^2 in Figure 5-6.

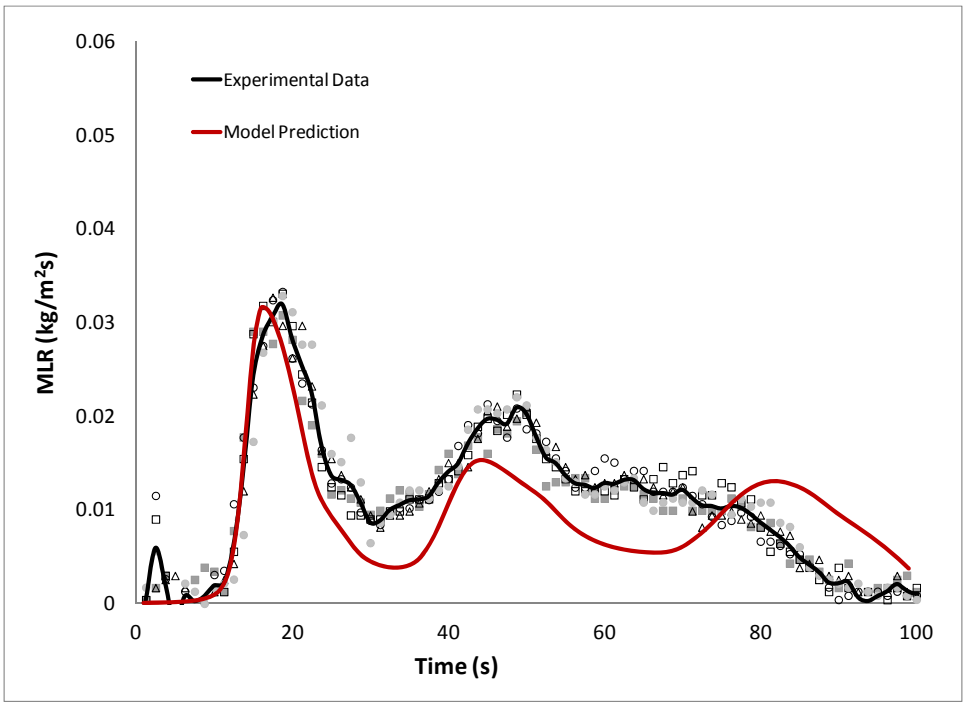

Figure 5-5: Mass Loss Rate Curve Collected with the Cone Calorimeter at an Incident Heat Flux of 40 kW/m^2 Presented with the Curve Predicted by the Final Thermakin Model

The curves predicted by the model for incident heat fluxes of 40 kW/m^2 and 80 kW/m^2 were qualitatively similar to the mass loss rate curve predicted for a heat flux of 60 kW/m^2. The curve predicted for 40 kW/m^2 corresponded well with the initial increase to the first peak of the experimental curve whereas the curve predicted for 80 kW/m^2 slightly overpredicted the rate of increase to first peak. The issues discussed about the accurate depiction of energy delivery to the sample in the model for the curves that were fit were observed for the mass loss rate curves for incident heat fluxes of 40, 60, and 80 kW/m^2.

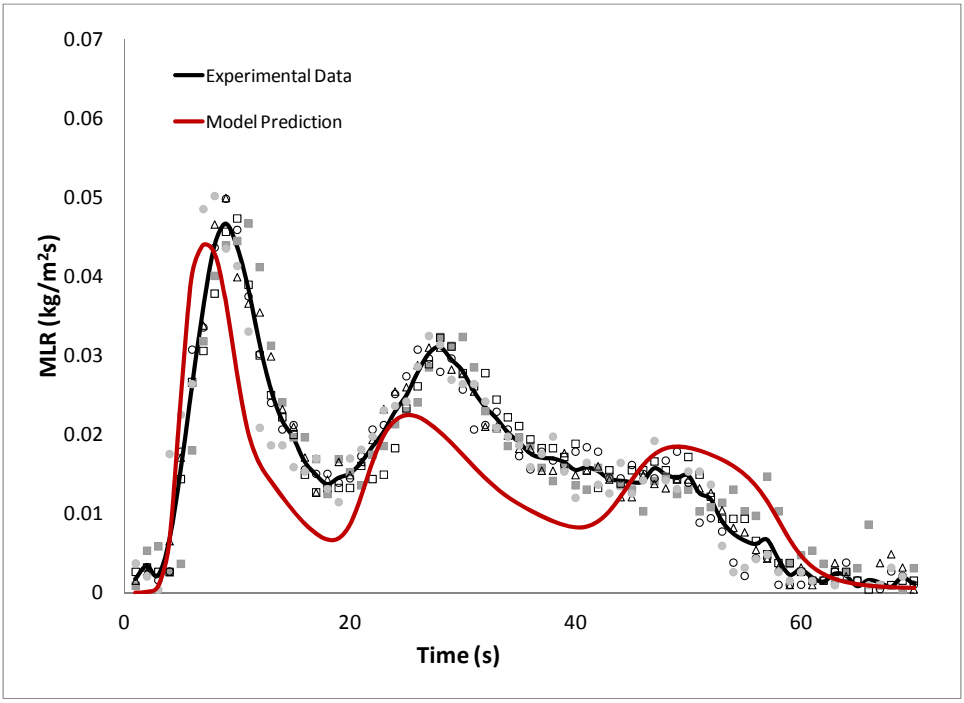

Figure 5-6: Mass Loss Rate Curve Collected with the Cone Calorimeter at an Incident Heat Flux of 80 kW/m^2 Presented with the Curve Predicted by the Final Thermakin Model

There is a systematic underprediction of the second peak and overprediction of the third peak mass loss rates for the heat fluxes 40 to 80 kW/m^2. This systematic trend could possibly be caused by a physical process that was not included in the model. Attempting to identify the possible process that caused this trend would be speculation at this point in the model development.

5.3 Temperature Profiles in the Insulation

The temperature profile data collected in the Kaowool insulation and below the sample at a heat flux of 20 kW/m^2 are provided in Figure 5-7 plotted in comparison with the temperature profiles predicted by Thermakin based on the bench-scale model. The distances specified at each curve correspond to the distance from the top surface of the sample to the thermocouple. The thermocouple 7.42 mm from the top surface was between the bottom surface of the sample the first layer of Kaowool insulation. The two

temperature curves with larger distances were located below a single quarter-inch sheet of insulation and below two sheets of quarter-inch insulation, respectively. The dashed lines correspond to the uncertainty of the prediction corresponding to the thickness of the thermocouples used to collect the experimental temperature data.

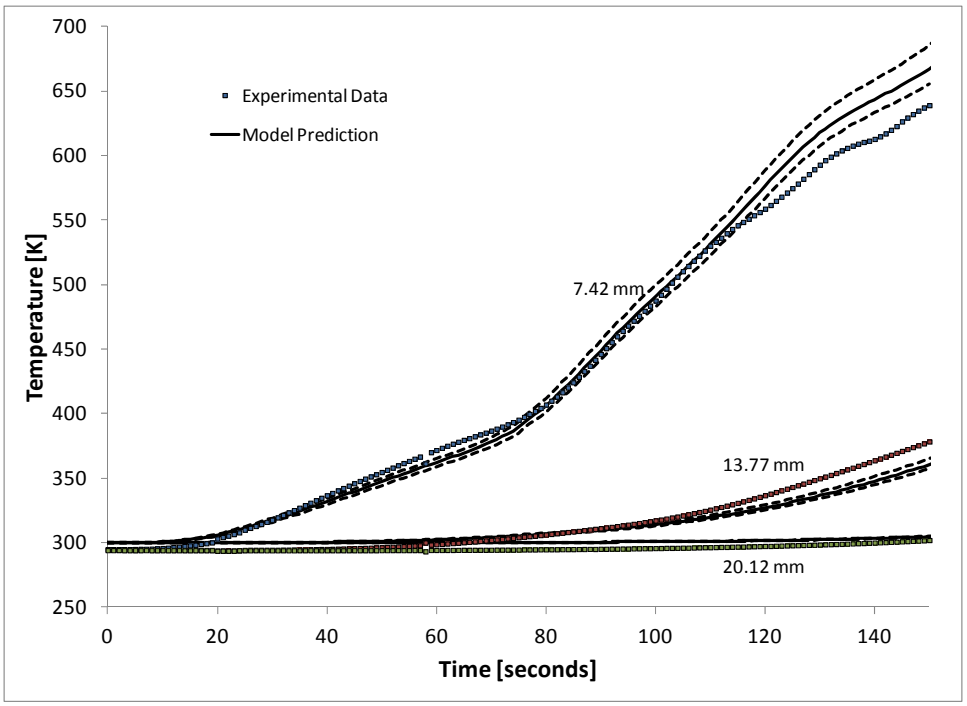

Figure 5-7: Temperature Profiles Collected Under the Sample at a Heat Flux of 20 kW/m^2 Presented in Comparison with Temperature Profiles Predicted with the Final Thermakin Model

Agreement between the Thermakin prediction and the experimental data that extended outside the range of the data targeted for fitting effectively validated the Thermakin model parameters for the corrugated cardboard and the Kaowool PM insulation.

The experimental temperature profiles collected in the insulation were accurately predicted by the bench-scale model. This agreement verifies the model on a large scale, i.e. for the sample as a whole. The predicted temperature profiles in the insulation depend on the rate at which energy was transferred through all the layers above the

insulation through the duration of the test. The model generated a prediction that was qualitatively and quantitatively similar to the experimental temperature profile over the entire duration of the simulation. This signifies the bulk energy transport through the entire sample is accurate in the model. The agreement between the model and measured temperature profiles also verifies that the thermal properties of the Kaowool insulation boards used in the model were physically accurate.

It is apparent that the model predicted mass loss rate profiles at the higher heat fluxes more accurately than at the low heat fluxes. The relative inaccuracy of the predictions at the lower heat fluxes could possibly be attributed to an invalid assumption about the heat transfer characteristics of the material at low heat fluxes. The thermal conductivity of most materials is a function of temperature, and the initial material components in the model were assumed to be constant to simplify the model.

6. Conclusions

The orientation of the cardboard sample was found to affect the rate of heat release and the mass loss rate of the sample during cone calorimeter testing. It was determined that the results obtained with the thick fluted section facing the heater yielded results comparable to the results obtained when the thin fluted section faced the heater and the edges of the sample were sealed with aluminum tape prior to ignition. The heat release rate data and mass loss rate data collected at heat fluxes ranging from 20 to 80 kW/m^2 were found to be repeatable at each heat flux.

Cone calorimeter tests were conducted to collect data used to estimate the thermal properties of the sample material components and verify the final model at heat fluxes ranging from 20 to 80 kW/m^2. Temperature profile data was collected with thermocouples inserted in the linerboards of several corrugated cardboard samples. The data collected with thermocouples during cone calorimeter tests was found to be repeatable at each heat flux that was tested. The temperature profile data acted as the target data to be fit by the model to determine the unknown and unmeasurable thermal properties of the sample material. The curve fitting procedure consisted of isolating a single parameter and adjusting that parameter to improve the agreement between the predicted temperature profiles and the experimental temperature profiles.

Data was collected for the corrugated cardboard samples on the milligram scale in TGA, DSC, and PCFC tests. The milligram scale data was used to determine the chemical kinetics describing the thermal degradation of the corrugated cardboard as well as the thermodynamic and energetic characteristics of the material for use as parameters in the bench-scale model.

The apparent kinetic mechanism that produced the best fit for the thermogravimetric data collected in nitrogen with a heating rate of 10 K/min consisted of four reactions. The reactions were characterized by the release of moisture, two reactions to describe the degradation of the initial material to an intermediate char, and the thermal degradation of the intermediate char to a final char. The apparent kinetic mechanism for the current study was found to be similar to some kinetic mechanisms reported in the literature, although the applications were considerably different for the mechanisms in the literature and, as a result, the kinetic parameters described significantly different mass loss rate curves.

The development of a homogeneous model was attempted although it was determined early in the development of the bench-scale model that the homogeneous model could not accurately represent the physical sample and would produce temperature profile and mass loss rate curves that did not agree with the experimental data. The final bench-scale model featured a non-homogeneous structure with three different initial components to describe the five layers of the physical sample.

The parameters of the bench-scale model that described the thermal properties of the material were measured directly or inferred from experimental data.

The flame heat flux was approximated according to temperature and heat flux data collected in cone calorimeter tests as well as observations of the flames produced during the tests. The flame heat flux was defined as a linear ramp with a duration of ten seconds followed by a steady heat flux of 30 kW/m^2 that was specified to last until the flame extinguished.

The mass loss rate profiles and temperature profiles predicted by the final non-homogeneous bench-scale model were consistent with the mass loss rate curves collected in cone calorimeter tests at heat fluxes ranging from 20 to 80 kW/m^2 and temperature profile data collected at heat fluxes of 20 and 60 kW/m^2

The final bench-scale model was able to accurately predict the temperature profiles of the insulation below the sample at a heat flux of 20 kW/m^2. This prediction verified that the bulk energy flow through the entire sample was represented accurately.

6.1 Future Work

The characterization and modeling of the pyrolysis of corrugated cardboard will continue in this laboratory. The continuing research will have an emphasis on oxidative pyrolysis to assess the effect of varying oxygen concentrations on the combustion of corrugated cardboard. The pyrolysis model developed in this investigation was based on the assumption that the pyrolysis occurred absent the presence of oxygen. This assumption was likely valid for the period of time when the flame completely covered the surface of the cardboard sample. There was a portion of the bench-scale tests before flame extinction when the flame covered a fraction of the cardboard surface. During the time when the flame did not completely cover the surface of the sample, it is possible that oxygen was allowed to react with the solid pyrolysis products effectively changing the mass loss and heat release rate characteristics.

The kinetic mechanism was constructed based on data collected with a heating rate of 10 K/min. The effective heating rate for the cone calorimeter tests varied over a wide range. It is possible that the kinetic mechanism describing the actual thermal degradation deviated from the mechanism defined in the final model, which could result

in errors in the mass loss rate curve. The effect of the heating rate on the kinetic mechanism and the resulting effects on the bench-scale mass loss rate profile will be examined in future work.

Smoldering combustion of the char that occurred after the flame was extinguished was not considered during this investigation. A model for smoldering char will be constructed with the Thermakin program as part of this ongoing research. The reaction mechanism used to describe the global mass loss rate while the char was smoldering will be complicated by the simultaneous oxidation and pyrolysis of char in the early part of the smoldering. The oxidation of char is a complicated process that depends on the diffusion of oxygen in to the carbonaceous char matrix.

Sprinkler protection is often activated in warehouse fires that involve corrugated cardboard early in the combustion process. As a result of sprinkler activation, water is introduced to the gaseous and condensed phase combustion system. Water affects the processes that occur in the gas and condensed phase during pyrolysis. Corrugated cardboard is a hydrophilic material, meaning the introduction of water to the samples may also affect the material and thermal properties and the geometry and structure of the sample. The effects of water on the pyrolysis and oxidation of corrugated cardboard and its pyrolysis products will be investigated in the continuation of the current project.

The model required several assumptions, though most of them were founded in physical theory or through observations and analysis of experimental data. A sensitivity analysis could likely assess the assumptions that cause the most significant deviations

from the physical experiments and procedures could be developed to eliminate uncertainty in these parameters.

7. Appendix I - Oxidative Pyrolysis

Oxidative pyrolysis of the virgin cardboard material was examined by testing the cardboard samples in TGA tests in atmospheres with 21% Oxygen and 10% Oxygen, both with balance Nitrogen. The tests conducted in each atmosphere had the same heating program that consisted of a twenty minute conditioning period at 40°C followed by linear heating from 40°C to 700°C at a rate of 10°C/min. The thermogravimetric data collected in these tests is displayed in Figure 7-1. The mass loss rate data was calculated as a numerical differentiation of the total mass data, so the experimental curves contain random noise, but the curves from each of the three tests displayed in the plots show consistent, repeatable data.

The thermogravimetric tests of corrugated cardboard powder conducted in two, well-defined atmospheres with oxygen yielded mass loss rate data with two, distinct peaks. The mass loss rate data collected in TGA tests is provided in Figure 7-1. The first large peak was associated with thermal degradation and the second large peak corresponded to the oxidation reaction. The peak associated with the release of moisture was present in the data, but was not displayed in the figure for the temperature range to emphasize the processes that deviated from the pure nitrogen atmosphere tests.

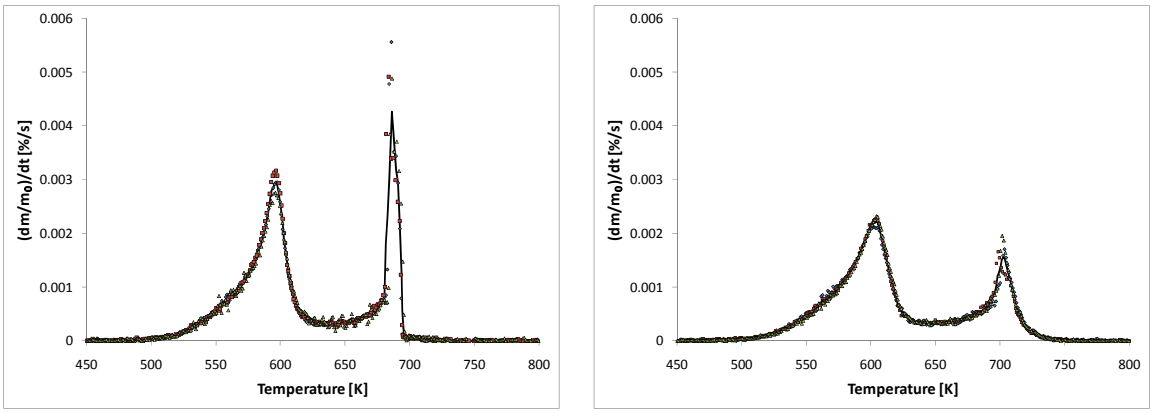

(a) (b)

Figure 7-1: Thermogravimetric Data Displayed as Mass Loss Rate for (a) 21% Oxygen Atmosphere (b) 10% Oxygen Atmosphere

Oxidation Kinetics Modeling

A set of kinetic parameters was determined to describe the degradation of the corrugated cardboard samples in oxidative atmospheres. Kinetics were individually determined for the mass loss rate data collected in 10% oxygen and 21% oxygen and were correlated as a function of the ambient oxygen concentration. The reaction mechanism was constrained by the requirement that the Arrhenius pre-exponential factor was a function of the ambient oxygen concentration, given in volumetric fraction, and the requirement that at 0% oxygen concentration the mechanism would revert to the pyrolysis mechanism given in Table 2.

The reaction mechanism including oxidation is provided in Table 7-1. Four oxidation reactions were included that were not present in the pyrolysis mechanism. The mechanism has sequential reactions, similar to the pyrolysis mechanism, but also incorporates parallel reactions that compete with reactions 3 and 4 in the inert pyrolysis mechanism, respectively. The competitive reactions 3a and 3b act to effectively speed reaction 3 without the loss of more mass. Reactions 4a and 4b act to effectively speed reaction 4 and decrease the final residual mass yield from approximately 20% of the initial mass to approximately 5% of the initial mass. In the description of the kinetic

parameters, the square brackets denote the volumetric fraction of the species inside the brackets. The kinetic parameters provided in the following table were developed with 10% and 21% oxygen, but can be extended to other oxygen concentrations.

Table 7-1: The Universal Reaction Mechanism for Corrugated Cardboard as a function of Ambient Oxygen Volume Fraction

#	Reaction Equation	A (sec^{-1})	E_a (J/mol)
1	$H_2O_\ell \rightarrow H_2O_g$	6.14	2.35×10^4
2	$CB_a \rightarrow 0.9CB_b + 0.1CB_{volatiles}$	7.95×10^9	1.3×10^5
3	$CB_b \rightarrow 0.37CB_{char,1} + 0.63CB_{volatiles}$	2.0×10^{11}	1.6×10^5
3a	$CB_b \rightarrow 0.59CB_{char,1} + 0.41CB_{volatiles}$	$4.76 \times 10^9[O_2]$	1.6×10^5
3b	$CB_b \rightarrow 0.48CB_{char,1} + 0.52CB_{volatiles}$	$1.11 \times 10^{21}[O_2]$	2.8×10^5
4	$CB_{char,1} \rightarrow 0.59CB_{char,2} + 0.41CB_{volatiles}$	2.61×10^{-2}	1.7×10^4
4a	$CB_{char,1} \rightarrow 0.48CB_{char,2} + 0.52CB_{volatiles}$	$1.24 \times 10^{-3}[O_2]$	1.7×10^4
4b	$CB_{char,2} \rightarrow 0.15\ ash + 0.85CB_{volatiles}$	$2.31 \times 10^{125}[O_2]$	1.69×10^6

The mass loss rate curve and total mass evolution curve collected in 21% oxygen and 10% oxygen are provided with the same curve predictions from Thermakin in Figure 7-2. The experimental data is indicated by the thick black line and the simulation data based on the reaction mechanism given in Table 7-1 is provided as the dashed line. The contribution to the mass loss rate profile from each reaction is displayed with dotted lines.

Although it was possible to obtain curve fits that correspond more accurately to the data, the fits displayed in the previous two figures provide good quantitative and qualitative predictions for the reaction kinetics of corrugated cardboard in an atmosphere

with oxygen, while maintaining as few reactions as possible. The agreement between the experimental data and the model prediction is surprisingly good considering the constraints imposed on the pre-exponential factors for the oxidative reactions.

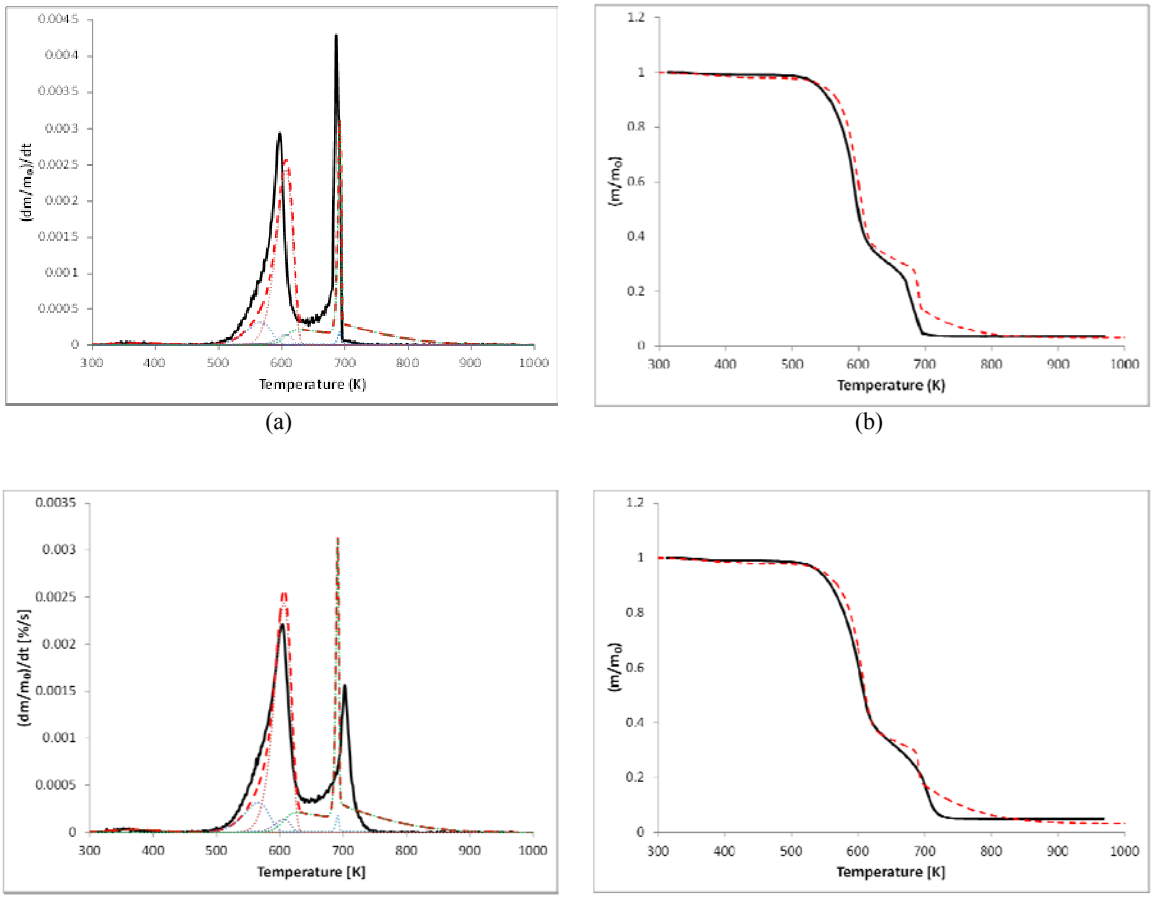

Figure 7-2: The Universal Reaction Mechanism Fit to (a) The Mass Loss Rate plot in 21% Oxygen (b) The Total Mass Curve in 21% Oxygen (c) The Mass Loss Rate plot in 10% Oxygen (d) The Total Mass Curve in 10% Oxygen

8. Appendix II – Char Smoldering

Char smoldering was not considered in the course of this investigation because of the relatively complex processes that govern char oxidation. Accurate representations of the smoldering processes that occur in cone calorimeter tests depend, in part, on the thermal history of the sample. A model to describe the portion of cone calorimeter tests with the flame present was required before a model for smoldering char could be constructed. A model dedicated to the char smoldering process was deemed outside the scope of the current study.

Char smoldering is qualitatively different from flaming combustion. Smoldering combustion is a condensed phase phenomenon characterized by oxygen attacking the carbon-rich char. Pyrolysis is characterized as an endothermic condensed phase phenomenon in contrast to the exothermic condensed phase phenomenon of oxidation. Pyrolysis can occur in an inert atmosphere and depends most significantly on the temperature of the material, which is governed by thermal processes and heat transfer. Char oxidation occurs in atmospheres that contain an oxidizer and the reaction depends on temperature and the concentration of oxidizer present at the gas-solid interface. The char oxidation reaction depends on thermal processes as well as mass transport of oxygen in to the porous char material, making the process considerably more complicated than inert pyrolysis.

Cone calorimeter data collected after self-extinction of the flame are presented in the following figures. The heat release rate and mass loss rate data are qualitatively similar at each heat flux and are characterized by a gradual decrease to the end of the test. It appears that the heat release rate curves have increasing initial magnitudes at flame

extinction as the incident heat flux was increased. The noise in the mass loss rate signal increased significantly with higher incident heat fluxes. The gradual decrease in the mass loss rate and heat release rate curves leads to the interpretation that the mass loss rate depends on the instantaneous mass of the sample. This interpretation agrees with the char oxidation process being controlled by diffusion of oxygen into the char because the rate of diffusion is proportional to the surface area of unreacted char.

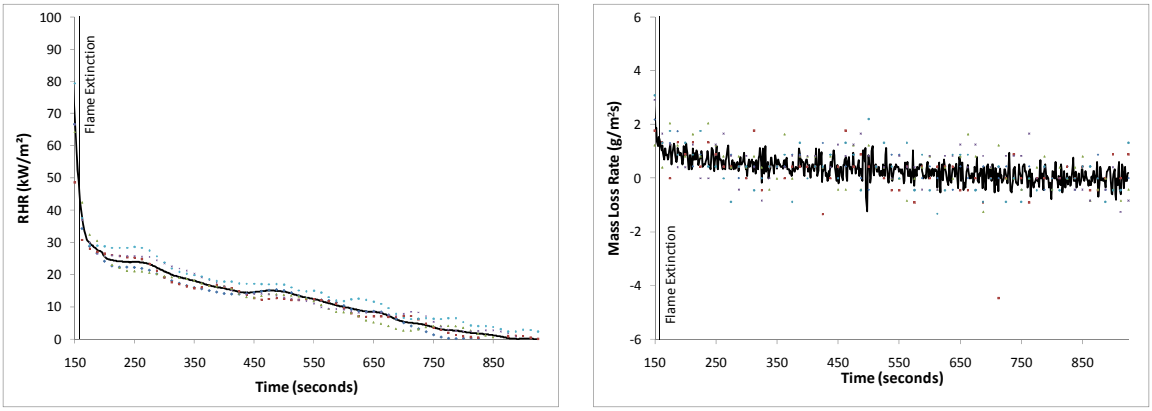

(a) (b)

Figure 8-1: Cone Calorimeter Data Collected After Flame Extinction for 20 kW/m2 Presented as (a) Heat Release Rate (b) Mass Loss Rate

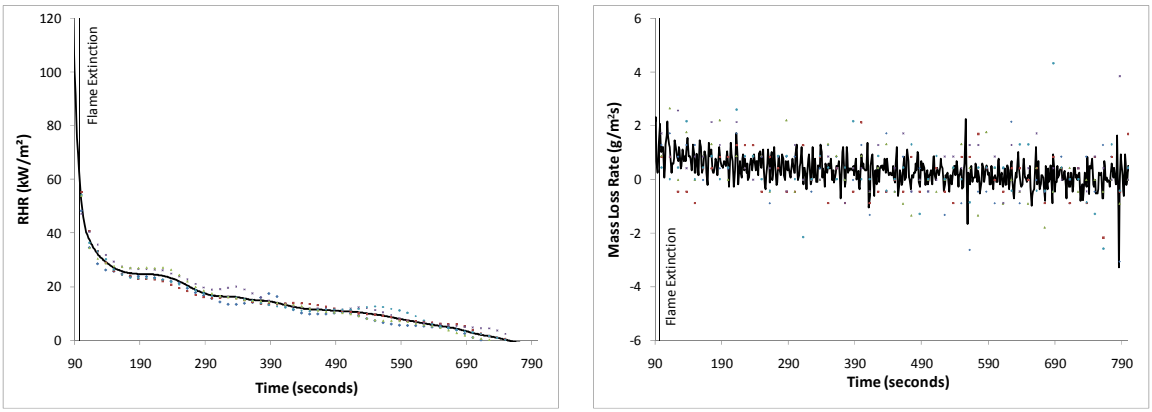

(a) (b)

Figure 8-2: Cone Calorimeter Data Collected After Flame Extinction for 40 kW/m2 Presented as (a) Heat Release Rate (b) Mass Loss Rate

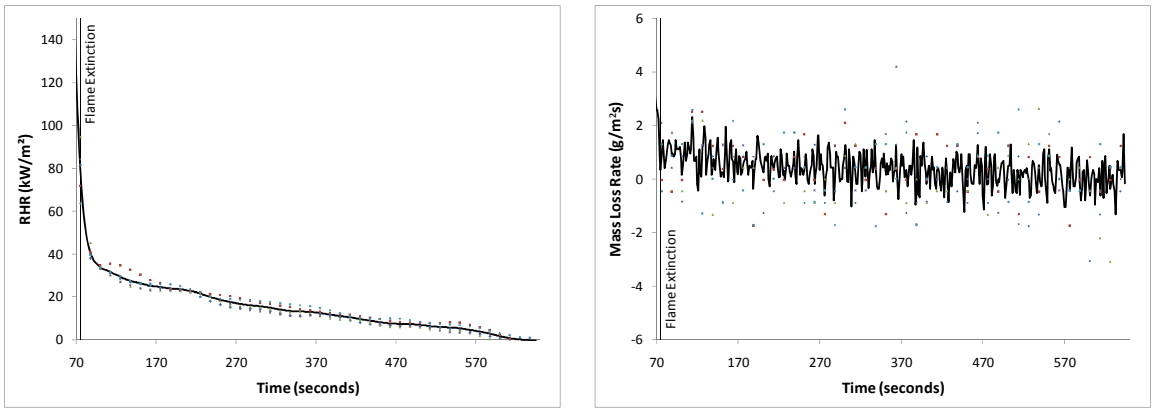

(a) (b)

Figure 8-3: Cone Calorimeter Data Collected After Flame Extinction for 60 kW/m2 Presented as (a) Heat Release Rate (b) Mass Loss Rate

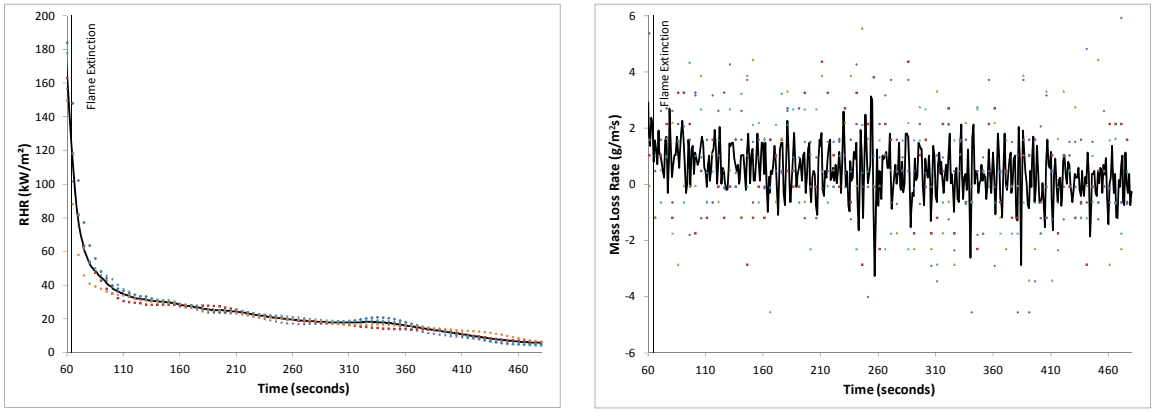

(a) (b)

Figure 8-4: Cone Calorimeter Data Collected After Flame Extinction for 80 kW/m2 Presented as (a) Heat Release Rate (b) Mass Loss Rate

9. Appendix III - Thermakin Input Files for Bench-Scale Model

Representative input files for the Thermakin program are provided below. The components file defines the material components with temperature-dependent material properties parameters. The reaction mechanism is also provided in the components file. The same components file was used for all heat fluxes because the material properties were not affected by the heat flux. The components were named arbitrarily in the initial stages of model development resulting in nondescript names. CB_A corresponds to moisture, CB_B denotes the initial material, CB_C denotes the intermediate, CB_ch1:3 denote the initial char, and CB_ch4:6 denote the final char. The numbers (1:3) for the solid cardboard components correspond to the layer described by the parameters. Components ending with 1 denote the linerboard, ending with 2 denote the C-flute layer, ending with 3 denote the B-flute layer. Parameters were adjusted in the components file to improve the agreement between the temperature profile prediction and the experimental data. Parameters were also adjusted according to the conditions of the experimental tests, e.g. the emissivity of all components was adjusted to 0.95 to simulate the tests with the sample surface painted black.

```
Final Components File - nMLR36.cmp


COMPONENT:       CB_A
STATE:           S
DENSITY:         10000  0  0  0
HEAT CAPACITY:   5230  -6.71  0.011  2
CONDUCTIVITY:    0.1  0  0  0
TRANSPORT:       1e-5  0  0  0
EMISSIVITY & ABSORPTION:  0.7  100

COMPONENT:       CB_B1
STATE:           S
DENSITY:         520  0  0  0
HEAT CAPACITY:   1800  0  0  0
CONDUCTIVITY:    0.1  0  0  0
TRANSPORT:       1e-5  0  0  0
EMISSIVITY & ABSORPTION:  0.7  100
```

```
COMPONENT:       CB_B2
STATE:           S
DENSITY:         49  0  0  0
HEAT CAPACITY:   1800  0  0  0
CONDUCTIVITY:    0.1  0  0  0
TRANSPORT:       1e-5  0  0  0
EMISSIVITY & ABSORPTION:  0.7  100

COMPONENT:       CB_B3
STATE:           S
DENSITY:         74  0  0  0
HEAT CAPACITY:   1800  0  0  0
CONDUCTIVITY:    0.1  0  0  0
TRANSPORT:       1e-5  0  0  0
EMISSIVITY & ABSORPTION:  0.7  100

COMPONENT:       CB_C1
STATE:           S
DENSITY:         468  0  0  0
HEAT CAPACITY:   1540  0  0  0
CONDUCTIVITY:    0.05  0  7.5e-11  3
TRANSPORT:       1e-5  0  0  0
EMISSIVITY & ABSORPTION:  0.775  100

COMPONENT:       CB_C2
STATE:           S
DENSITY:         44  0  0  0
HEAT CAPACITY:   1540  0  0  0
CONDUCTIVITY:    0.05  0  7.5e-10  3
TRANSPORT:       1e-5  0  0  0
EMISSIVITY & ABSORPTION:  0.775  100

COMPONENT:       CB_C3
STATE:           S
DENSITY:         67  0  0  0
HEAT CAPACITY:   1540  0  0  0
CONDUCTIVITY:    0.05  0  7.5e-10  3
TRANSPORT:       1e-5  0  0  0
EMISSIVITY & ABSORPTION:  0.775  100

COMPONENT:       CB_ch1
STATE:           S
DENSITY:         173  0  0  0
HEAT CAPACITY:   1280  0  0  0
CONDUCTIVITY:    0  0  1.5e-10  3
TRANSPORT:       1e-5  0  0  0
EMISSIVITY & ABSORPTION:  0.85  100

COMPONENT:       CB_ch2
STATE:           S
DENSITY:         16  0  0  0
HEAT CAPACITY:   1280  0  0  0
CONDUCTIVITY:    0  0  1.5e-9  3
TRANSPORT:       1e-5  0  0  0
EMISSIVITY & ABSORPTION:  0.85  100

COMPONENT:       CB_ch3
STATE:           S
DENSITY:         25  0  0  0
HEAT CAPACITY:   1280  0  0  0
CONDUCTIVITY:    0  0  1.5e-9  3
TRANSPORT:       1e-5  0  0  0
EMISSIVITY & ABSORPTION:  0.85  100
```

```
COMPONENT:       CB_ch4
STATE:           S
DENSITY:         102  0  0  0
HEAT CAPACITY:   1280  0  0  0
CONDUCTIVITY:    0  0  1.5e-10  3
TRANSPORT:       1e-5  0  0  0
EMISSIVITY & ABSORPTION:  0.85  100

COMPONENT:       CB_ch5
STATE:           S
DENSITY:         9.4  0  0  0
HEAT CAPACITY:   1280  0  0  0
CONDUCTIVITY:    0  0  1.5e-9  3
TRANSPORT:       1e-5  0  0  0
EMISSIVITY & ABSORPTION:  0.85  100

COMPONENT:       CB_ch6
STATE:           S
DENSITY:         14.8  0  0  0
HEAT CAPACITY:   1280  0  0  0
CONDUCTIVITY:    0  0  1.5e-9  3
TRANSPORT:       1e-5  0  0  0
EMISSIVITY & ABSORPTION:  0.85  100

COMPONENT:       CB_g_1
STATE:           G
DENSITY:         10000  0  0  0
HEAT CAPACITY:   2398  -1.6  0.0016  2
CONDUCTIVITY:    0.1  0  0  0
TRANSPORT:       1e-5  0  0  0
EMISSIVITY & ABSORPTION:  0.7  100

COMPONENT:       CB_g_2
STATE:           G
DENSITY:         10000  0  0  0
HEAT CAPACITY:   1280  0  0  0
CONDUCTIVITY:    0.1  0  0  0
TRANSPORT:       1e-5  0  0  0
EMISSIVITY & ABSORPTION:  0.7  100

COMPONENT:      KAOWOOL
STATE:          S
DENSITY:        256  0  0  0
HEAT CAPACITY:  1070  0  0  0
CONDUCTIVITY:   0.0519  -4e-5  1e-7  2
TRANSPORT:      1e-30  0  0  0
EMISSIVITY & ABSORPTION:  0  1000

MIXTURES
S SWELLING:           0
L SWELLING:           0
G SWELLING LIMIT:     1e-30
PARALL CONDUCTIVITY:  0.5
PARALL TRANSPORT:     0.5

REACTION:       CB_A + NOCOMP -> NOCOMP + CB_g_1
STOICHIOMETRY:  1      0         0        1
ARRHENIUS:      6.14e0  2.35e4
HEAT:           -24.45e5  0  0  0
TEMP LIMIT:     L  300

REACTION:       CB_B1 + NOCOMP -> CB_C1 + CB_g_2
```

```
STOICHIOMETRY:  1      0         0.9     0.1
ARRHENIUS:      7.95e9  1.3e5
HEAT:           0  0  0  0
TEMP LIMIT:     L  300

REACTION:       CB_B2 + NOCOMP -> CB_C2 + CB_g_2
STOICHIOMETRY:  1      0         0.9     0.1
ARRHENIUS:      7.95e9  1.3e5
HEAT:           0  0  0  0
TEMP LIMIT:     L  300

REACTION:       CB_B3 + NOCOMP -> CB_C3 + CB_g_2
STOICHIOMETRY:  1      0         0.9     0.1
ARRHENIUS:      7.95e9  1.3e5
HEAT:           0  0  0  0
TEMP LIMIT:     L  300

REACTION:       CB_C1 + NOCOMP -> CB_ch1 + CB_g_2
STOICHIOMETRY:  1      0         0.37     0.63
ARRHENIUS:      2e11  1.6e5
HEAT:           -1.26e5  0  0  0
TEMP LIMIT:     L  300

REACTION:       CB_C2 + NOCOMP -> CB_ch2 + CB_g_2
STOICHIOMETRY:  1      0         0.37     0.63
ARRHENIUS:      2e11  1.6e5
HEAT:           -1.26e5  0  0  0
TEMP LIMIT:     L  300

REACTION:       CB_C3 + NOCOMP -> CB_ch3 + CB_g_2
STOICHIOMETRY:  1      0         0.37     0.63
ARRHENIUS:      2e11  1.6e5
HEAT:           -1.26e5  0  0  0
TEMP LIMIT:     L  300

REACTION:       CB_ch1 + NOCOMP -> CB_ch4 + CB_g_2
STOICHIOMETRY:  1      0         0.59     0.41
ARRHENIUS:      2.61e-2  1.7e4
HEAT:           0  0  0  0
TEMP LIMIT:     L  300

REACTION:       CB_ch2 + NOCOMP -> CB_ch5 + CB_g_2
STOICHIOMETRY:  1      0         0.59     0.41
ARRHENIUS:      2.61e-2  1.7e4
HEAT:           0  0  0  0
TEMP LIMIT:     L  300

REACTION:       CB_ch3 + NOCOMP -> CB_ch6 + CB_g_2
STOICHIOMETRY:  1      0         0.59     0.41
ARRHENIUS:      2.61e-2  1.7e4
HEAT:           0  0  0  0
TEMP LIMIT:     L  300
```

The conditions files are used to define the sample geometry, the initial and boundary conditions for the computational domain, and the integration and output parameters. The conditions files varied according to the heat flux because the heat flux affected the boundary conditions of the computational domain. The flame heat flux

contribution was not turned on in the final versions of the conditions files and instead was approximated by the ramp function defined in the second external radiation program step in the top boundary conditions and the onset of the ramp was determined by monitoring the volatile mass flux from the sample. The onset of the heat flux ramp corresponding to the flame was defined as the critical mass flux. In the case provided below, the ignition time was 6 seconds, whereas for 20 kW/m^2 the ignition time was 55 seconds.

Final Conditions File for 60 kW/m^2 – nCND60_q.cnd

```
OBJECT TYPE:  1D

OBJECT STRUCTURE
****************

THICKNESS:  0.00064
TEMPERATURE:  300
MASS FRACTIONS:
CB_B1  0.98
CB_A   0.02

THICKNESS:  0.0034
TEMPERATURE:  300
MASS FRACTIONS:
CB_B2  0.98
CB_A   0.02

THICKNESS:  0.00064
TEMPERATURE:  300
MASS FRACTIONS:
CB_B1  0.98
CB_A   0.02

THICKNESS:  0.0021
TEMPERATURE:  300
MASS FRACTIONS:
CB_B3  0.98
CB_A   0.02

THICKNESS:  0.00064
TEMPERATURE:  300
MASS FRACTIONS:
CB_B1  0.98
CB_A   0.02

THICKNESS:  0.015
TEMPERATURE:  300
MASS FRACTIONS:
KAOWOOL  1

OBJECT BOUNDARIES
*****************

TOP BOUNDARY
```

```
MASS TRANSPORT: YES
CB_g_1  LIN  0.05  0
CB_g_2  LIN  0.05  0

OUTSIDE TEMP TIME PROG: 300  0
CONVECTION COEFF:  10

EXTERNAL RADIATION: YES
TIME PROG1:  6e4  0  6
TIME PROG2:  6e4  3000  10

REPEAT:  NO
ABSORPTION MODE: MAX

FLAME: YES
IGNITION MASS FLUXES:
CB_g_2  1e-3
OUTSIDE TEMP:  2270
CONVECTION COEFF:  0
RADIATION:  0

BOTTOM BOUNDARY

MASS TRANSPORT:  NO

OUTSIDE TEMP TIME PROG:  300  0
CONVECTION COEFF:  0

EXTERNAL RADIATION:  NO

FLAME:  NO

INTEGRATION PARAMETERS
**********************

ELEMENT SIZE:  5e-5
TIME STEP:     0.01
DURATION:      100

OUTPUT FREQUENCY:
ELEMENTS:    1
TIME STEPS:  100
```

Works Cited

1. *Warehouse commodity classification from fundamental principles Part I: Commodity & burning rates.* **Gollner, M. J., et al.** 2011, Fire Safety Journal, pp. 305-316.

2. **Stoliarov, S. I. and Lyon, R. E.** *Thermo-Kinetic Model of Burning.* Atlantic City : Federal Aviation Administration, 2008.

3. *Inert and Oxidative pyrolysis of a lignocellulosic material: Corrugated cardboard.* **Chaos, M., Khan, M. M. and Dorofeev, S. B.** Atlanta : s.n., 2011. 7th US National Technical Meeting of the Combustion Institute.

4. *Effects of External Radiant Heat Flux and Ambient Oxygen Concentration on nonlaming Gasification Rates and Evolved Products of White Pine.* **Kashiwagi, T., Ohlemiller, T. J. and Werner, K.** 1987, Combustion and Flame, pp. 331-345.

5. **Roper, F. G., Smith, C. and Cunningham, A. C.** The Prediction of Laminar Jet Diffusion Flame Sizes: Part II. Experimental Verification. *Combustion and Flame.* 1977, Vol. 29.

6. *The state-of-the-art in pyrolysis modelling of lignocellulosic solid fuels.* **Moghtaderi, Behdad.** 2006, Fire and Materials, pp. 301-334.

7. **Heikkinen, J. M., et al.** Thermogravimetry as a tool to classify waste components to be used for energy generation. *Journal of Analytical Applied Pyrolysis.* 2004, Vol. 71.

8. **David, C., et al.** Determination of a reaction scheme for cardboard thermal degradation using thermal gravimetric analysis. *Journal of Analytical Applied Pyrolysis.* 2003, 67.

9. **Gupta, Ashwani and Muller, Patric.** Pyrolysis of paper and Cardboard in inert and Oxidative Environments. *Journal of Propulsion and Power.* 1999, Vol. 15, 2.

10. **Antal, Michael Jerry Jr. and Varhegyi, Gabor.** Cellulose Pyrolysis Kinetics: The Current State of Knowledge. *Industrial & Engineering Chemistry Research.* 1995, Vol. 34.

11. **Prakash, N. and Karunanithi, T.** Kinetic modeling in Biomass Pyrolysis - A Review. *Journal of Applied Sciences Research.* 2008, Vol. 4, 12.

12. **Blasi, Colomba Di.** Comparison of semi-global mechanisms for primary pyrolysis of lignocellulosic fuels. *Journal of Analytical and Applied Pyrolysis.* 1998, Vol. 47.

13. **Broido, A.** [book auth.] F. Shafizadeh, K. Sarkanen and D.A. Tillman. *Thermal Uses and Properties of Carbohydrates & Lignins.* New York : Academic, 1976.

14. **Broido, A. and Nelson, Maxine A.** Char Yield on the Pyrolysis of Cellulose. *Combustion and Flame.* 1975, Vol. 24.

15. **Bradbury, Allan G.W., Sakai, Yoshio and Shafizadeh, Fred.** A Kinetic Model for Pyrolysis of Cellulose. *Journal of Applied Polymer Science.* 1979, Vol. 23, 11.

16. **Varhegyi, Gabor, Jakab, Emma and Antal, Michael Jerry, Jr.** Is the Broido-Shafizadeh Model for Cellulose Pyrolysis True? *Energy & Fuels.* 1994, Vol. 8.

17. **Shafizadeh, Fred and Chin, Peter P.S.** Thermal Deterioration of Wood. [book auth.] I. Goldstein. *Wood Technology: Chemical Aspects.* Washington, D.C. : American Chemical Society, 1977.

18. **Thurner, Franz and Mann, Uzi.** kinetic Investigation of Wood Pyrolysis. *Industrial and Engineering Chemical Process Design and Development.* 1981, Vol. 20.

19. **Chaos, Marcos, et al.** Evaluation of optimization schemes and determination of solid fuel properties for CFD fire models using bench-scale pyrolysis tests. *Proceedings of the Combustion Institute.* 2011, Vol. 33.

20. **Balci, Suna, Dogu, Timur and Yucel, Hayrettin.** Pyrolysis Kinetics of Lignocellulosic Materials. *Industrial & Engineering Chemistry Research.* 1993, Vol. 32.

21. **Wu, Chao-Hsiung, Chang, Ching-Yuan and Lin, Jyh-Ping.** Pyrolysis Kinetics of Paper Mixtures in Municiapl Solid Waste. *Journal of Chemical Technology & Biotechnology.* 1997, Vol. 68.

22. **Orfao, J.J.M., Antunes, F.J.A. and Figueiredo, J.L.** Pyrolysis klinetics of lignocellulosic materials - three independent reactions model. *Fuel.* 1999, Vol. 78.

23. *The Role of Thermal Decomposition in the Burning of Polymers.* **Lyon, R. E., Safronava, N. and Stoliarov, S. I.** Nottingham, U.K. : Interscience Communications, 2010.

24. *Combustion of a substitution fuel made of cardboard and polyethylene: Influence of the mix characteristics - Modeling.* **Salvador, S., Quintard, M. and David, C.** 2008, Fire and Materials, pp. 417-444.

25. **Gollner, M.J., Williams, F.A. and Rangwala, A.S.** Upward Flame Spread Over Corrugated Cardboard. *Combustion and Flame.* Submitted 2010.

26. *Combustion of a substitution fuel made of cardboard and polyethylene: influence of the mix characteristics - experimental approach.* **Salvador, S., Quintard, M. and David, C.** 2004, Fuel, pp. 451-462.

27. **Stoliarov, Stanislav I., et al.** Prediction of the burning rates of non-charring polymers. *Combustion and Flame.* 2009, Vol. 156.

28. **Stoliarov, I. Stanislav, et al.** *Prediction of the Burning Rates of Charring Polymers.* Atlantic City : Federal Aviation Administration, 2010. DOT/FAA/AR-TN09/59.

29. *The effect of variation in polymer properties on the rate of burning.* **Stoliarov, S. I., Safronava, N. and Lyon, R. E.** 2009, Fire and Materials, pp. 257-271.

30. **Staggs, J.E.J. and Whiteley, R.H.** Modelling the Combustion of Solid-phase Fuels in Cone Calorimeter Experiments. *Fire and Materials.* 1999, Vol. 23.

31. *Bench-Scale Flammability Experiments: Determination of Material Properties Using Pyrolysis Models for Use in CFD Fire Simulations.* **Chaos, Marcos, et al.** Nottingham, UK : Interscience Communications, 2010.

32. **International Trade Centre.** *Technical Notes on the Use of Corrugated Paperboard Boxes.* Geneva : s.n., 1993. Export Packaging Note No. 13.

33. **ASTM International.** *Standard Test Method for Heat and Visible Smoke Release Rates for Materials and Products Using an Oxygen Consumption Calorimeter.* s.l. : ASTM, 2009. E 1354-09.

34. **Parker, W.J.** *Calculations of the Heat Release Rate by Oxygen Consumption for Various Applications.* s.l. : National Bureau of Standards, 1982. NBSIR 81-2427.

35. **Huggett, Clayton.** Estimation of rate of heat release by means of oxygen consumption measurements. *Fire and Materials.* 1980, Vol. 4, 2.

36. **Lyon, Richard E. and Walters, Richard.** *A Microscale Combustion Calorimeter.* Atlantic City : Federal Aviation Administration, 2002. DOT/FAA/AR-01/117.

37. **National Institute of Standards and Technology.** NIST Chemistry Webbook. *Water.* [Online] NIST, 2011. [Cited: April 9, 2012.] http://webbook.nist.gov/cgi/cbook.cgi?ID=C7732185&Units=SI&Mask=4#Thermo-Phase. NIST Standard Reference Database 69.

38. **Siegel, Robert and Howell, John.** *Thermal Radiation Heat Transfer.* New York : Taylor & Howell, 2002.

39. **Matsumoto, T. and Ono, A.** Specific Heat Capacity and Emissivity Measurements of Ribbon-Shaped Graphite Using Pulse Current Heating. *International Journal of Thermophysics.* 1995, Vol. 16, 1.